IMPACT OF LAND USE/COVER AND CLIMATE CHANGE ON WATER BALANCE IN THE OUÉMÉ RIVER BASIN, BENIN

By

Ernestina Annan

(BSc. Agricultural Engineering; MPhil. Soil and Water Engineering)

A Thesis submitted to WASCAL Climate Change and Land Use, Department of Civil Engineering, Kwame Nkrumah University of Science and Technology in partial fulfilment of the requirements for the award degree of

DOCTOR OF PHILOSOPHY IN CLIMATE CHANGE AND LAND USE

February, 2025

DECLARATION

I hereby declare that this submission is my own work and that, to the best of my knowledge and belief, it contains no material previously published or written by another person nor material which to a substantial extent has been accepted for the award of any other degree or diploma at Kwame Nkrumah University of Science and Technology, Kumasi or any other educational institution, except where due acknowledgement is made in the thesis.

Ernestina Annan	………….	…………
(PG6992521)	Signature	Date

Certified by:

Prof. Wilson Agyei Agyare	………….	…………
(Main Supervisor)	Signature	Date

Certified by:

Prof. Kwaku Amaning Adjei	………….	…………
(Co-supervisor)	Signature	Date

Certified by:

Prof. Dr-Ing. Markus Disse	………….	…………
(Co-supervisor)	Signature	Date

Certified by:

Dr. William Amponsah	………….	…………
(Co-supervisor)	Signature	Date

Certified by:

Prof. Richard Akwasi Buamah	………….	…………
(Head of Department)	Signature	Date

ABSTRACT

The influence of land use/cover (LULC) and climate changes on hydrological processes are not fully understood in data-scarce regions such as the Ouémé River Basin, Benin. However, this is crucial for sustainable water management, infrastructure design, flood mitigation, and improving food security. This study assessed the impact of historical and projected future LULC changes, and climate change on hydrological components: surface runoff, lateral flow, aquifer recharge, and evapotranspiration. Using Landsat images from 1986, 2000, 2015, and 2023, LULC in the basin were categorised through a supervised classification in Google Earth Engine into Forests, Savanna, Settlements/bare lands, Water bodies, and Agricultural lands. The classified LULC maps were used to estimate water balance in the Soil and Water Assessment Tool (SWAT) model. LULC was then projected for 2030, 2063, and 2100 using the Cellular Automata-Markov projection, and future climate from 2021-2100 was projected using the ACCESS-CM2 model precipitation and ensemble mean temperature from five CMIP6 climate models. These were subsequently used to project future water balance, and a linear regression was used to examine the relationship between LULC, climate, and water balance components. The 1986 LULC map showed that the basin was predominantly Savanna (70 %), but these and Forests have reduced in 2023 by 24 % and 4 %, respectively; however, Settlements/bare lands and Agricultural lands have increased by 1 % and 27 %, respectively. These LULC changes resulted in increased surface runoff (32 mm/y) from 1986 to 2023, with a reduction in lateral flow (6 mm/y), baseflow (5 mm/y), aquifer recharge (22 mm/y), and evapotranspiration (6 mm/y). The highest rates of change were observed between 2015 and 2023. The projected future LULC changes under the business-as-usual scenario showed continued expansion of Settlements/bare lands and Agricultural lands at the expense of Forests and Savanna. The projected future climate under the "Sustainability" scenario, SSP1-2.6 showed gentler variability in rainfall patterns from 2021 – 2100, and more drastic changes in precipitation and temperature under the "Regional Rivalry" scenario, SSP3-7.0. The projected future climate resulted in an increase in surface runoff and a reduction in subsurface flow where temperature and precipitation increased; however, where precipitation reduced, surface and subsurface flow reduced. The combined future LULC and climate change increased surface runoff and reduced subsurface flow at a potential lower than LULC change alone and higher than climate change alone, with trends mirroring precipitation change patterns. The Partial Least Squares regression revealed that water balance in the basin was more sensitive to changes in Settlements/bare lands and Forests than Savanna and Agricultural land, and more sensitive to temperature than precipitation changes. The combined effect of increased runoff and reduced subsurface flows will increase the risk of people displacement and destruction of properties during flooding, and limit water availability for domestic and farming activities. Floods and droughts would lead to higher crop failures. Thus, sustainable land management practices such as reforestation, green urban spaces, conservation agriculture, and rainwater harvesting systems are recommended to limit runoff, reduce floods, and enhance water availability for domestic, industry and food production.

TABLE OF CONTENTS

LIST OF TABLES

LIST OF FIGURES

LIST OF ABBREVIATIONS

AGR	Agricultural Lands
AI	Artificial Intelligence
BSI	Bare Soil Index
CANMX	Maximum Canopy Storage
CDS	Climate Data Store
CENATEL	National Centre for Remote Sensing and Forest Cover Monitoring
CGLS	Copernicus Global Land Service
CHIRPS	Climate Hazards Group InfraRed Precipitation with Station Data
CI	Confidence Interval
CMIP	Coupled Model Intercomparison Project
CN	Curve Number
CORDEX	Coordinated Regional Climate Downscaling Experiment
CUP	Calibration and Uncertainty Program
DEM	Digital Elevation Model
EJ	Exajoules
EPCO	Plant Uptake Compensation Factor
ESA	European Space Agency
ESCO	Soil evaporation Compensation factor
ETM	Enhanced Thematic Mapper
FAO	Food and Agriculture Organisation
FRST	Forest Areas
GCM	Global Climate Model

GDP	Gross Domestic Product
GEE	Google Earth Engine
GIS	Geographic Information Systems
GLCC	Global Land Cover Characterization
GSAT	Global Surface Air Temperature
HRU	Hydrologic Response Units
IAM	Integrated Assessment Models
IFRC	International Federation of Red Cross and Red Crescent Societies
IPCC	Intergovernmental Panel on Climate Change
IWRM	Integrated Water Resources Management
KGE	Kling-Gupta Efficiency
LAI	Leaf Area Index
LHS	Latin-Hypercube Sampling
LST	Land Surface Temperature
LULC	Land Use/Cover
MIT	Massachusetts Institute of Technology
MJ	Megajoules
ML	Machine Learning
NASA	National Aeronautics and Space Administration
NDBI	Normalized Difference Built-up Index
NDVI	Normalized Difference Vegetation Index
NDWI	Normalized Difference Water Index
NSE	Nash-Sutcliff Efficiency

OA	Overall Accuracy
OLI	Operational Land Imager
PBIAS	Percent Bias
PET	Potential Evapotranspiration
PLS	Partial Least Squares Regression
PPU	Percent Prediction Uncertainty
RCM	Regional Climate Model
RCP	Representative Concentration Pathway
REMO	Regional Model
RIVERTWIN	A Regional Model for Integrated Water Management in Twinned River Basins
RSME	Root Mean Square Error
RSR	RMSE-observations Standard Deviation Ratio
SAV	Savanna Areas
SCP	Semi-Automatic Plugin
SCS	Soil Conservation Service
SDG	Sustainable Development Goal
SEZ	Special Economic Zones
SRES	Special Report on Emissions Scenarios
SRTM	Shuttle Radar Topography Mission
SSP	Shared Socio-economic Pathway
STB	Settlements/bare lands
SUFI	Sequential Uncertainty Fitting
SURF	Surface Runoff

SVM	Support Vector Machine
SWAT	Soil and Water Assessment Tool
TIRS	Thermal Infrared Sensor
TM	Thematic Mapper
TOA	Top of Atmosphere
UA	User Accuracy
USDA	United States Department of Agriculture
USGS	United States Geological Survey
VIP	Variable Importance in Projection

ACKNOWLEDGEMENTS

I am grateful to God for this PhD programme.

I appreciate KNUST for its inclusive and conducive learning environment.

I am very grateful to the West African Science Service Centre on Climate Change and Adapted Land Use (WASCAL) for the opportunity to benefit from the WASCAL scholarship scheme. I want to thank the German Federal Ministry of Education and Research (BMBF) for the funding, without which pursuing this PhD would have remained a distant dream. I appreciate WASCAL and BMBF for the opportunity to conduct part of my research in Germany, which added to my learning experience and network. I thank WASCAL Headquarters and WASCAL KNUST management for their immense support.

My heartfelt gratitude goes to my main supervisor, Prof. Wilson A. Agyare, for his thoughtful guidance, and to my co-supervisors, Prof. Kwaku A. Adjei, Prof. Dr.-Ing. Markus Disse, and Dr. William Amponsah, as well as my mentor, Dr. Jean Hounkpè, for their unwavering support throughout this PhD.

I appreciate the support from the FURIFLOOD research project and the UAWOS project in Germany.

I am also grateful to Prof. Disse and the Technical University of Munich, Dr. Michael Thiel of the University of Würzburg, Fabian Merk, and Mrs. Christiane Cretaine (and family), as well as Ms. Adowa Yéwa Tossoukpe, for their support and contributions during my research visit to Germany.

I want to thank Mr. Ernest Biney, and Mr. Albert Elikplim Agbenorhevi for their contributions to this research.

Finally, I am deeply grateful for the unwavering support of my family, especially my husband, and my friends.
God bless you all immensely!

DEDICATION

This book is dedicated to my parents, Mr. and Mrs. Annan, my husband, Sgt. Daniel Kwame Azumah, my son, Ethan Kekeli Kwesi Azumah, and my siblings, Alice, Sandra, and Rebecca, who have been instrumental in completing this PhD programme.

CHAPTER 1 INTRODUCTION

1.1 Background

Rapid population growth and urban expansion have increased the demand for food and water significantly (Olofintoye *et al.,* 2022). This increase in demand has led to the conversion of natural vegetation to cultivated lands to meet the food supply needs, with adverse implications for the overall ecosystem health and its ability to provide services. Land use/cover (LULC) is recognised for its crucial role in influencing hydrological processes in tropical basins where land surface dynamics and water are interrelated. In Benin, the Ouémé River Basin has been undergoing rapid shifts in LULC mainly due to agricultural extensification and urbanisation, similar to many parts of West Africa. Additionally, the changes in precipitation patterns and temperature due to climate change are further making water resources management in the region complex. This is especially true when choosing between the immediate satisfaction of needs and the long-term sustainability of these resources. The changes in LULC and climate change affect water availability (Mbaye *et al.,* 2015), surface runoff patterns, and the overall ability of the basin to support life under extreme pressure from the environment and climate. Hence, understanding the dynamics of LULC and climate change and how they impact hydrological processes is crucial to achieving sustainable agriculture and zero hunger, as outlined in the Sustainable Development Goals (SDGs) 2 and 6.2.

Agriculture is the main economic activity in Benin, with more than 90 % of production performed under rainfed conditions (Dossou *et al.,* 2021b). Therefore, agricultural productivity is limited by water availability, especially during the dry season, preventing some farmers from planting during the dry periods. Additionally, agriculture is important to Benin's Gross Domestic Product (GDP), contributing 26. 9 % and it also employs over 60 % of the country's workforce (World Bank, 2022). Thus, the limited water availability both spatially and temporally affects its use for domestic, agricultural, and industrial purposes (Togbévi *et al.,* 2020). Efforts have been made to improve access to potable water (World Bank, 2018), however, there is still limited information on the availability and variability across the country's landscape.

Ecosystem processes, such as the hydrological and carbon cycles are complex and difficult to predict, but regular assessment supports efforts to achieve SDG Target 6.5 ("*by 2030, implement integrated water resources management at all levels, including through transboundary cooperation as appropriate"*) (Mclntyre, 2023, p. 448) on integrated water resources management (IWRM), which is lagging globally (United Nations Environment Programme, 2021).

Characteristics such as LULC, soil properties, channel characteristics (length, roughness, width and depth), and catchment size and shape influence how a watershed responds to rain by controlling surface runoff generation and propagation as well as groundwater recharge (Mosavi *et al.,* 2020). The dynamics of how a catchment responds to rainfall can be assessed using LULC mapping to identify how changes in vegetation affect shifts in regional hydrology (Osseni *et al.,* 2022). This is integral to achieving SDG Target 15.1 ("*ensure the conservation, restoration, and sustainable use of terrestrial and inland freshwater ecosystems and their services, including forests, wetlands, mountains, and drylands by 2020, in line with obligations under international agreements"*) (Perron-Welch *et al.,* 2023, p. 1098) on ecosystem and biodiversity conservation.

Geographic Information Systems (GIS) enhance such LULC assessments by providing efficient means of processing large datasets and geographical areas and enabling analysis and visualization of changes in the land surface characteristics (Obodai *et al.,* 2019). When coupled with modelling tools, it provides valuable insights into future changes in LULC and climate, and how they could influence regional hydrology. Climate models for instance provide foresight into future climate scenarios, ensuring that water and landscape management strategies account for short-term fluctuations and long-term trends, which is essential for sustainable ecosystem management.

1.2 Problem Statement

Past studies within the Ouémé River Basin have explored the impacts of changes in LULC on water resources, with findings on surface runoff dynamics, groundwater recharge patterns, and their implications for local water management strategies. For instance, Hiepe (2008) studied how LULC affects water balance and soil erosion in the upper Ouémé basin (Bétérou catchment) using a 2000 LULC map from Landsat imagery and found that agricultural lands were more prone to soil erosion. Bossa *et al.* (2014) also modelled the effects of LULC change on land and water degradation in the Ouémé basin using LULC change scenarios from projected socio-economic changes, specifically population growth, and a baseline LULC of 2003 Landsat imagery. Their study found a higher sensitivity of water yield and evapotranspiration to climate change, and surface runoff and groundwater flow to LULC change (Bossa *et al.*, 2014). Hounkpè *et al.* (2019) also used LULC scenarios derived from socio-economic change scenarios to assess the impact of LULC change on flood characteristics in the Zou sub-catchment of the Ouémé basin assuming 2003 LULC from the RIVERTWIN project as a baseline. Their study found that expansion in agricultural lands and reduction in natural vegetation enhance the incidence of floods in the Zou catchment.

Abdulkadir *et al.* (2022) predicted water balance in the upper Ouémé basin (Bétérou catchment) from 1998-2007 using LULC map from the Global Land Cover Characterization (GLCC) for April 1992 to March 1993 and observed that evapotranspiration was the highest component of water loss from rainfall while lateral flow was the least. Similar findings have been reported by Sintondji *et al.* (2014), who modelled water balance at the Savè outlet of the Ouémé basin using a LULC map of 2003 by the National Centre of Remote Sensing and Forest Cover Monitoring (CENATEL), and Maforikan *et al.* (2023), who simulated water balance in the upper Ouémé basin (Bétérou catchment) using the 2003 LULC map from the RIVERTWIN project. Additionally, Olofintoye *et al.* (2022) predicted water balance values in the Bétérou catchment with the GLCC LULC map from April 1992 to March 1993 and compared simulated water balance values in 1998, 2008, and 2017. Their study observed an increase in precipitation and groundwater flow between 1998 and 2008, and a reduction between 2008 and 2017. Surface runoff and evapotranspiration however reduced over the period.

These past studies predicted water balance using single maps without considering LULC change or used derived scenarios of LULC from predicted socio-economic scenarios to assess changes in water balance in the future. Also, the studies did not explore the relationship between the LULC and the resulting changes in water balance, nor the consistency of the relationship across different periods. Additionally, most of the past studies focused on parts of the basin. Furthermore, even recent studies have used single LULC data dating as far back as 1993 to assess water balance in the basin and did not project future LULC changes beyond 2030. Also, they did not use the CMIP6 scenarios which consider how socio-economic factors (population, economic growth, urbanisation, technological development and development) lead to greenhouse gas emissions to project the influence of future climate on water balance. Furthermore, the combined impact of projected LULC and climate change on water balance has not been explored. Hence, there is a research gap in terms of understanding the impact of LULC and climate changes, and their combined influence on water balance across different spatial and temporal periods for the Ouémé River basin.

This study therefore builds upon existing research by assessing LULC change impacts on water balance across different periods in the Ouémé River Basin. Firstly, LULC types in the basin from historical years until the present are mapped, and the quantity and rates of change in LULC are assessed. Secondly, the derived LULC maps with spatio-temporal differences in the distribution of LULC types and observed climate data from 1998-2016 are used to estimate changes in water balance components such as surface runoff, baseflow, lateral flow, total aquifer recharge, and actual evapotranspiration. Furthermore, the effects of future LULC changes on water balance are estimated using LULC change modelling, considering the years 2030, 2063, and 2100. Finally, the Intergovernmental Panel on Climate Change (IPCC) Coupled Model Intercomparison Project phase 6 (CMIP6) Shared Socio-economic Pathways (SSPs) of climate emissions/concentration is used to predict water balance changes under two different climate mitigation and adaptation scenarios.

1.3 Justification

Water balance refers to rainfall distribution in a catchment and describes the hydrological cycle's processes (Gharun *et al.*, 2017). The primary source of water in the hydrological cycle is rainfall. Land surface characteristics affect how rainwater is distributed in a watershed. For instance, where there is a vegetative cover or tree canopy, rainfall is usually intercepted, and the rate and quantity of water flow on the land surface is reduced. However, where the land surface is bare or impervious, there is a direct impact of the rain onto the land, and the rate and amount of runoff are increased due to the absence of any obstacles (usually vegetation) (Guo *et al.*, 2019). When the native LULC in a region changes over time, it may affect the rainfall distribution, which pattern may differ from one catchment to another. Thus, assessing LULC changes is vital to understanding changes that may be occurring in the water balance of the catchment (Zhou *et al.,* 2023). Furthermore, climate, including precipitation patterns and temperature variations, affect the dynamics of the hydrological cycle in a region. Particularly, where precipitation intensity and amounts increase beyond the infiltration capacity of the soil, the runoff amounts will differ from when there is a reduction in precipitation over time. The combined influence of changes in LULC and climate spatio-temporally will present even more complex interactions with water balance.

The changes in rainwater distribution are closely associated with flooding in terms of peak flow, soil erosion, and water quality (pollution), which are all direct, visible outcomes of LULC changes (Guo *et al.,* 2019). The less visible changes such as a drop in the groundwater table, which indicate a reduction in groundwater, baseflow, and lateral flows into rivers and streams are also important because they have implications on water availability for domestic, farming, and industrial purposes. Particularly, in areas where groundwater serves as a primary source of drinking water, and water for other purposes as is the case in Benin, water balance assessment provides insights into possible risks of water availability or unavailability for abstraction. According to the World Resources Institute, 2023, demand for water in Sub-Saharan Africa is projected to increase by 163 % by 2050, meaning that water-related challenges may intensify, emphasising the need for urgent sustainable water resources management strategies.

Furthermore, water balance assessment is crucial for urban planning and infrastructure design, including drainage systems, road networks, and buildings. It is also essential in the evaluation of agricultural productivity, especially in regions where rainfed agriculture sustains local livelihoods, such as in the Ouémé River Basin (Hiepe, 2008). Water quality is influenced by soil erosion and sedimentation, which endanger aquatic life, leading to lower income for fish farmers in the basin.

More so, the projected increase in global surface runoff is found to be closely linked with changes in land surface characteristics together with changes in precipitation patterns (Zhou *et al.,* 2023). However, the projected variabilities in precipitation and temperature might amplify the risk of pluvial and flash floods (probably loss of lives and destruction to properties), extended dry periods, lower food productivity, and biodiversity losses (Chen *et al.,* 2021). Particularly, Sub-Saharan Africa could experience on average a reduction in maize productivity by about 5.8 % by 2100 if the increase in global surface temperatures approaches 4 ^{o}C (Lee *et al.,* 2021).

Therefore, effective water balance management by promoting water infiltration rates can reduce flood and erosion risks, protect and improve soil health, and ensure water security in quality and quantity to meet the increasing population's needs. This study therefore offers insights into the effects of spatio-temporal changes in LULC and climate on water balance in the Ouémé River Basin as a foundation for sustainable water and ecosystem management in the basin. This is to ascertain the sensitivity of the water balance components to changes in LULC, precipitation and temperature. The results of this study are beneficial for understanding and informing decisions regarding flood risk, sustainable water resources, and ecosystem management within the region, to improve food productivity and reduce land degradation.

1.4 Research Objectives

This study main objective was to assess the impact of LULC and climate change on water balance in the Ouémé River Basin. To achieve the main objective, this study specifically aimed to:

1. Assess the spatio-temporal changes in LULC for Ouémé River Basin.

2. Model water balance using LULC maps from Objective 1:
   2.1 Simulate water balance components using the LULC maps in SWAT.
   2.2 Assess the relationship between LULC changes and changes in surface runoff, subsurface flow, aquifer recharge, and actual evapotranspiration.
3. Evaluate future LULC changes impact on water balance components in the basin.
4. Evaluate future water balance under IPCC's CMIP6 Shared Socio-economic Pathways future climate scenarios, SSP1-2.6 (Sustainability) and SSP3-7.0 (Regional Rivalry).
5. Assess the combined effect of projected LULC and future climate on water balance.

1.5 Research Questions

The main research question is: What is the impact of LULC and climate change on water balance in the Ouémé River Basin, and what are the impacts on water resources and ecosystem sustainability?

Specifically:

1. What LULC changes have taken place in the Ouémé River Basin in the past?
2. What impact have past changes in LULC had on water balance?
   2.1 What changes in water balance have been influenced by LULC changes?
   2.2 What relationship do historical LULC changes have with water balance changes?
3. What potential impacts can future LULC changes have on water balance?
4. What potential impacts can future climate change have on water balance?
5. What are the potential impacts of combined future LULC and climate change on water balance?

CHAPTER 2 LITERATURE REVIEW

2.1 Introduction

Water scarcity and water pollution are two challenges facing many developing countries, specifically in Sub-Saharan Africa, which have high vulnerability to the effects of climate change and variability (Olofintoye *et al.,* 2022). Many of these countries also struggle with poverty, high reliance on rainfed subsistence farming for their livelihood, and rapid population growth which further increase their vulnerability (Santpoort, 2020). The growing population is a major driver of LULC changes, especially conversions of natural vegetation including forests and transitional savanna areas to expand food production and make room for settlements. These transformations on the land surface have brought about alterations in regional hydrology, revealed by the more erratic rainfall patterns and rising temperatures, and increasing incidences and impacts of floods and droughts across West Africa (Chalid and Mulyadi, 2021).

LULC on the one hand influences climate change, which also impacts water resources and the hydrological balance in a catchment. The SDG report for 2022 highlights a reversal of the progress made towards improving health, eradicating hunger, and making basic services accessible to all, due partly to the COVID-10 pandemic, conflicts, and climate change. Demand and pressure on land have increased, resulting in the expansion of croplands, urban areas, mining areas, and industrial centres at the expense of natural vegetation. These are drivers of LULC change and contribute to greenhouse emissions, thus worsening climate change.

Regular monitoring and water balance assessment at local and regional scales improve effective water resources management efforts to ensure environmental sustainability. This deepens the understanding of the impacts of human activities through LULC and climate change and provides valuable information for context-specific climate adaptation strategies (Ayanshola *et al.*, 2018).

In this section, relevant literature to the study topic was reviewed.

2.2 Change in LULC and Water Balance

2.2.1 Classification of LULC

Advancements in Remote Sensing (RS) and Geographic Information Systems (GIS) have provided accurate monitoring of diverse changes in the earth's features, including changes in LULC. LULC classification is a method of grouping land surface features (in pixels) from satellite images based on their spectral characteristics using algorithms. This provides insights into understanding environmental processes and changes that eventually affect ecosystem functioning. There are two primary methods of LULC classification: Supervised Classification and Unsupervised Classification (Sathya and Abraham, 2013). In a supervised classification the user directs the classification process by defining the number of LULC groups (categories) and setting reference areas based on which the LULC features would be trained (Lillesand *et al.,* 2015). This reference data is also referred to as ground truth data or training data. Because the supervised classification is based on user-defined training data and categories, it provides more accurate and detailed LULC mapping information. Unsupervised classification, on the other hand, allows the classification algorithm to automatically identify LULC groups without any pre-defined training data (Liu and Wu, 2017; Maxwell *et al.,* 2018). Although the unsupervised classification method is less accurate compared to the supervised, it is suited for exploratory studies.

2.2.2 LULC Datasets and Algorithms

Satellite imagery of the land surface is the main input in LULC classification, and they vary by the governing bodies, purpose, and spatial and temporal resolution. The evolution and launch of several satellites have made LULC data acquisition easier. One of the world's longest-running satellites for monitoring land and coastal areas is the Landsat series package, led by the United States Geological Survey (USGS) and the National Aeronautics and Space Administration (NASA). The first of the Landsat series mission was launched in 1972 and has since seen the launch of other satellites with up to 11 bands (the 6th failed), with the main aim of monitoring changes to land and coastal areas over time. It is a popularly used land use/cover package worldwide, and its image resolutions are moderate including 30 m, 60 m, and 15 m depending on the particular satellite. Secondly, there is the Copernicus Global Land Service (CGLS), a program under the European flagship program, Copernicus is run by the European Union and the European Space Agency (ESA). The CGLS package has biophysical variables (e.g., Leaf area index, Soil water index, etc.) to describe the evolution of land surface (vegetation, water, etc.), and it comes in moderate to coarse spatial resolutions (50 m to >= 1 km). The Global Land Cover Characterization Database maintained by USGS at a spatial resolution of 1 km and 24 LULC groupings is another package used in West Africa (Olofintoye *et al.,* 2022).

LULC classification algorithms often used include Maximum Likelihood Classification, Support Vector Machines (SVM), and Decisions Trees, such as Random Forests. The Random Forest algorithm is a robust ensemble learning tool that improves classification accuracy where the datasets are complex and non-linear (Belgiu and Dăgut, 2016). It builds decision trees with randomly collected data and makes a final decision from the average of the trees. It is less susceptible to overfitting and efficiently manages large datasets even with missing data. It is sensitive to input data quality, including the training data and satellite imagery.

The training data is divided into two, a portion is used for training (usually 70 %) and validation (the remaining 30 % is not used for training). The accuracy of LULC classification is evaluated based on the validation data using metrics such as overall accuracy (OA), producer's accuracy (PA), and user's accuracy (UA). Furthermore, additional metrics including quantity disagreement and allocation disagreement are used to quantify the source error in the classification process since the kappa statistic has been discovered to be inadequate for accuracy evaluations (Pontius Jr and Millones, 2011; Obodai *et al.,* 2019). Where there are multiple classified maps, the absolute change, relative, and rate of change of the LULC categories can be calculated between maps to quantify the changes over time and space.

2.2.3 The Hydrological Cycle

The hydrological cycle is the primary natural process that controls how water moves between land, atmosphere, and oceans to sustain life and stability on earth. The primary energy that drives the hydrological (water) cycle is solar energy from the sun, which leads to water evaporation from oceans, and plants through evapotranspiration, and lands into the atmosphere, to condense and fall back as precipitation (Chakravarty and Kumar, 2019). Upon reaching the earth, this precipitation can flow over the land surface as surface runoff, be abstracted by plants, or recharge groundwater storage, carrying on the cycle.

Changes in LULC and climate affect the hydrological cycle. Human interventions and interactions on land, including expansion of agricultural lands, deforestation, and urbanisation (Aladejana *et al.,* 2018) alter infiltration rates, resulting in changes in hydrological components, such as surface runoff, aquifer recharge, evapotranspiration, lateral flow, and baseflow (Hounkpè and Diekkrüger, 2018). These impacts are augmented by the uncontrolled emission of greenhouse gases contributing to rising global surface temperatures, and unpredictable rainfall patterns. These climate changes have been associated with more regular and intense droughts and floods, further stressing the water resources the growing population relies on (Lamboni *et al.,* 2019; Hounkpè *et al.,* 2022). Thus, this study assesses the interrelationship among LULC change, climate change, and changes in hydrological processes by assessing the relationships between LULC, climate and water balance changes to provide insights for informed water resources decisions in the basin.

2.2.4 Hydrological Response to LULC Change

The presence of vegetation on a land area plays a pivotal role in how the area responds to rainfall. This means that changes in vegetation cover through the expansion of urban and agricultural production lands inform the movement, distribution (Cornelissen *et al.,* 2013) and water quality in the area (Yehouenou *et al.,* 2017). In catchments where forest areas are cleared for farming or urban development, the land's capacity to intercept rainfall and retain water is reduced due to vegetation loss, which may result in enhanced soil detachment and transport, runoff, and reduced groundwater recharge (Biao, 2017). An increase in surface runoff can cause higher peak flows leading to flooding, reduced baseflow during dry periods, and more droughts that limit farmers from cropping all year round (Barbier and Hochard, 2018). The impervious surfaces of urban areas such as tarred roads and pavements worsen these effects by providing little or no room for water infiltration into the soil. This increases the risk of flash floods through increasing stormwater volumes during high-intensity rainfall events.

Across West Africa, existing research has shown that urbanisation contributes to changes in seasonal river flow patterns, and pollution through increased sediment transport from exposed soil surfaces (Bossa, 2012). Expansion in agricultural lands also alters evapotranspiration, especially in semi-arid areas (Togbévi *et al.,* 2020).

2.2.5 LULC Change Impact on Water Balance in the Ouémé River Basin

Existing research on LULC change in the Ouémé River Basin has shown a trend of reducing natural vegetation and increasing Agricultural lands and Settlements/bare lands. Bodjrènou *et al*. (2023a) assessed the changes in LULC within the Ouémé River Basin using Landsat images from 1975, 2000, and 2013 and found that the predominant Savanna areas had declined from about 78 % to 57 % over the period while residential areas and cultivated areas expanded. Their study also found that the period between 2000 and 2013 had higher changes in LULC than between 1975 and 2000. This demonstrates increasing rates of agricultural and urban expansion in the basin. Within the Ouémé Delta, beneath the Bonou outlet, Osseni *et al.* (2022) also revealed a considerable reduction in vegetation with the main drivers of changes in LULC alluding to the fertility of existing alluvia soils in the basin for agriculture and urbanisation. Hounkpè *et al.* (2019) assessed the impact of LULC changes on flood hazard within the Zou subbasin of the Ouémé basin using projected LULC scenarios based on expected socio-economic change scenarios (population, economic, etc.) from 2020-2029. The study found that agricultural lands expanded while forest and savanna areas reduced over time. Their study also revealed a strong positive linear relationship between increasing Agricultural lands and an increase in flood magnitude and a negative relationship with increasing Forest and Savanna. This depicts that Agricultural land expansion increases higher flood magnitudes, whereas Forests and Savanna reduce it, indicating the importance of vegetation in reducing flood risk on the land surface. Bossa *et al.* (2014) also undertook a scenario-based assessment of LULC change impacts on sediment transport and found that, Savanna conversion into croplands increased surface runoff in the Ouémé basin from 2000-2029. Groundwater water flow decreased while sediment yield increased due to lower infiltration rates, and higher exposure of the soil surfaces to the impact of raindrops on cultivated lands compared with savanna areas. Togbévi and Sintondji (2021) assessed the hydrological response of the Couffo basin at the south.

These studies did not consider multiple LULC maps over time to simulate water balance in the basin as done in this study. The few studies that considered LULC changes over time used LULC scenario maps based on expected socio-economic changes to predict water balance in the basin, however, the use of classified maps provides a surer way to assess spatio-temporal changes in LULC, which can then be used to assess changes in water balance. Secondly, existing research has not explored the relationship between LULC cover and water balance components such as surface runoff, lateral flow, base flow, actual evapotranspiration, and aquifer recharge using regression analysis as done in this study. Therefore, this study could offer deeper insights into spatio-temporal variations in LULC, its effects on specific water balance components, and their sensitivity to changes in specific LULC types.

2.3 Climate Change and Water Balance

2.3.1 Hydrological Changes Due to Climate Change

Globally, water resources are highly impacted by changes in climate, through changes in precipitation patterns and temperature variabilities, and these changes affect patterns of water balance processes (Mbaye *et al.,* 2015). In extension, these changes in water balance component patterns affect freshwater availability and long-term water resources dependability. The rising population growth rate is increasing demand for land utilization for farming activities, industry, and city building in West Africa, making the region highly susceptible to the adverse impacts of climate change on water resources.

Climate change is evidenced through lower and irregular rainfall, rising surface temperatures, extended drought periods, and an increase in evapotranspiration rates. These variations in the climate worsen water shortages, which in turn limit water availability for domestic, farming, and industrial processes, and limit food productivity (Soumaoro, 2021; Incoom *et al.,* 2020; Ayanshola *et al.,* 2018) through reduced soil moisture (and nutrients) for plant growth. Additionally, climate changes increase the vulnerability to flooding through an increase in peak flows and result in the reduction of river water levels thereby reducing ecosystem services provision.

Therefore, climate change plays a vital role in changes in a catchment's water balance, especially because rainfall is the main input into river basin water balance.

2.3.2 Water Balance Response to Climate Change in the Ouémé River Basin

Existing research has shown the significant influence changes in climate have on the Ouémé River Basin's hydrological processes. Biao (2017) assessed the impacts of climate change on river discharge trends using CMIP 5 Representative Concentration Pathway (RCP) scenarios RCP4.5 (intermediate emissions scenario with 4.5 W/m^2 radiative forcing by 2100) and RCP8.5 (high emissions scenario with 8.5 W/m^2 radiative forcing by 2100) at Bètèrou and Bonou stations of the Ouémé River Basin. The study found a reduction in river discharge at both stations and under the two future climate scenarios, with shifts toward extreme events including droughts, particularly for the extreme future scenario RCP8.5. Hiepe (2008) also assessed the impacts of climate change on soil erosion and found that climate change contributed to intensified rainfall events, which resulted in more severe soil erosion.

Hounkpè (2016) also assessed heavy rainfall characteristics from 1921-2012 over the Ouémé River Basin and found that there was a general increase in heavy rainfall events over the basin; however across different return periods, there was a reduction in heavy rainfall events from the east to the west of the basin. The areas from the central to the upper Ouémé basin also had a decreasing likelihood of heavy rainfall events; however, this reduction in frequency was accompanied by more intense rainfall patterns which could lead to floods. To assess the impact of climate change on Benin, Dossou *et al.* (2021a) correlated Land Surface Temperature (LST) with NDBI (Normalized Difference Built-up Index), NDWI (Normalized Difference Water Index), NDVI (Normalized Differences Vegetation Index), and Potential Evapotranspiration (PET). Their study found a strong positive correlation coefficient between LST and NDBI and a strong negative coefficient between NDBI and NDVI. This suggests that expansion in built-up areas increases land surface temperature, while an increase in vegetation reduces land surface temperature. Hounkpè *et al.* (2022) investigated the impact of climate change on high discharge in the Ouémé River Basin using the WaSiM model and found that an increase in rainfall intensity increased the vulnerability of communities to floods, especially when combined with LULC changes such as deforestation, urbanisation, and agricultural expansion.

Furthermore, Alamou *et al.* (2017) assessed future water resources availability under CMIP5 RCP4.5 and RCP8.5 in the Mékrou Basin, above the Ouémé Basin across three future periods, 2011-2040, 2041-2070, and 2070-2100. The study revealed a significant increase in PET until the end of the 21st century, with a higher increase rate under the RCP8.5 scenario than RCP4.5. Rainfall however, increased at a steady rate from 2011-2040 and decreased from 2041-2100, while mean annual discharge increased across the period and both scenarios with the magnitude of change varying with the projected period and RCP scenario. Similar findings were made by Lawin *et al.* (2019) who evaluated climate change impact on discharge in the Bétérou basin and the study revealed increasing discharge under the RCP4.5 and RCP8.5 future climate scenarios from the REMO regional climate model. Regarding crop production, Sonneveld *et al.* (2012) revealed that a reduction in rainfall amounts and increased variability caused by climate change led to more frequent crop failures in staples such as maize and yam production in the Ouémé basin.

Alterations in a catchment's hydrology due to climate change also affect the ecosystem's ability to provide services, reduce freshwater availability and increase hazard risks. The study by Togbévi *et al.* (2020) assessed the effect of climate change on hydrological ecosystem services such as household water supply and crop water needs in the Ouriyori subbasin of the Ouémé. Their study discovered that, seasonal changes in rainfall and temperature resulted in high water stress conditions, which led to lower crop yields. Dossou *et al.* (2021a) examined the Ouémé River Basin's ecosystem response to climate change between 2000 and 2016, and identified that, the south is highly sensitive to a reduction in water levels in water bodies and an increase in land surface temperatures compared to the north.

Generally, existing studies have not determined the relationship between climate change indicators, precipitation and temperature, and water balance components using regression analysis. The new IPCC socio-economic cum radiative forcing (SSP-RCP) future scenarios of climate change have also not been used to assess future water balance patterns. These updated scenarios enhance understanding of future climate change scenarios by providing socio-economic factors underpinning future emissions. Hence, this study builds on existing research in the basin by assessing the relationship between changes in precipitation, temperature, and water balance, using the sustainability (SSP1-2.6) and Regional Rivalry (SSP3-7.0) future climate scenarios from CMIP6.

2.4 LULC and Climate Change Modelling

2.4.1 Modelling LULC Change

Modelling of LULC change approaches includes Agent-Based Modelling, Neural Networks, Markov Chain, and Cellular Automata (CA) methods (Varga *et al.,* 2019). These methods differ in their approach to projecting future changes in LULC. Pure CA models project changes in a cell based on time and the current state of its neighbouring cells at each time step. However, this bottom-up approach may not be able to capture the complexity of LULC systems where demand often drives LULC changes. The Markov chain also projects LULC changes using probabilities based on the current state and the period between two historical maps. In Agent-based modelling the nearest neighbours change over time, introducing higher complexity while they are static in CA modelling. Most LULC change models use the classical land rent theories by Von Thünen and Ricardo, where land is allotted to purposes (uses) that return the highest economic rent based on their properties and location (Fujita and Thisse, 2013; McDonald, 2018). The CA-Markov model was used in this study to project future LULC changes in the basin. This model incorporates the spatial dimension of LULC change in CA with the Markov chain transition probabilities, which enables it to effectively project LULC changes in complex systems, capturing spatial (allocation) and temporal (quantity) patterns and interactions compared to statistical models (Viana *et al.,* 2023).

2.4.2 Climate Change Modelling

Climate models or General Circulation Models are computer programs developed to represent physical processes that describe how energy and matter are transferred through the atmosphere, land and ocean (Eltahir and Krol, 2021). Climate models are built by quantifying Earth system processes and defining them with mathematical equations, setting some baseline conditions, and climate forcing (e.g., greenhouse gas radiation) for projections and solving the equations repeatedly (Randall *et al.*, 2007). Climate models use a three-dimensional grid to divide the Earth's surface, namely: horizontal dimension (Latitude, Longitude), vertical dimension (to measure vertical variations in Atmosphere or Ocean), and Time dimension (e.g., hourly, daily, monthly). These dimensions define the resolution of the climate model, and the smaller the grid size (dimensions), the higher the resolution. Additionally, the higher the resolution, the higher the accuracy but is computationally intensive.

Global Climate Models (GCM) cover the entire earth while Regional Climate Models (RCM) are downscaled versions of GCMs with higher resolution and detail than the GCMs. Global models can be downscaled using dynamic or statistical methods, and the biases can be reduced with bias-correction methods including Quantile Mapping, Linear Scaling, and Delta Approach. Examples of RCMs include REMO (Lawin *et al.,* 2019) and CORDEX (Lamboni *et al.,* 2019) models; and examples of GCM models that are widely used are the global models developed under the IPCC CMIP framework. These models comprise projections of historical and future climate under varying emissions/concentration scenarios. Over the years, the IPCC climate report scenarios have been used to model climate change globally. The CMIP5 RCP scenarios in 2008 replaced the Special Report on Emission Scenarios (SRES) from 2000 used in the Third and Fourth IPCC reports. Since 2021, the CMIP6 SSP scenarios have been introduced for the assessment of natural and human-induced changes in the environment's impact on climate as an improvement of CMIP5 models. CMIP6 SSP scenarios enable future climate projections from socio-economic conditions and global effective radiative forcing (Lee *et al.,* 2021). The CMIP6 SSP scenarios provide socio-economic factors that would lead to the concentrations of GHGs, which is lacking in the CMIP5 RCP scenarios. The CMIP6 models have more detailed physics, improved land, ocean and ice processes, spatial resolution and representation of regional climate patterns compared to CMIP5 (Almazroui *et al.*, 2020). Some CMIP5 models applied in the basin include CORDEX and REMO regional climate models. Environmental changes such as greenhouse gas (GHGs) emissions from fossil fuels, deforestation and land degradation (Wheeler *et al.*, 2016; O'Neill *et al.,* 2017), and fertilizer application (Walling and Vaneeckhaute, 2020) are considered in the SSP scenarios. These factors are important because they provide scenarios of climate mitigation and adaptation actions that can be used to assess the impacts of human activities on climate change better (Lee *et al.,* 2021).

Presently, the CMIP6 SSP scenarios have not been explored for water balance assessment, and this study aims to fill this gap.

2.5 Water Balance Modelling in a Watershed

Limitations of measuring techniques and the variations in the temporal and spatial scales at which hydrological processes occur make the hydrological model crucial for understanding changes in the hydrology of an area (Beven, 2012). Hydrological modelling provides insights into the processes involved in water flow and projections for future scenarios, such as flood forecasting for early warning. Hydrological models have been developed for different aspects of water resources management. Challenges common to models is the inability to accurately mimic the physical properties of a watershed, due to uncertainties from the input data, model type, parameterization, and human errors (Cornelissen *et al.,* 2013).

2.5.1 Hydrological Model Types

Hydrological models vary based on their structure and functionality and thus, influence the outputs from water resource studies. Generally, hydrological models can be defined as Deterministic or Stochastic, based on their mathematical structure. Deterministic models have a unique input which leads to a unique output, while in Stochastic models the same input may lead to different outputs. Hydrological models are also defined by their ability to represent the physical characteristics of the basin: Physically-based models derive the hydrological processes using the principles of physics and thermodynamics, while Conceptual models simplify the processes in their derivation. Some quasi-physical models have a blend of physically-based and conceptual models. Furthermore, hydrological models can be referred to as Lumped, Distributed, or Semi-distributed according to their spatial complexity. Lumped models consider the watershed as a single homogeneous entity and use mean parameter values for simulating hydrological processes; distributed models consider the spatial distribution of variables and basin processes at a fine resolution (more detailed) (Paudel *et al.,* 2011). On the other hand, semi-distributed models divide the watershed into subunits (sub-basins) and treat each subunit as lumped (Hounkpè and Diekkrüger, 2018). Distributed models offer more detail but have potentially greater uncertainty due to higher complexity and require more input data and computation time compared to the lumped and semi-distributed models (Jajarmjzad *et al.,* 2012).

2.5.2 Hydrological Models Applied in West Africa

The Soil and Water Assessment Tool (SWAT) is a continuous semi-distributed small watershed to river-basin scale model used to simulate the quality and quantity of surface and groundwater and to predict the impact of land use and management practices, as well as climate change (Arnold *et al.,* 1998). SWAT was developed partly by the United States Department of Agriculture (USDA) Agricultural Research Service and the Texas A&M AgriLife Research. Minimum input data required to run the SWAT model include precipitation and temperature, soil, elevation and topography, and LULC data.

Another example of hydrological models used in West Africa is the "UHP-HRU Model, a spatially differentiated version of the UHP model" specifically designed for Benin (Cornelissen *et al.,* 2013; Giertz *et al.,* 2006) and the Water Flow and Balance Simulation Model (WaSiM), a spatially distributed model designed for water flow simulations above and below the land surface. Data requirements include meteorological (precipitation, temperature, etc.), LULC, and soil data in gridded format. It can also be used to conduct an impact assessment of climate and LULC change on hydrology (Schulla, 2014).

The "Water Evaluation and Planning System (WEAP)" Model (Höllemann *et al.,* 2010) is used to study transboundary water allocation in assessing water demand and availability. Other models include "Génie Rural à 4 Paramètres Journaliers" (GR4J) (Cornelissen *et al.,* 2013), 1-D SVAT model (Giertz *et al.,* 2006), HEC-HMS, to mention a few have also been used for hydrological modelling of watersheds in Africa. These models generally require rainfall data, temperature, land use, potential evapotranspiration, soil water retention capacity and topography, and discharge data (Nounangnonhou *et al.,* 2018). Artificial Intelligence (AI) methods such as Machine Learning (ML) techniques are also being introduced into hydrological modelling because it is capable of handling large datasets and learning patterns quickly. AI has been applied in soil and water quality assessments, which are usually challenging in inaccessible or data-scarce regions (Werther *et al.,* 2021; Al-Naji *et al.,* 2021).

In this study, SWAT was used because it can integrate physically-based processes with conceptual approaches (semi-distributed) to simplify complex hydrological processes in large river basins like the Ouémé River basin (Arnold *et al.,* 1998). It also incorporates uncertainty and sensitivity analysis of parameters affecting water flow in the separate SWAT-CUP tool, which makes calibration and validation efficient. SWAT has been applied and validated globally, including in West Africa. It is easily accessible with a user-friendly interface. SWAT inputs and outputs data formats are compatible with other software such as ArcGIS and QGIS, and programming languages like Python, thereby enabling efficient data transfer and analysis. Due to its continuous processing method, it requires continuous climate data and hydrological data such as discharge, which is challenging due to data scarcity in Africa. However, calibration and validation in the SWAT-CUP provide a way to successfully calibrate discharge with the available data while still accounting for missing data (Abbaspour, 2015).

2.6 Challenges in Water Balance Modelling and Assessment

2.6.1 Water Balance Modelling Challenges

Hydrological modelling provides valuable insights that enhance water resources management; however, there are challenges and uncertainties. One major challenge is the unavailability and/or inaccessibility of long-term, high-resolution observed data on variables, such as streamflow, precipitation and temperature, soil moisture, LULC, and evapotranspiration. Usually, the available data are inconsistent, attributable to faulty or outdated measuring equipment or human errors which affect the accuracy of the models. The introduction of remote sensing tools has provided ways to efficiently and accurately monitor environmental changes (Odusanya *et al.,* 2021). However, it is not without shortfalls such as spatial and temporal resolution constraints and biases, which also introduce uncertainties in the model when used. In cases where satellite data are combined with ground-truth observations, modelling accuracy is improved but does not eliminate the uncertainties (Bodjrènou *et al.,* 2023b).

Spatial and temporal resolutions play an important role in water balance assessment. Assessment at larger spatial scales like the regional scale can capture overall trends, but it often misses the details peculiar to localised water management. Additionally, long-term assessments may capture variations that short-term assessments may not, which could lead to better conclusions about water availability and stability.

2.6.2 Uncertainties in Water Balance Assessment

Uncertainties in hydrological modelling stem from uncertainties in the models themselves. In SWAT, for instance, the water balance simulation depends on assumptions that simplify the catchment characteristics, and this can introduce some errors (Bailey *et al.,* 2020). The sensitivity of the models to the quality of input data, particularly climate data, makes calibration and validation quite challenging especially in data-scarce areas. These issues are compounded by the unpredictable nature of climate and LULC changes, particularly in regions like West Africa where changes are occurring very rapidly. Climate models also vary in their assumptions about future emissions and trends of precipitation and temperature (Hayhoe *et al.,* 2017; Lawin *et al.,* 2019). Hence, these uncertainties make long-term projections of impacts on water balance more complex.

In this study, available data including climate, LULC, soil, and discharge were used to assess the impacts of LULC changes on water balance components such as baseflow, surface runoff, lateral flow, actual evapotranspiration and total aquifer recharge using the SWAT model. The simulation in SWAT was divided into three periods, 1998-2008, 2008-2016, and 1998-2016, to assess the effects of changes in LULC on water balance components over multiple periods assuming constant climate and soil data.

This is so that, any changes in water balance can be ascribed solely to LULC changes. The impact of future scenarios of changes in precipitation and air temperature patterns on water balance was evaluated using IPCC CMIP6 future climate model projections.

CHAPTER 3 MATERIALS AND METHODS

3.1 Introduction

This section outlines the data sources and methods used to assess the impacts of LULC changes and climate change on water balance in the Ouémé River Basin, Benin. The study area is first described, and then the classification of LULC types for different historical years is outlined. This is followed by water balance simulations using the LULC maps developed based on the classification. The subsequent sections focus on the projection of future LULC impact on water balance, future climate impacts on water balance, and the combined influence of projected future LULC and climate changes on water balance in the basin.

3.2 Study Area

The Ouémé River basin is situated between latitudes 6° 30’ N and 10° 00’ N, and longitudes 0° 52’ E and 3° 05’ E (Hiepe, 2008). It is the largest river basin in Benin, West Africa, covering about 43 % of the country’s land surface area. The basin spans a total area of 49,280 km^2 (at Bonou outlet), with 89 % of its area in Benin, and 10 % and 1 % in Nigeria and Togo, respectively (Hounkpè, 2016). The basin is bounded to the north by the Atakora Mountains and discharges into the Ouémé Delta and the Gulf of Guinea at Cotonou, with an average flow rate of 170 m^3/s. According to the Köppen climate classification, the Ouémé River Basin falls within the Tropical Savanna climate zone (Peel *et al.,* 2007).

The largest tributaries of the Ouémé River are the Okpara River on the east side which discharges into Lake Nokoué towards Cotonou and the Zou River on the west which discharges into the Porto-Novo Lagoon (Fig. 3.1). Gauged sub-catchment stations within the Oueme River Basin, include from the north Bétérou station, Kaboua, Affon-Pont, Donga-Pont, Térou-Igbomakoro, Vossa, Savè (Atchakpa), Zou (Atchérigbé), and Bonou stations (Hounkpè, 2016, p. 13; Bossa *et al.,* 2014, p. 3156; Bossa, 2016, p.6). Due to data unavailability and inconsistencies, the Bétérou and Bonou stations were used to calibrate and validate the hydrological modelling in SWAT.

The Bétérou outlet is within the Upper Ouémé with 14,400 km^2 sub-catchment area and elevations between 228 m and 617 m (Olofintoye *et al.,* 2022). Luvisols dominate that sub-catchment, and LULC consists of savanna areas, croplands, and urban areas. The Bonou outlet falls in the Lower Ouémé where streamflow from the Ouémé basin drains into the Ouémé Delta south of Bonou.

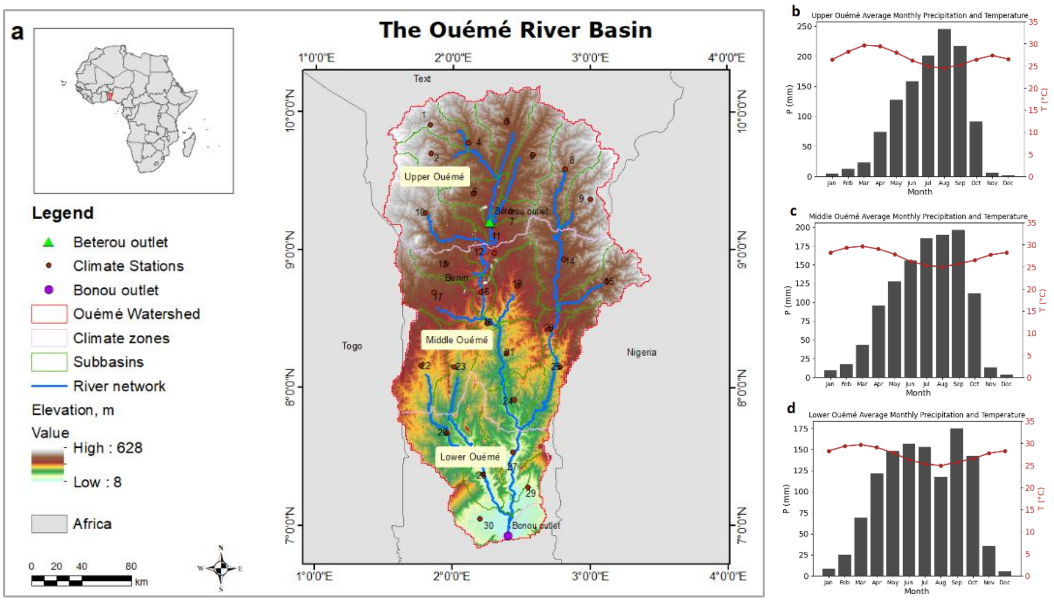

Figure 3.1: Elevation map (a) showing the river networks, climate stations, mean rainfall, and temperature (1998-2016) for the Upper (b), Middle (c), and Lower (d) parts of the Ouémé River Basin

3.2.1 Geology

The geology of Benin is primarily composed of two types of rocks: (1) sedimentary rocks, found in the coastal areas in the south (including a portion of the lower Ouémé River Basin), the Kandi, and Volta basins; and (2) metamorphic and crystalline rocks within the Dahomeyan basement, which covers most of the Ouémé River Basin (Hounkpèand Diekkrüger, 2018). Due to the solid and compact nature of the metamorphic and crystalline rocks, they have low permeability, which slows groundwater recharge. However, where fractures are present, they create pathways that enhance water infiltration (Bossa, 2012). The impermeable nature of these rocks results in increased surface runoff, particularly during heavy rainfall events, contributing to high peak river flows. As a result, baseflow is typically lower and more seasonal compared to sedimentary formations.

The eastern side of the Dahomeyan basement consists of a granite gneissic unit, characterized by amphibole-gneiss, biotite-gneiss, and syntectonic granites, which have a medium metamorphic gradient (Darko *et al.,* 2019). In contrast, the western side is composed of granulitic and aluminous gneiss, including aluminous gneiss with hypersthene, biotite-gneiss, and gneiss with pyroxenes, exhibiting a high metamorphic gradient. These variations in the metamorphic gradients and rock types across the eastern and western regions influence water movement, as the differing rock properties affect both surface and subsurface hydrology (Wright *et al.,* 1985).

3.2.2 Topography, Soil, and Hydrography of the Basin

The land surface of the Ouémé River Basin is predominantly characterized by high peneplains (upper and lower slopes), which are nearly flat surfaces formed through prolonged soil erosion (Bossa, 2012). This history of erosion shapes the soil properties, which in turn strongly influence the basin's hydrology. Tropical Ferruginous Soils (*Ferrugineux Tropical Lessive*) which extend from the centre to the northern parts of the basin are the dominant soil type (Fig. 3.2). These soils are formed through clay translocation and iron segregation, processes that promote horizon differentiation after earlier ferricretes were eroded (Faure and Volkoff, 1998). The ferruginous soils, particularly in the lower slope areas, are leached and indurated. Hydrologically, these soils tend to have reduced infiltration capacity due to their hardened layers, promoting surface runoff and increasing erosion risk. The inland valleys where Gleysols (hydromorphic soils) dominate have higher water retention, which supports groundwater recharge but may become waterlogged in some areas. This can influence streamflow dynamics and wetland formation in these valleys. Generally, Ferric Acrisols/Lixisols are present on the upper slopes (Bossa *et al.,* 2014) with lower fertility, typically exhibiting moderate infiltration capacities, which can reduce runoff and promote subsurface flow. However, during intense rainfall events, these soils may contribute to lateral flow and baseflow into streams, influencing the basin's hydrological processes. Ferrallitic soils are found in the southern parts of the basin on the coastal sedimentary rocks as 'Terre de Barre' and inland on some parts of the

Dahomeyan crystalline basement. These soils are highly weathered and kaolinitic, rich in sesquioxides, and deep and sandy to loamy Acrisols (Faure and Volkoff, 1998). The ferrallitic soils, while having a high porosity, are often associated with lower nutrient retention due to leaching. Hydrologically, they support infiltration and groundwater recharge, though, in regions where the texture becomes finer within the soil profile, surface runoff may increase due to reduced permeability. These provide insights into the spatial diversity in hydrological characteristics in the basin due to variations in soil properties across the basin.

The landscape of the coastal sedimentary basin which contains the lower part of the Ouémé River Basin is tabular with low plateaus, and the hydrographic networks are widely spaced. The crystalline Dahomenyan basement is drained mainly by the Ouémé river southwards and rivers leading to the Niger River northwards. The upper portion of the Ouémé River Basin is characterized by steep convex slopes and lowering of thalwegs. The land surface of the basin is slightly undulating with generally low relief, strongly fractured with seasonally waterlogged linear depressions (Bossa, 2012; Faure and Volkoff, 1998).

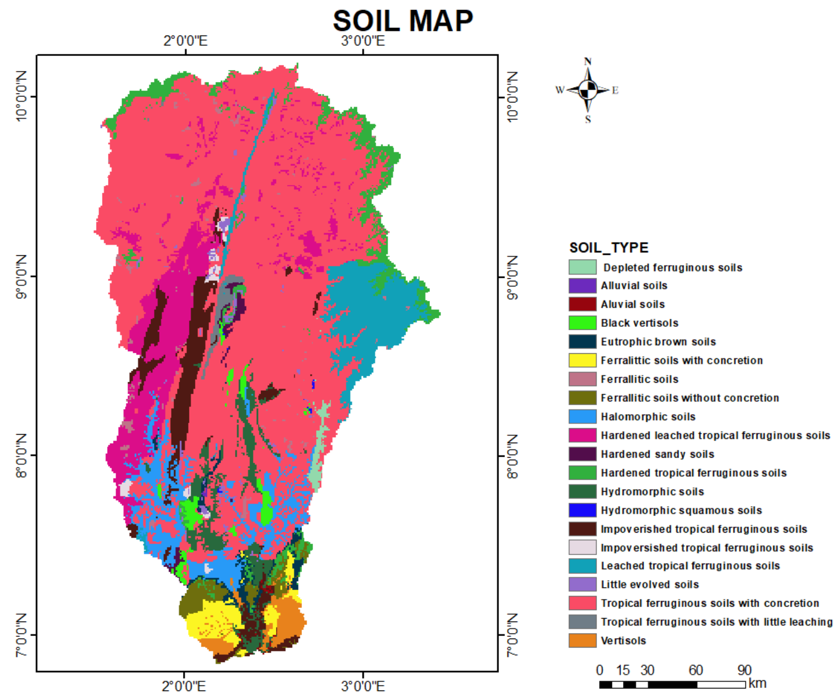

Figure 3.2: Soils found in the Ouémé Basin
(*Source: van Engelen and Ting-tiang, 1993*)

3.2.3 Climate

The Ouémé Basin has two main seasons, namely, the wet and dry seasons. The south, within the Guinean agroecological zone has a bimodal rainfall regime with two wet and two dry seasons, a short dry season during August, and a longer dry season from November to March. However, in the north, there is a single wet season from April to September and a dry season that ranges from October to March (Faure and Volkoff, 1998). The annual rainfall ranges from 900 mm to 1400 mm (from 1998 to 2016) and the mean temperature is between 25 °C and 30 °C (Olofintoye *et al.,* 2022) (Fig. 3.1). The central part (Middle Ouémé) exhibits characteristics of the Upper and Lower Ouémé (transitional regime), with rainfall amounts from April to June higher than those in Upper Ouémé but less than that in Lower part. However, according to (Faure and Volkoff, 1998), "Benin has four bioclimatic zones, namely; (1) a littoral humid tropical zone (1200 to1400 mm of annual rainfall), (ii) a littoral and inland subhumid zone (900 to 1200 mm annual rainfall), (iii) a wetter inland zone (1200 to 1400 mm of annual rainfall), and (iv) a continental dry northern zone (1200 to 900 mm of annual rainfall)" (Faure and Volkoff, 1998).

There are four National climate stations within the Ouémé River Basin located at Parakou, Bohicon, Djougou and Savè (Atchapkpa) and about twenty-four rainfall stations (Bossa *et al.*, 2014, p. 3156) scattered over the basin with a higher cluster in the north-west due to the establishment of the AMMA-CATCH observatory site. Missing data, equipment malfunction and inadequacies of long-term observed data that are uniform across the stations influenced the selection of the gridded rainfall data (Rauch et al., 2024) sourced from the Karlsruhe Surface Database (KASS-D) and the West African Historical Precipitation Database (WAHPD) based on observation data (89 stations in total) and geostatistical modelling for the Oueme River Basin. This data has been successfully utilised for studies in the basin and West Africa (Merk *et al.*, 2024; Bliefernicht *et al.*, 2022). The period 1998-2016 was selected due to its alignment with the baseline period (1995-2014) for the climate change analysis and data availability to the researcher.

3.2.4 Vegetation

The Ouémé River Basin lies mainly within the littoral and inland subhumid zone and a smaller portion of the wetter inland zone. The landscape in the Ouémé River Basin is made up of forests (including riparian), woodlands and savannas, agricultural landscapes, and degraded lands (Bossa *et al.,* 2014; Bodjrènou *et al.,* 2023a). The southern part of the basin is dominated by semi-deciduous tropical forests, with a mix of evergreen and deciduous tree species. These forests thrive in areas with higher rainfall and relatively fertile ferrallitic soils, which are leached but retain moisture and nutrients necessary for dense vegetation. Common tree species found in the basin include; African Mahogany (*Khaya senegalensis*), African Whitewood (*Triplochiton scleroxylon*), and Shinglewood (*Terminalia superba*) (Lokono *et al.,* 2017). These forests contribute significantly to carbon sequestration and biodiversity conservation (Wheeler *et al.*, 2016), and thereby regulation of local microclimates. However, deforestation due to agricultural expansion and settlement growth is a pressing issue in the southern zones. Northward, vegetation transitions into savanna ecosystems, which dominate the middle and north of the basin. These areas are characterized by wooded savannas and tree savannas, with sparse tree cover interspersed with grasses and shrubs. Species such as the Shea tree (*Vitellaria paradoxa*), African Locust Bean (*Parkia biglobosa*), and African Copaiba Balsam tree (*Daniellia oliveri*) are common in the wooded savannas (Lokonon *et al.,* 2018). The savanna regions are supported by the less fertile ferruginous soils, which are more prone to soil erosion, but still capable of supporting these drought-tolerant species. The savanna vegetation plays an important role in livestock grazing and subsistence farming, though it is highly vulnerable to land degradation from overgrazing and shifting cultivation. Riparian zones along the Ouémé River and its tributaries feature gallery forests and wetland vegetation. The inland valleys support dense grasslands and seasonally flooded wetlands that provide important ecosystem services, including flood regulation, water purification, and habitats for wildlife. The middle and upper parts of the basin have been converted into agricultural lands, primarily for subsistence farming of crops such as maize (*Zea mays*), yams (*Dioscorea spp.*), and cassava (*Manihot esculenta*). Tree and crop plantations including cotton, cashew, cowpea, soybean, and oil palm are also present in this region (Dossou *et al.,* 2021a). The expansion of agriculture has replaced native savanna vegetation, leading to soil degradation and loss of biodiversity. In some areas, particularly near settlements and in over-exploited lands, the vegetation is sparse, consisting of degraded woodlands and shrublands. These areas, often referred to as fallow lands or bare lands, are increasingly vulnerable to erosion and loss of productivity.

3.3 Spatio-temporal Changes in LULC

3.3.1 Data Sources

Data for the LULC classification based on data quality, availability, accessibility and the ability to provide substantive information on LULC changes were selected (Fig. 3.3). Four Landsat images of the basin from the dry season of the years 1986, 2000, 2015 and 2023 were sourced from the USGS database in Google Earth Engine (GEE) (Table 3.1). The period selection was guided by the need for a balance between capturing significant temporal changes in LULC, and the availability of high-quality satellite images. Though a 15-year interval was initially planned, constraints in image quality (for instance years before 1986) and accessibility necessitated some adjustments. The years 2000 and 2015 correspond with the establishment of the Millennium Development Goals (MDGs) and the Sustainable Development Goals (SDGs), respectively, which are significant efforts towards achieving environmental sustainability. The 2023 also ensured that the most current state of LULC was incorporated to improve the relevance of the study for current and future planning.

Google Earth Engine is a cloud computing system with a host of satellite imagery that covers various aspects of earth observation assessments. Images were selected from 1st January to 31st March, and extended to 30th April where the image quality was insufficient. These dry season images have less cloud cover compared to the rainy season. A high percentage of cloud cover over the image obscures details on the images and affects the accuracy values obtained during classification. Therefore, images with lower cloud cover are recommended to improve accuracy in LULC classification.

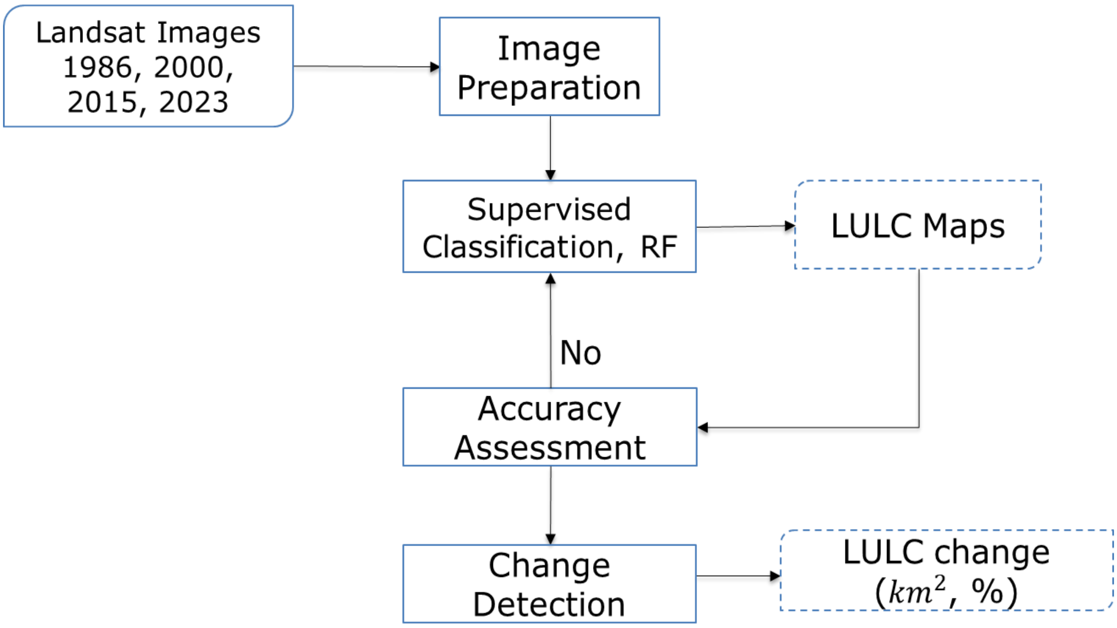

Figure 3.3: LULC Classification Workflow

The GEE cloud computing database enables faster data analyses through cloud processing and in-built algorithms, which made assessing LULC changes in the large Ouémé River Basin faster and more efficient (Noi Phan *et al.,* 2020). GEE also integrates various datasets with varying resolutions, which are updated from time to time.

Table 3.1: Satellite Data Applied in the LULC Classification

Year	LULC Data Used	Resolution	Number of Images	Month
1986	Landsat 5 TM	30 m	27	1st January – 30th April
2000	Landsat 7 ETM+	30 m	23	1st January – 30th April
2015	Landsat 8 OLI/TIRS	30 m	55	1st January – 31st March
2023	Landsat 8 OLI/TIRS	30 m	57	1st January – 31st March

3.3.2 Data Composition

The composition of time series images is an important step in LULC classification. The "Simple-Composite Landsat" algorithm is available in GEE (Qiu *et al.,* 2023). This algorithm uses the Tier 1 Landsat images which are radiometrically and geometrically corrected and selects a subset from each location, converting them to Top of Atmosphere (TOA) reflectance using Equation 3.1 and 3.2 for Landsat 5TM/7 ETM+ (Chander *et al.,* 2009) and Landsat 8 OLI/TIRS (US Geological Survey, 2019), respectively. The algorithm selects the lowest range of cloud and shadow percentages at each point and uses the "Simple Landsat Cloud Score" algorithm to calculate the median of the least cloudy pixels (Tassi and Vizzari, 2020).

This Simple-Composite Landsat algorithm retains the spatial and spectral fidelity of the input images, which is important in LULC change detection and can be challenging when compositing with the surface reflectance (SR) images where data gaps are created during cloud-masking. The algorithm has proven to enhance the effective compositing of Landsat images and yield high mapping accuracy values (Qiu *et al.,* 2023; Xie *et al.,* 2019).

$$\rho_\lambda = \frac{\pi L_\lambda d^2}{ESUN_\lambda \cos\theta_s} \qquad [3.1]$$

$$\rho_\lambda = \frac{M_\rho Q_{cal} + A_\rho}{\sin(\theta_s)} \qquad [3.2]$$

Where;

$\rho_\lambda =$ Planetary TOA reflectance [unitless]

$\pi =$ Mathematical constant equal to approximately 3.14159 [unitless]

$L_\lambda =$ Spectral radiance at the sensor's aperture $[W/(m^2 sr \mu m)]$

$ESUN_\lambda =$ Mean exoatmospheric solar irradiance $[W/(m^2 \mu m)]$

$\theta_s =$ Solar zenith angle [degrees]

$M_\rho =$ Band-specific multiplicative rescaling factor from the metadata

$Q_{cal} =$ Quantized and calibrated standard product pixel values (DN)

$A_\rho =$ Band-specific additive rescaling factor from the metadata

Therefore, the code for input in GEE for image composition requires;

i. Image Collection (e.g., Landsat 5 TM Tier 1 scenes)

ii. Region of interest (roi) which is a shapefile of the study area
iii. Period of interest (e.g., 1986-01-01 to 1986-03-31)
iv. Select input bands of interest

3.3.3 LULC Classification

A stratified random sampling method was used to select training samples (data) by polygons for the LULC types, and training data for each LULC type was collected randomly according to the proportion of the image covered by the LULC types, as recommended in LULC classification (Olofsson *et al.,* 2014). Polygons were used instead of point to enable uniform collection of pixel data on LULC types, considering the large size of the basin. These training data, also referred to as ground-truth data or reference data were collected from Google Earth Pro, field visit, and GEE base maps, following the good practices for LULC change assessment outlined by Olofsson *et al.* (2014). The ground-truth polygons were first collected for the most current year, 2023, through field visits to the study area and the high-resolution satellite layer of Google Maps using the Google Earth Pro interface. Then the 'historical imagery' tool in Google Earth Pro was used to visualise land surface maps from historical years, which helped in collecting reference data for 1986, 2000, and 2015. These sets of training data were imported into GEE and superimposed as a shapefile onto the composited Landsat images, and using their spectral characteristics through indices and visual interpretation of the land features, more training samples were collected in GEE per image. In all, a total of 1471 training samples (Table 3.2) were collected throughout the basin for the four images (1986, 2000, 2015, and 2023).

The next step in the classification process is training (the main classification) and validation (used for accuracy assessment). Seventy percent (70 %) of the total samples per year was used for training while 30 % was used for validation. The variable 'count' was applied to the algorithm to determine the number of images sampled for compositing in each year. To ensure higher accuracy of classification of features in the raster images, auxiliary variables including NDVI and BSI (Bare Soil Index) were computed for the composite images of each time step and added to the image band set (Polykretis *et al.,* 2020; Tassi and Vizzari, 2020).

Table 3.2: Training Samples used for the LULC Classification

Year	Total Number of Sample Polygons per LULC Class				
	Forest	Settlement/Bare land	Savanna	Agriculture	Water
1986	68	57	44	86	36
2000	39	44	56	89	21
2015	89	82	92	253	33
2023	34	46	73	197	32

Five LULC classes (Table 3.3) were selected based on the FAO West African Land Cover Reference System (Di Gregorio *et al.,* 2022), representing key ecosystems in West Africa: Forest areas, Savannas, Agricultural lands, Settlements/bare lands, and Water bodies. These classes were derived by re-grouping commonly used LULC classes in the basin, such as those from the RIVERTWIN project (Bossa, 2012), which includes classifications like Gallery forest, Humid forest, and Dry dense forest. The selected classes also reflect the natural and human-induced changes that influence the hydrological cycle. The Forests play a significant role in evapotranspiration, retain soil moisture, reduce surface runoff and enhance groundwater recharge. Savannas serve as transitional zones with moderate water balance effects. Agricultural lands increase surface runoff and reduce infiltration, while settlements/bare lands lead to higher runoff and more extreme hydrological responses.

In GEE, the Random Forest algorithm was used to perform a supervised classification to categorize the land surface features of the four composited images into the five different LULC classes. The ecosystem within the Ouémé River Basin consisted mostly of a mixture of LULC types per area, where settlement areas were interspersed with farmlands, trees, plantations, and business centres, making it complex to map. The Random Forest Classifier can handle high-dimension data with complex interactions between variables, although it is sensitive to errors in the input data (Hengle *et al.,* 2015). Moreover, it has been proven to yield higher accuracy in land cover mapping and projections in Africa and many other parts of the world (Xie *et al.*, 2019). The classification step therefore requires;

- a composited image
- feature collection containing training/validation polygons collected for each LULC class and given the same property name and specify percentage for training and validation.
- the output bands of interest (e.g., Landsat 5 bands, NDVI, BSI)
- extract confusion matrices of the training and validation
- Output folder to export classified map (e.g., google drive).

Table 3.3: Description of LULC Classes in the Ouémé River Basin

LULC Type	Description
Forest areas	Areas with dense trees (including riparian forests) are mostly classified as forests.
Settlements/Bare lands	Cities, roads, bare (cleared) areas, towns.
Savanna areas (Woodlands)	Areas with sparse trees interspersed with grass, shrubs, and bushes. .
Agricultural lands	Croplands, plantations, fallow lands.
Water bodies	Rivers, lakes, wetlands, and areas covered with water for all or most of the year.

3.3.4 Classification Accuracy Assessment

For each LULC map classified per year, a cross-tabulation matrix, also known as confusion or error matrix of the validation samples in pixels was extracted from GEE and used to assess how well the classified maps depict the reality on the ground. General summary statistics for classification accuracy assessments include overall accuracy (OA), producer's accuracy (PA), user's accuracy (UA), and kappa statistics. Recently, the kappa statistic has been found insufficient in explaining LULC change, therefore, two other indices, quantity and allocation disagreement which are recommended were also used. Overall accuracy values greater than 85 % are generally considered indicative of strong to almost perfect agreement between the reference and predicted categories (García-Álvarez *et al.,* 2022).

Additionally, area-based statistics, recommended to address uncertainties and biases that could arise from the sampling and classification process, were conducted (Olofsson *et al.,* 2014). This area-based analysis intends to incorporate the standard error based on the total area of each LULC class. This way, the producer's and user's accuracies are assessed based on the map data and not just the validation data (30 % of training samples). Accuracy was determined at the category scale (per each LULC class) and for the overall classified image. The original confusion matrix from the validation step was converted into an area-based matrix representing the entire study area to compute unbiased area-based summary statistics of the classified image using Card's equations (Olofsson *et al.,* 2014; Pontius Jr and Millones, 2011). This method involves calculating the area proportion from stratum weight, W_i of the predicted map, based on which the area-based summary statistics are recalculated. These statistics include the percentages of omission and commission errors quantified by the user and producer accuracies, respectively, standard error of area estimates, and corrected area estimates with 95 % confidence to account for uncertainty. Equations used for these computations accessed from the NASA Applied Remote Sensing Training Program (NASA- Applied Remote Sensing Training Program, 2018) are presented in Appendix 1.

Quantity disagreement represents the difference between the classified map and validation data due to imperfections in the proportions of the categories, calculated as the difference between omission and commission errors (sum of the proportion of the category in the classified map minus the sum of the proportion of the category in the reference from the error matrix) (Pontius Jr and Millones, 2011). Allocation disagreement is the differences arising from mismatches in the spatial locations of the categories, expressed as "the sum of exchange (pairwise) and shift (non-pairwise) confusion between categories" (Obodai *et al.,* 2019).

3.3.5 Change Detection

Once the classification accuracy was within acceptable ranges, the absolute magnitude of change in the area of the different LULC classes, their relative changes between the years, and the rate of change were estimated. The change detection was conducted using the "post-classification" tool under "Land Cover Change" within the Semi-Automatic Classification Plugin (SCP) in the QGIS interface. This step develops a change map that illustrates the changes in the LULC types between two time points, and a change matrix that indicates the transitions and/or persistence of the LULC types. The following Equations (3.3, 3.4, 3.5) were used to calculate the magnitude of change (km^2), the annual rate of change (%) and relative change (%) from the change matrices (García-Álvarez *et al.,* 2022; Puyravaud, 2003). LULC maps were created using ArcGIS and QGIS software.

$$\text{Absolute change, AC} = A_2 - A_1\ (km^2) \qquad [3.3]$$

$$\text{Relative change, RC} = \frac{A_2 - A_1}{A_1}\ (\%) \qquad [3.4]$$

$$\text{Rate of Change, q} = \left(\frac{A_2}{A_1}\right)^{\frac{1}{t_2 - t_1}} - 1\ (\%/y) \qquad [3.5]$$

Where A_2 is the area of the LULC in the year t_2, and A_1 is the area in the year t_1.

The transition intensities were also generated for each land category between the LULC maps years (1986-2000, 2000-2015, 2015-2023) which tells the demand for the categories and which ones are more susceptible to change (Pontius Jr, 2022). The uniform transition intensity is calculated as the sum of the losses/gains over a period (Equation 3.6 and 3.7). The transition intensity analysis reveals how the LULC types change between the years (Equation 3.8 and 3.9). An active transition depicts a higher rate of change in the LULC category greater than the overall rate of LULC change in the basin (uniform transition intensity), while a dormant category transition has a rate of change lower than the uniform transition intensity for that period (Pontius Jr, 2022; Aldwaik and Pontius Jr, 2012).

$$\text{Gain} = \text{Total area of category}_{\mathbf{map2}}\ (\%) - \text{area of category persistent}\ (\%) \qquad [3.6]$$

$$\text{Loss} = \text{Total area of category}_{\mathbf{map1}}\ (\%) - \text{area of category persistent}\ (\%) \qquad [3.7]$$

$$\text{Gain intensity}\ (\%) = \left(\frac{\text{Gain}}{\text{Total area of category}_{\text{map2}}}\right) \times 10 \qquad [3.8]$$

$$\text{Loss intensity (\%)} = \left(\frac{\text{Loss}}{\text{Total area of category}_{\text{map1}}}\right) \times 100 \qquad [3.9]$$

3.4 Modelling Water Balance Based on Historical LULC in the Basin

In this section, water balance was simulated using the four LULC maps developed in Objective 1 in the Soil and Water Assessment Tool (SWAT) hydrological model. Afterwards, the absolute areas of the LULC types across the different maps were regressed against the absolute amounts of average surface runoff, lateral flow, baseflow, total aquifer recharge, and actual evapotranspiration to examine the relationships between them, and the direction of those relationships.

3.4.1 SWAT Model Set-up

The SWAT model is a continuous semi-distributed river basin simulation model, quasi-physically based in nature, developed for the prediction of the long-term impact of land management decisions on water, sediment, and agricultural chemicals in watersheds (Arnold *et al.,* 1998). In SWAT, the catchment is first divided into sub-basins based on topography, and then into Hydrologic Response Units (HRUs), which SWAT uses to simulate loadings from the catchment (Arnold *et al.,* 1998) (Fig. 3.4).

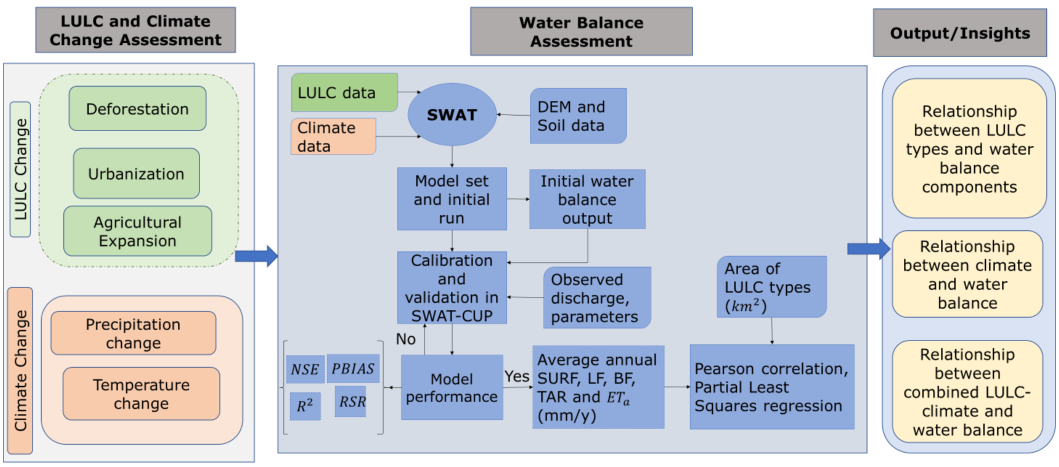

Figure 3.4: Conceptual Framework of the Study[1]

[1] surface runoff (*SURF*), lateral flow (*LF*), baseflow (*BF*), total aquifer recharge (*TAR*) and actual evapotranspiration (ET_a). Nash-Sutcliffe Efficiency (NSE), Percent Bias (PBIAS), Coefficient of Determine (R^2), RMSE-observations Standard Deviation Ratio (*RSR*)

An HRU refers to the total area in a subbasin with a particular LULC, management, and soil, capturing the diversity of LULC and soils in the sub-basins. Loadings from each HRU are calculated separately and summed to obtain the total sub-basin loadings. Thresholds of LULC, soil, and slope are used to define HRUs (Her *et al.,* 2015) which are used to generate parameter characteristics for the sub-basins, such as surface runoff curve numbers and saturated hydraulic conductivity for water balance simulations. Using threshold values of 2 % LULC type, 10 % soil type, and 20 % slope levels in defining HRUs provided an effective balance between model detail and computational efficiency in this study. The lower LULC threshold enables finer differentiation among areas reflecting the dynamic nature of LULC changes over time, which is a primary focus of this analysis, in contrast to soil and slope, which are relatively stable over time in the basin. Due to the nearly flat terrain characteristic of the basin landscape, three slope divisions were used for the SWAT model setup namely, 0-5 %, 5-10 %, and above 10 %. Daily temperature and precipitation data from 1998-2016 were the climate input (Table 3.4).

Table 3.4: Datasets Applied in this Study

Sn.	Data Type	Source	Resolution
1.	DEM (Digital Elevation Model	SRTM (Shuttle Radar Topography Mission)	30m
2.	Land Cover Maps	Specific Objective 1	30m
3	Daily precipitation and temperature (1998-2016)	ERA 5 reanalysis, (Rauch *et al.,* (2024)	
4.	Soil map	FAO soil database	1km
	Measured discharge	DGEau[2], Benin	

3.4.2 Hydrology

SWAT generates hydrological components using the water balance Equation 3.10, as shown in Fig. 3.5. It predicts runoff from the basin outlet by predicting the sub-basins and routing to the channel (Neitsch *et al.*, 2011).

$$SW_t = SW_0 + \sum_{i-1}^{t}\left(R_{day} - Q_{surf} - ET_a - w_{seep} - Q_{gw}\right) \qquad [3.10]$$

Where:

[2] DGEau – Direction Générale de l'Eau

SW_t is the final soil water content (mm H_2O)

SW_0 is the initial soil water content (mm H_2O)

R_{day} is the amount of precipitation on day i (mm H_2O)

Q_{surf} is surface runoff on day i (mm H_2O)

ET_a is actual evapotranspiration on day i (mm H_2O)

w_{seep} is the amount of water entering the vadose zone on day i (mm H_2O)

Q_{gw} is the amount of return (interflow) flow on day i (mm H_2O)

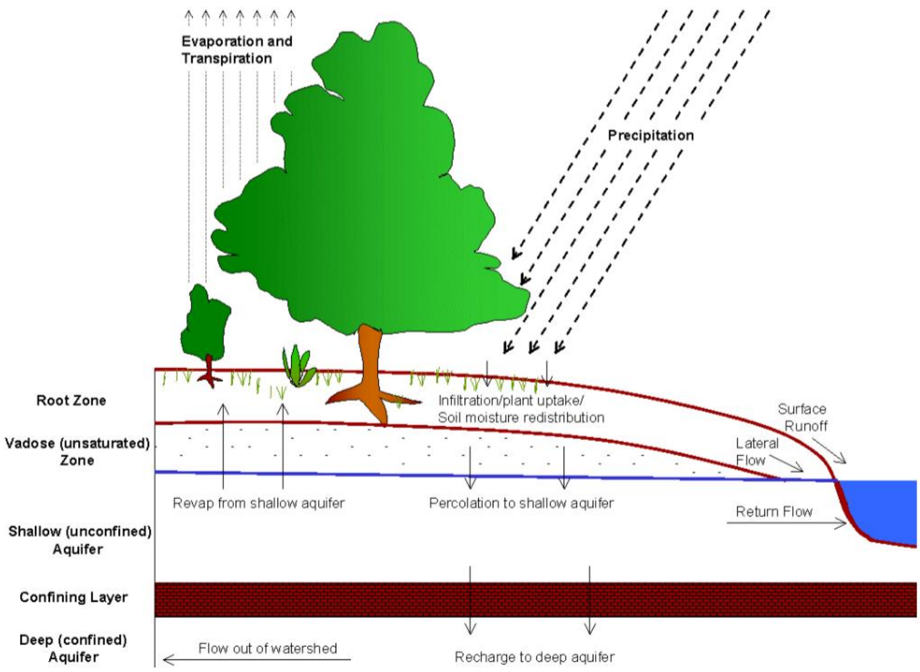

Figure 3.5: Schematic Hydrological Cycle in the SWAT Model
(*Source: Neitsch et al., 2011)*

3.4.2.1 *Surface Runoff*

Surface runoff is the flow that occurs along a slope whenever the rate of water application to the ground surface exceeds the infiltration rate. In SWAT, surface runoff can be estimated by either the modified Soil Conservation Service (SCS) curve number method (Equation 3.11) or the Green and Ampt infiltration method (Green and Ampt, 1911). To use the latter, hourly rainfall is required, but the SCS curve number method can be run with daily rainfall, hence it was employed in this study (Neitsch *et al.,* 2011). In this method, surface runoff is calculated as a function of initial abstraction and retention parameters in addition to daily rainfall as follows:

$$Q_{surf} = \frac{(R_{day} - I_a)^2}{(R_{day} - I_a + S)} \quad [3.11]$$

Where:

Q_{SURF} is surface runoff (mm H_2O)

R_{day} is rainfall for the day (mm H_2O)

S is the retention parameter (mm H_2O),

I_a is initial abstractions (mm H_2O) including surface storage, infiltration before runoff, and canopy storage, expressed as $0.2S$.

Daily curve number based on land use, soil, and antecedent moisture characteristics (Neitsch *et al.,* 2002) is used to estimate the retention parameter (Equation 3.12).

$$S = \left(\frac{25400}{CN}\right) - 254 \quad [3.12]$$

CN is the curve number, ranging from 30 to 100, and represents runoff potential for different land uses, hydrological soil groups and antecedent moisture conditions. Lower CN values correspond to lower runoff potential and vice versa. The CN values defined for the LULC types and soil hydrologic groups from SWAT and FAO soil databases are presented as follows:

Table 3.5: Calibrated CN values Applied in the Study

LULC type	SWAT name	Soil hydrologic group			
		A	B	C	D
Forest areas	FRSD	31	59	72	79
Settlements/bare lands	URBN	67	77	83	87
Savanna areas	RNGB	39	61	74	80
Agricultural lands	AGRL	45	#	77	83

SWAT calculates the time of concentration (where it takes longer than a day for runoff from a large sub-basin to get to the outlet from the beginning of a rainfall event) using the sub-basin slope length and channel velocity. SWAT includes a surface runoff storage (lag) feature to control the total amount of the surface runoff entering the main channel on any one day, denoted as surlag (Equation. 3.13). For a given time of concentration, more water is held in storage as surlag decreases, which smooths the streamflow hydrograph simulated.

$$Q_{surf} = \left(Q'_{surf} + Q_{stor,i-1}\right)\left(1 - e^{\frac{-surlag}{t_{con}}}\right) \qquad [3.13]$$

Where:

Q_{surf} is surface runoff entering the main channel on a given day (mm H_2O)

Q'_{surf} is surface runoff generated in the sub-basin on a day (mm H_2O)

$Q_{stor,i-1}$ is surface runoff lagged (stored) from the previous day (mm H_2O)

Surlag is surface runoff lag coefficient.

SWAT also estimates the maximum runoff flow rate that occurs during a rainfall event (peak runoff) which is indicative of the erosive power of a storm and is used to predict sediment loss using the Modified Rational formula (Neitsch *et al.,* 2011) (Equation. 3.14).

Peak runoff, $q_{peak} = \frac{\alpha_{tc} \cdot Q_{surf} \cdot Area}{3.6 \cdot t_{conc}}$. [3.14]

Where:

α_{tc} is fraction of daily rainfall occurring during the time of concentration

Q_{surf} is surface runoff (mm H_2O)

Area is area of sub-basin (km^2)

t_{conc} is time of concentration for the sub-basin and 3.6 is a conversion factor

3.4.2.2 *Lateral Flow*

Lateral flow occurs along the slope below the surface (above the groundwater table). SWAT calculates lateral flow (Equation. 3.15) using the Kinematic Storage model (Sloan and Moore, 1984) with saturated hydraulic conductivity, soil slope, hill slope length, and drainable volume of water as follows:

$$Q_{lat} = 24 \cdot H_o \cdot V_{lat} = 0.024 \cdot \left(\frac{2 \cdot SW_{ly,excess} \cdot K_{sat} \cdot slp}{\emptyset_d \cdot L_{hill}}\right) \qquad [3.15]$$

Where:

Q_{lat} is lateral flow (mm/d)

H_o is the saturated thickness normal to the hillslope at the outlet expressed as a fraction of the total thickness (mm/mm)

V_{lat} is the velocity of flow at the outlet (mm/h)

$SW_{ly,excess}$ is the drainable volume of water (mm H_2O)

K_{sat} is the saturated hydraulic conductivity (mm/h)

Slp is slope (m/m)

$\emptyset_d$ is drainable porosity (mm/mm)

L_{hill} is hill slope length (m)

A lateral flow storage feature lags a portion of the lateral entering to the main channel when the t_{conc} > a day.

3.4.2.3 *Groundwater Flow and Storage*

An aquifer is a geologic unit that can store and transmit water easily. An aquifer can be confined (bounded above and below by a geologic formation with a lower hydraulic conductivity compared to an aquifer) or unconfined (bounded above by the water table). SWAT simulates in each sub-basin an unconfined aquifer (shallow aquifer) which contributes to baseflow entering the main channel with the sub-basin and a confined aquifer (deep aquifer) which may contribute to streamflow outside the basin (Neitsch *et al.,* 2011). The unconfined aquifer is recharged through percolation to the water table, while the confined is recharged from the land surface upstream end where the aquifer is exposed to the water table. Groundwater storage loses water mainly by discharge into water bodies (rivers and lakes), or upward movement from the water table into the capillary fringe (a saturated zone above the water table). Water balance in the shallow aquifer is determined from recharge through percolation and reductions through baseflow, seepage into the deep aquifer, and upward flow into the soil

(W_{revap}) or withdrawal through wells and boreholes (Equation 3.16). SWAT calculates the fraction of baseflow with a baseflow recession constant as shown in Equation 3.17 and 3.18. SWAT also calculates the water balance in the deep aquifer using Equation 3.19, and the amount of water that enters the soil zone during water deficiencies using Equation 3.20.

$$aq_{sh,i} = aq_{sh,i-1} + W_{rchrg,sh} - Q_{gw,i} - W_{revap} - W_{deep} - W_{pump,sh} \qquad [3.16]$$

Where:

$aq_{sh,i-1}$ is the amount of water stored in the shallow aquifer on day i (mm H_2O)

$aq_{sh,i-1}$ is the amount of water stored in the shallow aquifer on day $i - 1$ (mm H_2O)

$W_{rchrg,sh}$ is the amount of recharge entering the shallow aquifer on day i (mm H_2O)

$Q_{gw,i}$ is baseflow or groundwater flow into the main channel on day i (mm H_2O)

W_{revap} is amount of water moving into the soil zone in response to water deficiencies on day i (mm H_2O)

W_{deep} is the amount of water percolating from the shallow aquifer into the deep aquifer on day i (mm H_2O) calculated using a percolation coefficient

$W_{pump,sh}$ is the amount of water removed from the shallow aquifer by pumping or withdrawals on day i (mm H_2O)

Equation 3.17 and 3.18 are used to calculate groundwater or baseflow in the main channel.

$$Q_{gw,i} = Q_{gw,i-1} \cdot e^{-\alpha_{gw} \cdot \Delta t} + W_{rchrg,sh} \cdot (1 - e^{-\alpha_{gw} \cdot \Delta t}), \text{ if } aq_{sh,i} > aq_{shthr,q} \qquad [3.17]$$

$$Q_{gw,i} = 0, \qquad \text{if } aq_{sh,i} \leq aq_{shthr,q} \qquad [3.18]$$

$Q_{gw,i-1}$ is baseflow into the main channel on day $i - 1$ (mm H_2O)

α_{gw} is the baseflow recession constant

$aq_{shthr,q}$ is the threshold water level in the shallow aquifer for groundwater flow to the main channel to occur mm H_2O

Δt is time step (1 day)

The water balance for the deep aquifer is expressed as:

$$aq_{dp,i} = aq_{dp,i-1} + W_{deep} - W_{pump,dp} \quad [3.19]$$

Where:

$aq_{dp,i}$ is the amount of water stored in the deep aquifer on day i (mm H_2O)

$aq_{dp,i-1}$ is the amount of water stored in the deep aquifer on day $i - 1$ (mm H_2O)

$W_{pump,dp}$ is the amount of water removed from the deep aquifer by pumping on day i (mm H_2O)

During soil water deficiencies, water entering the vadose zone is calculated as:

$$W_{revap} = \beta_{rev} \cdot E_o \quad [3.20]$$

3.4.2.4 *Potential Evapotranspiration*

There are four methods SWAT provides for calculating evapotranspiration in the basin. These are the Priestley-Taylor method (Priestley and Taylor, 1972), Penman/Monteith method (Monteith, 1965; Allen *et al.,* 1989), Hargreaves method (Hargreaves and Samani, 1985), and the 'read in' method where calculated potential evapotranspiration using other methods aside those as mentioned earlier can be inputted into SWAT. Generally, potential evapotranspiration represents the amount of water transpired by a short crop of uniform height, completely shading the ground with an unlimited water supply (Kirkham, 2005). The Penman-Monteith method combines components such as the latent heat flux density, slope of saturation vapour pressure-temperature curve, canopy resistance, net radiation, and air, and water vapour pressure. The Priestly-Taylor method is suitable for estimating potential evapotranspiration in low advective conditions and is known to underestimate PET in semi-arid and arid areas.

Due to data scarcity in the study region, the Hargreaves method for estimating Potential Evapotranspiration (PET) was applied (Hargreaves and Samani, 1985). This method requires maximum and minimum air temperature for a given day and extraterrestrial radiation (Equation 3.21) (Arnold *et al.,* 1998).

$$\lambda E_o = 0.0023 \cdot H_0 \cdot (T_{mx} - T_{mn})^{0.5} \cdot (T_{av} + 17.8) \qquad [3.21]$$

Where:

λ is the latent heat of vaporization (MJ/kg)

E_o is the potential evapotranspiration (mm/d)

H_0 is the extraterrestrial radiation (MJ/m^2d)

T_{mx} is the maximum air temperature for a given day (°C)

T_{mn} is the minimum air temperature for a given day (°C)

T_{av} is the mean air temperature for a given day (°C)

The Hargreaves method has shown performance comparable to the more widely used Penman-Monteith method in data-scarce regions, including parts of the basin in Benin and West Africa (Kilinzo *et al.,* 2011; Adjei *et al.,* 2023; Maforikan *et al.,* 2023).

3.4.2.5 *Actual Evapotranspiration*

After determining the potential evapotranspiration, SWAT calculates the evaporation of rainfall intercepted by the plant canopy first, then calculates the maximum amount of transpiration and the maximum amount of soil evaporation (Chun *et al.,* 2018) using a modified Ritchie (1972) approach. When the evaporative demand is more than the water stored in the canopy, SWAT divides the remaining water demand between the vegetation (transpiration) and soil (evaporation). The amount of potential transpiration under ideal conditions is calculated as a function of leaf area index (LAI) and potential evapotranspiration (Equation 3.22 and 3.23):

$$E_t = \frac{E_o' \cdot LAI}{3.0} \qquad \text{for } 0 \leq \text{LAI} \leq 3.0 \qquad [3.22]$$

$$E_t = E'_o \qquad \text{for LAI} > 3.0 \qquad [3.23]$$

Where:

E_t is the maximum transpiration on a given day (mm H_2O)

E'_o is the potential evapotranspiration adjusted for evaporation of water from plant canopy (mm H_2O)

SWAT partitions the evaporative demand between the soil layers using a depth distribution to obtain the maximum allowable evaporation per layer (Equation 3.24).

$$E_{soil,z} = E"_s \cdot \frac{z}{z+exp(2.374-0.00713\cdot z)} \qquad [3.24]$$

Where:

$E_{soil,z}$ is the evaporative demand at depth z (mm H_2O)

$E"_s$ is the maximum soil water evaporation on a given day (mm H_2O)

z is the depth below the surface (mm)

The coefficients in Equation 3.23 are selected to ensure 50 %, and 95 % of the evaporative demand is extracted from the top 10 mm and 100 mm of the soil, respectively. SWAT allows modification of the distribution of soil evaporative demand with the soil evaporation compensation factor (ESCO).

The outputs from the SWAT water balance simulation include average basin precipitation, surface runoff, lateral flow, baseflow/groundwater flow (shallow and deep), “revap” amount, deep aquifer recharge, total aquifer recharge, total water yield, percolation out of the soil, potential and actual evapotranspiration. The water balance for the sub-basins and HRUs is also obtained as output.

3.4.3 Model Calibration and Validation

SWAT input parameters related to soil, LULC, and channel characteristics of the basin were generated following the initial model run. From these, sixteen parameters were selected for calibration and validation based on their significant impact on hydrology, soil properties, and land use, as used in existing research (Odusanya *et al.,* 2021; Maforikan *et al.,* 2023; Hounkpè, 2016) and the SWAT documentation (Neitsch *et al.,* 2002). These parameters were calibrated and validated using the SWAT-Calibration and Uncertainty Program (CUP) (Abbaspour, 2015). They include SCS runoff curve number (CN2), Groundwater delay (GW_DELAY in days), Threshold depth of water in the shallow aquifer required for return flow to occur (GWQMN), Baseflow Alpha factor, days (ALPHA_BF), Groundwater 'revap' coefficient (GW_REVAP), Threshold depth of water in the shallow aquifer for 'revap' to occur, mm (REVAPMN), Maximum rooting depth of soil profile (SOL_ZMX), Depth from soil surface to bottom of layer (SOL_Z), Moist bulk density (SOL_BD), Available water capacity of the soil layer (SOL_AWC), Saturated hydraulic conductivity (SOL_K), Manning's "n" value for the main channel (CH_N2), Effective hydraulic conductivity in main channel alluvium (CH_K2), Maximum canopy storage (CANMX), Soil evaporation compensation factor (ESCO), Plant uptake compensation factor (EPCO).

The SWAT model was calibrated first at Bétérou outlet (9° 11' 56" N, 2° 16' 50" E) and then at Bonou outlet (6° 54' 35" N, 2° 26' 35" E) with observed discharge data from 2000-2002 and the 2000 LULC map, utilising the period 1998-1999 for model warmup. The 2000 LULC map was calibrated because it falls within and more closely represents the LULC during the calibration period. This calibration method was applied because the Bétérou sub-basin contributes directly to Bonou sub-basin as outlined in the SWAT-CUP user manual (Abbaspour, 2015). After calibration at Bétérou, final parameter ranges were used to initialise calibration at Bonou. The SUFI-2 (Sequential Uncertainty Fitting - 2) algorithm was employed, which uses the Latin-Hypercube Sampling (LHS) method to simulated discharge. During the calibration process, SWAT approximates the total uncertainty by computing the 95 Percent Prediction Uncertainty (95 PPU) between the 2.5 % and 97.5 % ranges of the cumulative simulated discharge distribution. The parameter uncertainty range is initially broader and progressively narrowed based on the objective function while ensuring that most of the observed discharge points lie within the 95 PPU band. The p-factor and r-factor values are used to assess the uncertainty in the calibration and validation. The p-factor indicates the fraction of observed data falling within the 95 PPU range, with values between 0 and 1. Values closer to 1 indicate that more of the observed data falls within the 95 PPU, denoting most of the uncertainty in the observed data is accounted for. The r-factor describes the thickness of the 95 PPU, with lower values indicating a narrower uncertainty range (less uncertainty) and good model precision. The selected parameters were propagated and updated until values of simulated discharge were very close to the observed discharge, indicated by satisfactory objective function values as outlined by (Moriasi *et al.,* 2007). Validation was performed with observed discharge data for 2003-2008 at both stations.

Calibration and validation performances were evaluated using statistical metrics such as the Coefficient of Determination (R^2), Nash-Sutcliffe Efficiency (NSE), Percent Bias (PBIAS), and RMSE-observations Standard Deviation Ratio (RSR). The R^2 measures the proportion of variance in the observed discharge data that is explained (captured) by the simulated discharge data (Equation 3.25). The NSE is a normalised metric which assesses the predictive capacity of the model comparing it to using the mean value of the observed discharge values (Equation 3.26). It ranges from 0 to 1, with a value of 1 indicating a good fit between the simulated and observed discharge. The PBIAS assesses the bias in the simulated discharge, with negative values indication overestimation while positive values indicate underestimation (Equation 3.27). The RSR also standardizes the root mean square error using the standard deviation of the observed data (Equation 3.28). The Kling-Gupta Efficiency (KGE) also measures the goodness-of-fit between the simulation and observed discharge values (Equation 3.29).

$$R^2 = \frac{\left[\sum_i (Q_{obs,i} - \overline{Q}_{obs})(Q_{sim,i} - \overline{Q}_{sim})\right]^2}{\sum_i (Q_{obs,i} - \overline{Q}_{obs})^2 \left(Q_{sim,i} - \overline{Q}_{sim}\right)^2} \qquad [3.25]$$

$$NSE = 1 - \frac{\sum_i (Q_{obs} - Q_{sim})_i^2}{\sum_i \left(Q_{obs,i} - \overline{Q}_{obs}\right)^2} \qquad [3.26]$$

$$PBIAS = 100 \left(\frac{\sum_{i=1}^{n} (Q_{obs} - Q_{sim})_i}{\sum_{i=1}^{n} Q_{obs,i}}\right) \qquad [3.27]$$

$$RSR = \frac{\sqrt{\sum_{i=1}^{n} (Q_{obs} - Q_{sim})_i^2}}{\sqrt{\sum_{i=1}^{n} \left(Q_{obs,i} - \overline{Q}_{obs}\right)^2}} \qquad [3.28]$$

$$KGE = 1 - \sqrt{(r-1)^2 + (\alpha - 1)^2 + (\beta - 1)^2} \qquad [3.29]$$

Where:

Q_{obs} and Q_{sim} are observed and simulated discharge (m^3/s),

$\overline{Q}_{obs}$ and $\overline{Q}_{sim}$ are mean observed and simulated discharge respectively, and (σ and β are mean and standard deviation respectively)

3.4.4 Relationship between LULC Change and Water Balance

The final parameter range which gave satisfactory results was used to simulate water balance for the other LULC maps: 1986, 2015 and 2023 maps. The calibrated and validated SWAT model for the basin using observed discharge data from 1998-2008 was used to predict discharge for 2008-2016 in SWAT (where observed discharge data was absent). The water balance components were simulated for three distinct periods based on the available climate data period: 1998-2008, 2008-2016, and 1998-2016 without changing climate and soil data inputs. The isolation of LULC as the primary variable was to ensure that any changes observed in the water balance components were solely due to changes in LULC such as deforestation, agricultural expansion and urbanisation. This approach resulted in twelve sets of water balance outputs, combining each LULC map with each period, enabling the assessment of temporal variations in the impact of land cover change on water balance components.

Key water balance variables from the SWAT simulation output assessed include average annual surface runoff (mm), baseflow (mm), lateral flow (mm), total aquifer recharge (mm) and actual evapotranspiration (mm). Statistical analyses were used to examine the response of these water balance components to changes in the different LULC types across the LULC maps and assess the effect of LULC types on each component and the consistency of their relationship across the three simulation periods. These analyses are correlation, independent t-test, and Partial Least Squares (PLS) regression analysis. Initially, the average annual values of the water balance components per simulation were assessed for normality using the Shapiro-Wilk test, and the distribution was visualised in a Quantile-Quantile (Q-Q) plot.

3.4.4.1 Correlation Analysis

Following the assessment of normality, Pearson's correlation coefficient was employed to examine the strength and direction of the relation between the different LULC types and the water balance components, which include average annual surface runoff (mm), lateral flow (mm), baseflow (mm), actual evapotranspiration (mm), and total aquifer recharge (mm). This analysis was conducted across the three simulation periods to identify any significant correlations. The inputs were the area (km^2) of LULC classes for each map and the absolute amounts (mm/y) of the water balance components simulated per map. The correlation was assessed for the three periods simulated.

3.4.4.2 Independent t-test Analysis

An independent t-test was performed to examine if the mean values of the water balance components from the three simulations from the 1986 LULC map were statistically different from those obtained from the 2023 LULC. The test was applied at a 5 % significance level and 95 % confidence interval. The null hypothesis of the independent t-test assumes the mean water balance from the two LULC maps are equal, while the alternative hypothesis assumes the means are significantly different.

A p-value less than 0.05 signifies a statistically significant difference between the means from the 1986 map and those from the 2023 map. This suggests that the LULC change (deforestation, urbanisation, and agricultural expansion) between 1986 and 2023 led to notable differences in the water balance components over time. The test statistic value and sign also depict the level of difference between the means relative to the variability in the data and the direction. A smaller t-value suggests there is more variability in the data, making it harder to distinguish between the two groups.

The input for the test includes the area of LULC types from the 1986 and 2023 maps and their corresponding absolute values of the water balance components.

3.4.4.3 Partial Least Squares (PLS) Regression Analysis

As a result of the high multicollinearity among the LULC types in this study, Partial Least Squares (PLS) regression was used to model the relationship between the LULC types and the water balance components for each simulation period (Equation 3.30). The PLS regression is a supervised learning method which handles collinearity in predictor (independent) variables by creating new (latent) variables from linear combinations of the original predictors that have the closest relation with the response variables (Geladi and Kowalski, 1986). Hence, the latent variables are created for both the predictor and response variables (Equation 3.31 and 3.32), and their loadings show the contributions of each of the original predictor and response variables to the latent variables. The PLS regression is especially recommended where the predictors are strongly correlated with relatively few samples and multiple response variables, and ordinary linear regression often fails. The regression coefficients (Equation 3.30) produced for each predictor variable quantify the expected change in the water balance components when there is a unit change in a particular LULC category. This offers insights into the effects of the LULC types on the water balance components, and how sensitive the different water balance variables are to specific LULC types changes (Aladejana *et al.,* 2018). In this study, the predictor variables are the areas of the LULC types while the response variables are the absolute amounts of surface runoff, lateral flow, baseflow, total aquifer recharge, and actual evapotranspiration.

$$\hat{Y} = XB_{PLS} = XW(P^TW)^{-1}Q^T \qquad [3.30]$$

Where:

$\hat{Y}$ is the predicted response variable (surface runoff, lateral flow, baseflow, actual evapotranspiration and total aquifer recharge)

X is the matrix of predictors (LULC types)

B_{PLS} is the matrix of regression coefficients estimated by the PLS model

W is the weight matrix that relates X to the latent scores T

$(P^TW)^{-1}$ rescales the weights in W to align with the variance captured in each component

Q is the matrix of the loadings for Y

P is the matrix of the loadings for X

In PLS regression, actual predictor and response variables are projected (decomposed) onto latent components as expressed in Equation 3.31 and 3.32. Further details on PLS regression can be found in Abdi (2010) and Geladi and Kowalski (1986).

$$X = TP^T + E \qquad [3.31]$$

$$Y = UQ^T + F \qquad [3.32]$$

Where:

X is the matrix of the predictor variables

Y is the matrix of the response variables

T is the matrix of latent scores for X

U is the matrix of latent scores for Y

3.5 Future LULC Change Impact on Water Balance

This section projected the possible future LULC change that can occur based on the 'business-as-usual' trend shown in the classified maps in Objective 1. The classified LULC maps were used as input into the IDRISI Selva software for the analyses. The section begins with validation of the most current map and then a projection of future LULC for 2030, 2063 and 2100, and simulating water balance with the derived future maps. The years 2030, 2063 and 2100 were selected in line with the SDGs, African Agenda 2063 and IPCC global change projection timelines, respectively to enable evaluation of the results with the outcomes of these goals.

3.5.1 Validation of Projected 2023 LULC Map

Accurate projection of LULC in a region requires validation of the projection methods being applied. The combined Cellular-Automata (CA) – Markov projection was utilised for projecting future LULC. The Markov transition tool can project the probability of LULC types to transition into other forms or persist over a future period based on the change between two known periods (Equation 3.33). The CA-Markov improves the LULC projection by incorporating the spatial pattern of change (from the CA component) in addition to the quantities generated by the Markov probabilities (Pontius Jr and Malanson, 2005). It determines the future state of a cell (LULC class) based on its current state and the state of its neighbouring cells (Equation 3.34). The transition probabilities and areas were first estimated using the Markov transition in IDRISI Selva with the 1986 and 2015 maps and the time between them as input. The estimated transition probabilities and areas were used as input into the CA-Markov tool to simulate the LULC for the year 2023. The simulated 2023 map was assessed against the classified 2023 LULC map for its overall agreement, as well as quantity and location agreement. The validate tool in IDRISI Selva environment was utilised for this purpose. The total agreement, K-standard, K-location are some of the metrics produced after validation.

$$S_{i,j}(t+1) = f\left(S_{i,j}(t), N_{i,j}(t), T\right) \qquad [3.33]$$

Where:

$S_{i,j}(t+1)$ is the future state (LULC class) of the cell at location (i, j) at time $t + 1$ from CA-Markov projection

$S_{i,j}(t)$ is the current state of the cell at time t

$N_{i,j}(t)$ is the states of the neighboring cells

T is the Markov transition probabilities matrix expressed as;

$$T = \begin{bmatrix} P_{ij} & \cdots & P_{in} \\ \vdots & \ddots & \vdots \\ P_{nj} & \cdots & P_{nn} \end{bmatrix} \quad [3.34]$$

Where:

P_{ij} is the probability of transitioning from LULC class i to j

n is the number of LULC classes, each row summing to 1 as the total probability of transitioning from one class must equal 1

3.5.2 Projection of Future LULC Maps

The CA-Markov projection of the 2023 LULC map demonstrated a reasonable ability to learn from earlier LULC scenarios and make predictions. However, it also highlighted some deviations from reality. Hence, the 2023 classified map was used as a baseline to project future LULC for 2030, 2063, and 2100 to enhance the credibility and reliability of future projections and reduce error propagations from the simulated 2023 map as recommended (Padial-Iglesias *et al.,* 2021; Foody, 2010). The 2023 and 2015 classified LULC maps were used to project the 2030 LULC map, the 2023 and 2030 maps were used to project for 2063, and the projected 2030 and 2063 maps were used to estimate LULC for 2100. The absolute change in the land cover categories and the rate of change in the LULC types for the periods 2023-2030, 2030-2063 and 2063-2100 were calculated. This was to understand the quantity of change (%) and the rate of change (%/y) that could be expected between those years.

3.5.3 Simulation of Future Water Balance Based on Projected LULC

The projected LULC maps of 2023, 2030, 2063 and 2100 were used to simulate water balance in the calibrated and validated SWAT model to obtain the quantities of surface runoff, baseflow, lateral flow, total aquifer recharge and actual evapotranspiration using the same climate data from 1998-2016. This ensures that any changes in water balance can be attributed solely to changes in LULC. The PLS regression was then implemented with the areas of the LULC types per future map (predictor variables), and their corresponding water balance component amounts (response variables) as input. The coefficients of the LULC types in predicting each water balance component were assessed to determine how sensitive the water balance components are to the different LULC types.

3.6 Future Climate Change Impact on Water Balance

In this section, future climate in the Ouémé River Basin was first projected, and then the projected climate was used to simulate water balance to ascertain possible future changes in water balance resulting from future climate change likely to be expected.

3.6.1 Future Climate Projection

3.6.1.1 Data Acquisition and Bias Correction

Climate projections were performed using six (6) available Global models and their ensemble from the sixth IPCC Coupled Model Intercomparison Project (CMIP6) by the World Climate Research Programme (WCRP) framework which has been successfully used in Africa (Tanimu *et al.,* 2024; Zoungrana *et al.,* 2024; Taonda *et al.,* 2024) (Table 3.6). Factors that informed the selection of the models were the availability of historical and future data for the scenarios considered, accuracy in capturing seasonal climate patterns in the basin compared to the reference data, and the validation of the models in other parts of Africa. The historical and future climate scenario data for these models were downloaded from the Copernicus Climate Data Store (CDS) website (Copernicus Climate Change Service – Climate Data Store, 2021a) and tested, after which the best-performing model for the basin was selected for the water balance simulations. To improve the accuracy of the models at the watershed scale, the historical and future scenario projected data of the models were downscaled and bias-corrected to reduce the systematic errors in model data due to factors such as coarse resolution. Statistical downscaling and Quantile Mapping methods were used to downscale and bias-correct the historical and future climate data of the global climate models to match the distribution of the reference (observed) data in the basin. The reference precipitation data used is the Climate Hazards Group InfraRed Precipitation with Station Data (CHIRPS), downloaded from the CDS website (Copernicus Climate Change Service-Climate Data Store, 2021b). The CHIRPS data has a latitude-longitude resolution of $0.05^{o} \times 0.05^{o}$ (~5.3 × 5.3 km) and precipitation data from 1981 to present. For reference temperature data, the three-hourly European Centre for Medium-Range Weather Forecasts Reanalysis 5 (ERA 5) data was used, also downloaded from the CDS website (Copernicus Climate Change Service – Climate Data Store, 2023). The ERA 5 reanalysis data has a latitude and longitude resolution of $0.25^{o} \times 0.25^{o}$ and a horizontal resolution of 31×31 km, with data from 1940 to the present.

The CMIP6 models have historical and future climate projections including data from 1850 – 2014, and 2015 – 2100, respectively. The six models used for the precipitation and temperature projection are described in Table 3.6. Two scenarios of IPCC CMIP6 future socio-economic cum radiative change, the Shared Socio-economic Pathways (SSPS) were considered, namely, the SSP1-2.6 and SSP3-7.0 scenarios. Mean bias error (*mbe*) and correlation coefficient were used to evaluate the bias-corrected models' precipitation and temperature data compared to the references. A negative *mbe* value signifies an underestimation while positive values indicate an overestimation.

3.6.1.2 Scenarios: SSP1-2.6 and SSP3-7.0

Climate scenarios describe how future climate may develop based on assumptions about key drivers including population growth, lifestyle, technological innovation, and economic processes. They can also be defined by geophysical forces such as emissions of greenhouse gasses (GHGs), aerosols and/or land use patterns (Lee *et al.,* 2021). In the IPCC Sixth Assessment Report (AR6), potential future climate change is assessed by emissions and concentration-driven scenarios with Model Intercomparison Project (MIP) scenarios based on a combination of Shared Socio-economic Pathways (SSPs) and climate forcing (previously Representative Concentration Pathways-RCP). The SSPs are socio-economic developments regarding urbanisation, population, economic collaborations, and human and technological developments that describe different global futures in the absence of climate change and additional climate policy. The implications of these socio-economic developments are defined in the form of emission and concentration outcomes dependent on Integrated Assessment Models (IAM models used to assess the interrelationship between different factors). The emission-driven scenario requires using the carbon and other gas cycle model emissions and the concentration-driven climate projection has a default concentration of CO_2, CH_4, N_2O, among other GHGs coupled with aerosol emissions without considering the carbon cycle feedback. These scenarios provide insights to describe differing situations of evaluating climate mitigation, adaptation and residual damage. The first number in the scenario name refers to the SSP situation, while the second number refers to the approximate global effective radiative forcing (W/m^2) reached by 2100. Two scenarios assessed in this study are SSP1-2.6 and SSP3-7.0.

The SSP1-2.6, known as the 'Sustainability' scenario depicts a future climate where the world shifts gradually but pervasively towards a more sustainable path, emphasizing more inclusive development that respects perceived environmental boundaries and is driven by an increasing commitment to achieving development goals and low challenges to mitigation and adaptation. It is also characterized by a 2.6 W/m^2 radiative forcing by the year 2100, and mean temperature values below 2.0^{o} relative to 1850 – 1900 climate with net zero CO_2 emissions by the second half of the century (O'Neill *et al.,* 2017; Riahi *et al.,* 2017). The SSP3-7.0 is known as the 'Regional Rivalry' scenario where there is resurgent nationalism, concerns about competitiveness and security, and regional conflicts push countries to increasingly focus on national and regional issues, and low international priority for addressing environmental concerns thereby leading to strong environmental degradation (O'Neill *et al.,* 2017). It is characterized by a 7.0 W/m^2 radiative forcing by 2100, and is an intermediate-to-high reference scenario with high non-CO_2 emissions, including high aerosol emissions. These scenarios were chosen because SSP1-2.6 has more simulations and represents better the current state of the world where conscious efforts are being made toward climate adaptation for sustainability, and the SSP3-7.0 scenario has been argued in the IPPC Sixth Report to be more plausible to unfold compared to the extreme warming scenario, SSP5-8.5.

The main drivers of emissions across the SSPs include population growth of 8.5 – 9.7 billion by 2050 and, an increase in global Gross Domestic Product (GDP) of 2.7 – 4.1 % per year between 2015 and 2050, with energy demand reaching 480 to 750 EJ/y (compared to approximately 390 EJ/y in 2015) in the absence of any new climate policies (Lee *et al.,* 2021).

3.6.1.3 Data Analysis

Global land precipitation and surface air temperature are two physical indicators of global climate change according to the IPCC (Chen *et al.,* 2021). To assess the change in precipitation and temperature that is likely to occur over the basin, the projected average values across the basin were examined relative to the baseline climate from 1995 to 2014 as done by the IPCC future scenario analysis (Lee *et al.,* 2021). This 20-year baseline period depicts the recent past climate and encompasses the years used in the initial SWAT modelling. The IPCC future periods namely, near-term (2021-2040), mid-term (2041-2060), and long-term (2081-2100) (Lee *et al.,* 2021) projections of precipitation, and minimum and maximum temperature were compared with the baseline values and the change between them were calculated. This revealed the average changes in precipitation and temperature (minimum and maximum) projected to occur under the SSP1-2.6 and SSP3-7.0 future scenarios over the catchment area, which has potential impacts on the hydrology within the basin.

Table 3.6: CMIP6 Climate Models Applied in this Study

Model	Full Name	Institute	Horizontal resolution (atmosphere)	Horizontal resolution (ocean)
ACCESS-CM2	Australian Community Climate and Earth System Simulator – Climate Model 2	Australian Bureau of Meteorology in collaboration with other Institutions.	$1.875^{o} \times 1.25^{o}$ (85L)	1^{o} (50L)
MPI-ESM1-2-LR	Max Planck Institute Earth System Model version 1.2 – Low Resolution)	Max Planck Institute of Meteorology	$1.875^{o} \times 1.875^{o}$ (47L)	$1.5^{o} \times 0.5^{o}$ (40L)
MIROC-ES2L	Model for Interdisciplinary Research on Climate – Earth System version 2 for Long-term simulations)	Japan Agency of Marine-Earth Science and Technology, University of Tokyo, and National Institute for Environmental Studies.	$2.8^{o} \times 2.8^{o}$ (40L)	$1^{o} \times 0.5^{o}$ (62L)
IPSL-CM6A-LR	Institut Pierre-Simon Laplace Climate Model version 6A – Low Resolution	Institut Pierre-Simon Laplace (IPSL)	$2.5^{o} \times 1.25^{o}$ (79L)	$1^{o} \times 0.5^{o}$ (75)
EC-Earth-Veg-LR	EC – Earth System version 3 – Vegetation – Low Resolution	EC-Earth Consortium	$0.7^{o} \times 0.7^{o}$ (91L)	1^{o} (75L)
AWI-ESM-1-1LR	Alfred Wegener Institute Earth System Model Version 1.1 – Low resolution	Alfred Wegener Institute (AWI)	$1.875^{o} \times 1.875^{o}$ (47L)	1^{o} (40L)

3.6.2 Future Water Balance Based on Future Climate Data

Given the better performance of the ACCESS-CM2 model bias-corrected precipitation (Taonda *et al.*, 2024), and the ensemble mean temperature (maximum and minimum) data compared to the other models, they were used for the water balance simulations. The future temperature and precipitation data for both SSP1-2.6 and SSP3-7.0 scenarios were extracted and prepared according to the stations used in the SWAT model set-up in the format applicable in SWAT. The data were divided into the near term (2020-2040), mid-term (2041-2060) and long term (2081-2100) future scenarios of the IPCC climate action framework to ascertain the periodical differences as well.

The relationship between future climate changes (precipitation and temperature), and simulated future water balance was then assessed between the scenarios SSP1-2.6 and SSP3-7.0. This aids in understanding how the different concentration scenarios influence the relationship between climate and water balance, providing insight into scenario-specific climate change impacts on water balance. The inputs were mean catchment values of precipitation (mm) and temperature (^{o}C) across the future periods (near term, mid-term and long term), and the simulated average annual values of surface runoff (mm), lateral flow (mm), baseflow (mm), total aquifer recharge (mm), and actual evapotranspiration (mm) for the future periods.

3.7 Assessing the Impact of Combined Future LULC and Climate Change on Water Balance

To assess the possible impact of future LULC changes and climate change on water balance simultaneously, the projected LULC for 2030, 2063 and 2100 were used together with the projected temperature and precipitation change for SSP1-2.6 and SSP3-7.0 scenarios according to the future periods. The near term (2021-2040) future climate was combined with LULC for 2030, while the mid-term future climate (2041-2060) was combined with LULC for 2063, and long term (2081-2100) future climate with the 2100 LULC for the SWAT modeling.

The average annual surface runoff, lateral flow, baseflow, total aquifer recharge and actual evapotranspiration were then assessed in terms of their absolute, relative and rates of change, and the relationship between the combined LULC-Climate change and water balance.

CHAPTER 4 RESULTS AND DISCUSSION

4.1 Assessment of the Spatio-temporal LULC Change

Under this section, results from the first objective on the spatio-temporal differences in the LULC type distribution across the four historical LULC maps for 1986, 2000, 2015 and 2023, as well as their rates of change, are described.

4.1.1 Mapping LULC in the Basin

The results of the LULC mapping in the basin for 1986, 2000, 2015 and 2023 revealed that, the Ouémé River Basin was originally covered with Savanna areas and Woodlands in its major parts (Table 4.1). These LULC types occupied more than 70 % of the basin in 1986, followed by Agricultural lands and Forest areas (Fig. 4.1). Settlement/bare areas and Water bodies had the least cover in the basin. In 2023, Agricultural land covered most of the basin (51 %), followed by Savanna, Settlements and bare lands, Forests and Water bodies. This indicates a considerable decline in Savanna and Forest areas, in contrast to an expansion in Agricultural lands and Settlement areas.

Table 4.1: Area (km^2) and Percentage Cover of the LULC Classes from 1986 to 2023

LULC Class	1986		2000		2015		2023	
	km^2	(%)	km^2	(%)	km^2	(%)	km^2	(%)
Forest areas	3108.78	(6.31)	2096.11	(4.25)	1164.92	(2.36)	677.08	(1.37)
Settlements/bare lands	273.49	(0.55)	372.76	(0.76)	603.65	(1.22)	807.47	(1.64)
Savanna areas	34368.08	(69.74)	32468.83	(65.89)	28729.48	(58.30)	22501.23	(45.66)
Agricultural land	11487.08	(23.31)	14310.59	(29.04)	18702.80	(37.95)	25263.42	(51.26)
Water bodies	42.79	(0.09)	31.95	(0.06)	79.38	(0.16)	31.03	(0.06)
Total	49280.23	(100.00)	49280.23	(100.00)	49280.23	(100)	49280.23	(100)

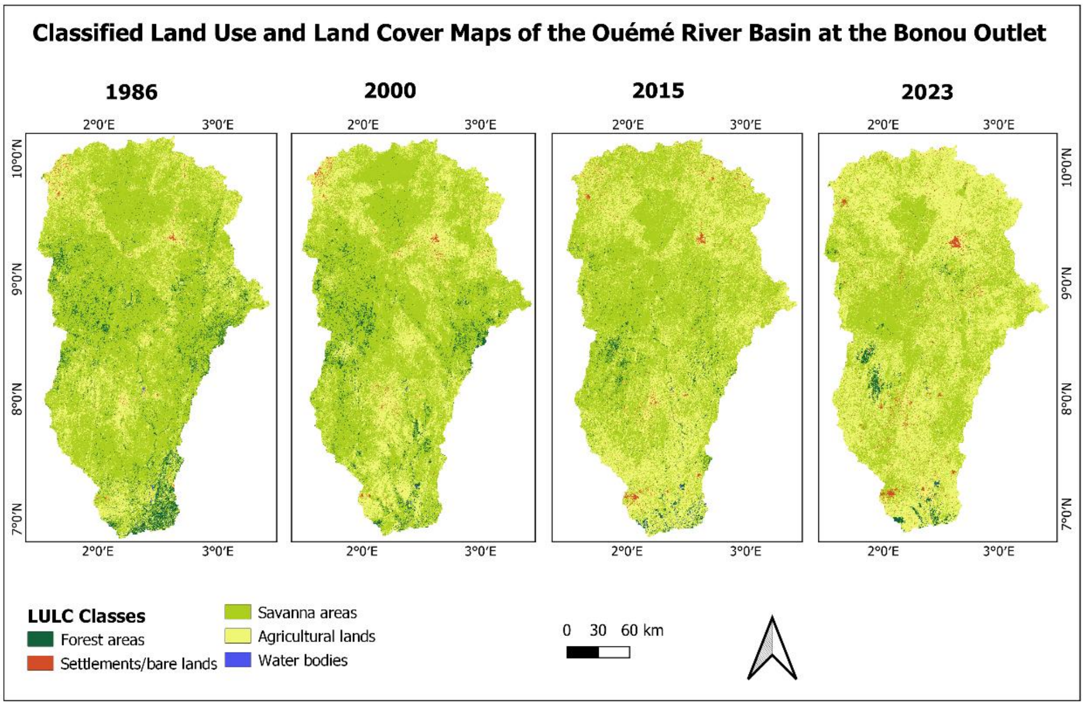

Figure 4.1: Classified LULC Maps of the Ouémé River Basin with Outlet at the Bonou Outlet for 1986, 2000, 2015 and 2023

4.1.2 Accuracy Assessment

The supervised classification of LULC in the Ouémé River Basin for 1986, 2000, 2015 and 2023 yielded pixel-based overall accuracy values greater than 90 %. Additionally, the kappa, and producer's and user's accuracy values were all greater than 85 %, for all four classified maps (Table 4.2 and 4.3), indicating the reliability of the LULC maps for further analysis of changes in the basin.

Table 4.2: Pixel and Area-based Accuracy of the Classified Maps

Statistic	1986	2000	2015	2023
Pixel-based				
Overall Accuracy (%)	92.90	92.58	90.63	92.93
Kappa Statistic	0.90	0.89	0.86	0.90
Area-based				
Overall Accuracy (%)	93.65	93.54	90.61	91.82

The area-based accuracy analysis for the 2023 classified map yielded an overall accuracy value of 91.8 % ± 0.4, with total commission (overestimation) and omission (underestimation) errors of 8.2 %. The quantity and allocation disagreement values were 2.3 % and 5.9 % respectively. Notably, the commission errors in Agricultural land estimation were of the equal magnitude to the omission errors in Savanna areas estimation. Additionally, the results indicated a 1 % underestimation in Settlement areas and bare lands.

Conversely, the 1986 classified map, based on the area proportion analysis, demonstrated an overall accuracy value of 93.7 % ± 0.6, and a total error of 6.3 %. The exchange and shift errors (allocation disagreement) were 3.3 % and 0.8 %, respectively, representing more than 50 % of the total error. The quantity disagreement was 2.2 %.

Regarding omission, Savanna areas estimation had the highest omission errors of about 3 % followed by Agricultural lands, Settlements and bare lands, Forest areas and Water bodies having the least omission errors. This suggests that areas that should have been classified as the aforementioned LULC types were either left out or misclassified as other LULC types. The value of exchange errors for Savanna areas was the same as that for Agricultural lands, indicating that most of the errors originated from misclassification between those two LULC types. Additionally, Settlements and bare lands were largely underestimated, leading to a producer's accuracy value of less than 50 %.

Similar results were obtained for the 2000 classified map, which had an overall accuracy value of 93.5 % ± 0.5, and producer accuracy values ≥ 70 % for most classes, except for settlement areas and bare lands which have a value of 37 %. Furthermore, the area-based accuracy for the 2015 map yielded an overall accuracy of 90.6 % ± 0.5, with producer and user accuracy values ≥ 59 % and ≥ 87 % respectively.

Most errors were confusion between Savanna and Agricultural land, although a few Forests were misclassified as Savanna. Furthermore, some pixels of Water bodies were misclassified as forest and savanna areas, particularly along riparian forests and swamps. The area of Water bodies was higher in the 2015 classified map than the range of values observed in the other years, indicating an overestimation. The raw error matrix for the classified maps, together with the producer's (PA), user's (UA), overall accuracy (OA) and area proportions of the LULC classes are provided in Table 4.3.

The corresponding area-based unbiased error matrix consisting of the area proportions of each LULC class and their producer, user and overall accuracies, and adjusted areas at 95 % confidence interval are also shown in Table 4.4.

Table 4.3: Confusion Matrices (pixel counts) of Classified Maps of the Ouémé River Basin

		Reference								
	Years	LULC Class	Forest areas	Settlement/ bare lands	Savanna areas	Agriculture lands	Water bodies	Total	UA	OA
Map	**1986**	Forest areas	933	0	52	2	0	987	0.95	0.93
		Settlement/bare land	0	591	7	56	0	654	0.90	
		Savanna areas	43	3	2897	55	2	3000	0.97	
		Agriculture lands	0	67	147	1192	0	1406	0.85	
		Water bodies	2	1	6	1	194	204	0.95	
		Total	978	662	3109	1306	196	6251		
		PA	0.95	0.89	0.93	0.91	0.99			
	2000	Forest areas	1138	0	64	4	0	1206	0.94	0.93
		Settlement/bare land	0	795	27	102	0	924	0.86	
		Savanna areas	53	10	4440	109	2	4614	0.96	
		Agriculture lands	14	94	242	2449	0	2799	0.88	
		Water bodies	4	0	1	0	236	241	0.98	
		Total	1209	899	4774	2664	238	9784		
		PA	0.94	0.88	0.93	0.92	0.99			
	2015	Forest areas	1159	0	75	3	1	1238	0.94	0.91
		Settlement/bare land	0	1820	22	125	0	1967	0.93	
		Savanna areas	47	11	5471	377	0	5906	0.93	
		Agriculture lands	11	106	646	5217	0	5980	0.87	
		Water bodies	8	0	5	2	247	262	0.94	
		Total	1225	1937	6219	5724	248	15353		
		PA	0.95	0.94	0.88	0.91	1.00			
	2023	Forest areas	656	0	7	0	0	663	0.98	0.93
		Settlement/bare land	0	2783	30	49	0	2862	0.97	

Savanna areas	10	25	5319	343	0	5697	0.93
Agriculture lands	8	58	615	6177	0	6858	0.90
Water bodies	1	5	2	1	237	246	0.96
Total	675	2871	5973	6570	237	16326	
PA	0.98	0.97	0.89	0.94	1.00		

Table 4.4: Area-based Error Matrices and Adjusted Area Estimates at 95 % Confidence Interval of Classified Maps

		Reference							
	Year	LULC Class	Forest areas	Settlement/ bare land	Savanna areas	Agricultural lands	Water bodies	Total	UA
Map	**1986**	Forest areas	0.0596	0.0000	0.0033	0.0001	0.0000	0.0631	0.95 ± 0.01
		Settlement/bare lands	0.0000	0.0050	0.0001	0.0005	0.0000	0.0055	0.90 ± 0.02
		Savanna areas	0.0100	0.0007	0.6735	0.0128	0.0005	0.6974	0.97 ± 0.01
		Agricultural lands	0.0000	0.0111	0.0244	0.1976	0.0000	0.2331	0.85 ± 0.2
		Water bodies	0.0000	0.0000	0.0000	0.0000	0.0008	0.0009	0.95 ± 0.03
		Total	0.070	0.017	0.701	0.211	0.001	1	
		Standard error of area (km^2)	77.92	68.31	149.47	138.69	16.21		
		PA	0.86 ± 0.02	0.30 ± 0.04	0.96 ± 0.01	0.94 ± 0.01	0.64 ± 0.07		
		Adj. Area ± CI (km^2)	3431 ± 153	829 ± 134	34557 ± 293	10398 ± 272	64 ± 32		
	2000	Forest areas	0.0401	0.0000	0.0023	0.0001	0.0000	0.0425	0.94 ± 0.01
		Settlement/bare lands	0.0000	0.0065	0.0002	0.0008	0.0000	0.0076	0.86 ± 0.02
		Savanna areas	0.0076	0.0014	0.6340	0.0156	0.0003	0.6589	0.96 ± 0.01
		Agricultural lands	0.0015	0.0098	0.0251	0.2541	0.0000	0.2904	0.88 ± 0.01
		Water bodies	0.0000	0.0000	0.0000	0.0000	0.0006	0.0006	0.98 ± 0.02
		Total	0.049	0.018	0.662	0.271	0.001	1	
		Standard error of area (km^2)	56.15	53.74	119.42	115.35	9.96		
		PA	0.82 ± 0.02	0.37 ± 0.03	0.96 ± 0.01	0.94 ± 0.01	0.69 ± 0.06		
		Adj. Area ± CI (km^2)	2423 ± 110	872 ± 105	32604 ± 234	13336 ± 226	45 ± 20		

2015	Forest areas	0.0221	0.0000	0.0014	0.0001	0.0000	0.0236	0.94 ± 0.01
	Settlement/bare lands	0.0000	0.0113	0.0001	0.0008	0.0000	0.0122	0.93 ± 0.01
	Savanna areas	0.0046	0.0011	0.5400	0.0372	0.0000	0.5830	0.97 ± 0.01
	Agricultural lands	0.0007	0.0067	0.0410	0.3311	0.0000	0.3795	0.88 ± 0.01
	Water bodies	0.0000	0.0000	0.0000	0.0000	0.0015	0.0016	0.94 ± 0.03
	Total	0.028	0.019	0.583	0.369	0.002	1.000	
	Standard error of area (km^2)	35.74	35.93	123.45	121.98	1.48		
	PA	0.80 ± 0.02	0.59 ± 0.02	0.93 ± 0.01	0.87 ± 0.01	0.99 ± 0.01		
	Adj. Area ± CI (km^2)	1356 ± 70	944 ± 70	28713 ± 242	18192 ± 239	76 ± 3		
2023	Forest areas	0.0136	0.0000	0.0001	0.0000	0.0000	0.0137	0.99 ± 0.01
	Settlement/bare lands	0.0000	0.0159	0.0002	0.0003	0.0000	0.0164	0.97 ± 0.01
	Savanna areas	0.0008	0.0020	0.4263	0.0275	0.0000	0.4566	0.93 ± 0.01
	Agricultural lands	0.0006	0.0043	0.0460	0.4617	0.0000	0.5126	0.90 ± 0.01
	Water bodies	0.0000	0.0000	0.0000	0.0000	0.0006	0.0006	0.96 ± 0.02
	Total	0.015	0.022	0.473	0.490	0.001	1.000	
	Standard error of area (km^2)	16.48	34.28	114.52	115.58	0.37		
	PA	0.91 ± 0.02	0.71 ± 0.02	0.90 ± 0.01	0.94 ± 0.01	1.00		
	Adj. Area ± CI (km^2)	739 ± 32	1098 ± 67	23290 ± 224	24123 ± 227	30 ± 0.7		

4.1.3 Change in LULC over Time

The period between 2015 and 2023 exhibited the fastest rates of losses and gains in LULC, spanning fewer years compared to the periods 1986 – 2000 and 2000 – 2015. Specifically, Savanna and Forest areas showed sharp reductions in area at rates of 3.0 %/y and 6.6 %/y, respectively, while Agricultural lands and Settlement areas/bare lands exhibited sharp increases at rates of 3.8 %/y and 3.7 %/y respectively (Fig. 4.2). However, during the periods 1986 – 2000 and 2000 – 2015, the results revealed gradual annual changes, with reductions in Savanna areas (0.4% and 0.8 %) and Forest areas (1.9 % and 4.3%) and increase in Agricultural lands (1.5 % and 1.8 %).

The magnitude of Forest cover loss exhibited a declining pattern over the period, yet the annual rate of deforestation increased, particularly during the period 1986 – 2000 compared to 2000 – 2015. Approximately 78 % of the Forests in 1986 have undergone degradation, resulting in a reduction of 2,431 km^2 in area and an average of 64 km^2 loss per year. Similarly, by 2023, Savanna areas experienced a decline of approximately 11,867 km^2, representing a total loss of about 35 % of its 1986 cover, with an average annual loss of 312 km^2.

On the other hand, Agricultural land increased by more than 100 % of their quantity in 1986, primarily as croplands (maize, beans, cassava, yam, pepper and other vegetables) and plantations (cashew, oil palm, cotton, orange, teak), with an annual increase of 363 km^2. Settlements and bare land also expanded by over 100 % of their 1986 area, resulting in a total gain of 534 km^2, with an annual increase of 14 km^2per year expansion primarily in settlement areas. The increase rate during 2000 – 2015 was higher than during 1986 – 2000 for Settlements and bare lands, attributable to increasing population growth and urbanisation rates. Overall, the average annual rates of change between 1986 and 2023 were as follows: Forest areas > Settlements/bare lands > Agricultural lands > Savanna areas > Water bodies, corresponding to -4.0 %, 3.0 %, 2.2 %, -1.1 % and -0.9 % respectively.

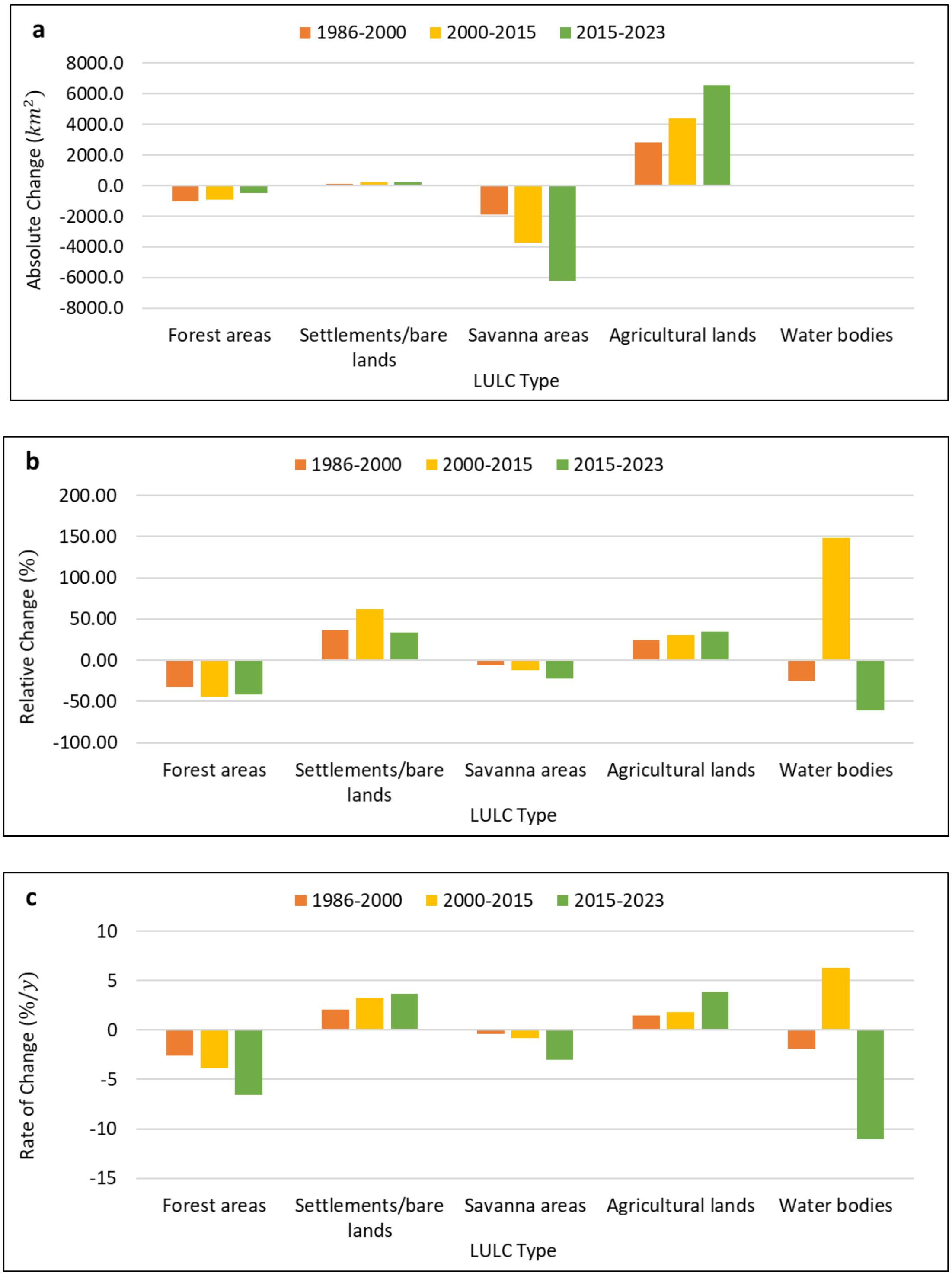

Figure 4.2: Absolute Change (a), Relative Change (b) and Annual Rate of Change (c) of LULC in the Ouémé River Basin

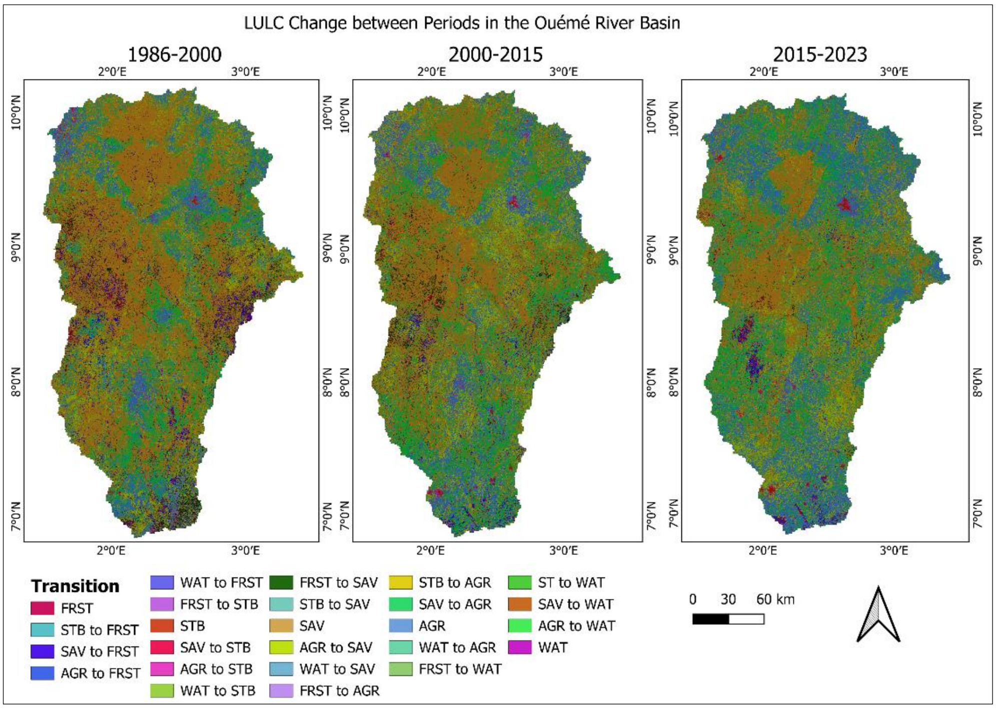

Figure 4.3: LULC Change Map over Time in the Ouémé River Basin[3]

Analysis of the transitions between the LULC map and the years revealed significant insights. The uniform transition intensity in LULC types between 2015- 2023 was higher than that for 2000 – 2015, with 1986-2000 having the least (Table 4.5). The period from 1986 and 2000, had Forest areas transitioning actively (higher intensity than the uniform intensity over the period), with the intensity of loss higher than the intensity of gain. Settlements/bare lands also transitioned actively but with higher gaining intensity than loss intensity. This is similar for Agricultural lands and Water bodies within the same period. Savanna areas, however, showed a higher loss intensity than gain intensity though the transition was dormant (lower than the uniform intensity over the period). Similar trends were observed for 2000 – 2015, except for Water bodies which had a higher gain intensity than loss intensity. However, from 2015 to 2023, Forest areas and Settlements/bare lands had lower transition intensities than the other two periods. Secondly, Savanna areas had higher transition intensities than earlier periods, and the loss intensity was active while the gain intensity was dormant.

[3] *FRST* – Forest areas, *STB* – Settlements/bare lands, *SAV* – Savanna areas, *AGR* – Agricultural lands and *WAT* – Water bodies

On the other hand, agricultural lands had lower transition intensities compared to the earlier years, with an active gain intensity but dormant loss intensity.

In summary, it can be inferred that Savanna and Forests have been actively converted into Agricultural land and Settlements/bare areas. Notable areas witnessing massive settlement expansion include Parakou and Djougou in the north, Bohicon and Ketou in the south, and Save and Dassa-Zoume in the central parts of the basin. Agricultural land expansion, on the other hand, occurred throughout the basin (Fig. 4.3), particularly in the north southeast and west, entering into the savanna areas/woodlands, protected areas, 'classified forest' areas and along water bodies.

Table 4.5: Transition Intensities of LULC over Time

LULC category	Gain (%)	Gain Intensity (%)	Loss (%)	Loss Intensity (%)
	1986 – 2000 (uniform intensity = 36.09)			
Forest areas	2.88	67.62	4.93	78.17
Settlements/bare lands	0.65	85.41	0.44	80.11
Savanna areas	15.03	22.81	18.88	27.07
Agricultural lands	17.50	60.28	11.78	50.52
Water bodies	0.03	49.44	0.05	62.25
	2000 – 2015 (uniform Intensity = 42.31)			
Forest areas	1.74	73.74	3.63	85.41
Settlements/bare lands	1.08	88.01	0.61	80.58
Savanna areas	15.98	27.41	23.57	35.77
Agricultural lands	23.38	61.59	14.46	49.80
Water bodies	0.14	83.84	0.04	59.86
	2015 – 2023 (uniform intensity = 43.19)			
Forest areas	0.88	63.70	1.87	78.90
Settlements/bare lands	1.26	76.63	0.84	68.74
Savanna areas	13.91	30.47	26.55	45.54
Agricultural lands	27.11	52.89	13.80	36.36
Water bodies	0.03	55.38	0.13	82.56

4.2 Modelling Water Balance Based on Historical LULC

4.2.1 SWAT Model Calibration and Validation

The uncertainty assessment of the SWAT model calibration at Bétérou yielded a p-factor of 0.63 and an r-factor of 1.09, while validation results showed a p-factor of 0.54 and an r-factor of 1.19 (Fig. 4.4). At Bonou, the calibration produced a p-factor of 0.45 and an r-factor of 1.32, with validation p-factor value of 0.42 and r-factor value of 1.28 (Figure 4.5). P-factor values ≥ 0.5 and r-factor values < 1.5 are generally considered acceptable (Abbaspour, 2015).

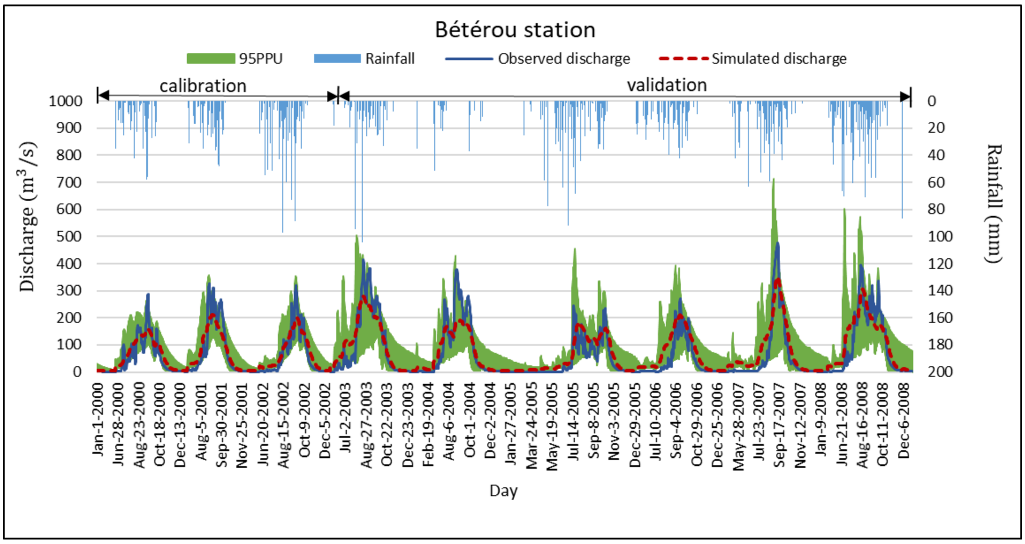

Figure 4.4: Calibration and validation results at Bétérou station, showing simulated versus observed discharge, rainfall and the 95 PPU range

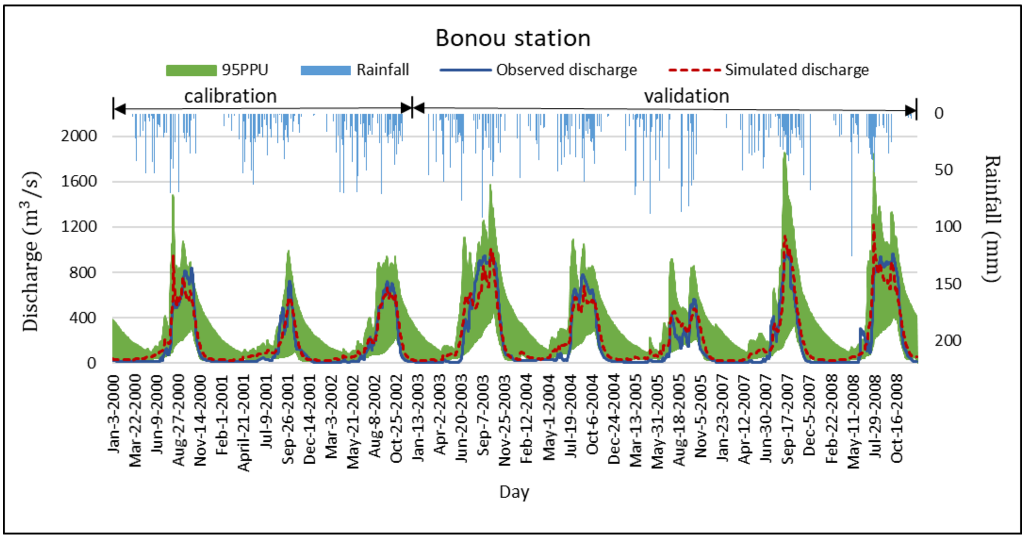

Figure 4.5: Calibration and validation results at Bonou outlet, showing simulated versus observed discharge, Rainfall and the 95 PPU range

Despite the satisfactory performance, the negative Percent Bias (PBIAS) values obtained during both calibration and validation phases indicate a general overestimation of discharge by the model, although it remains within acceptable limits.

The SWAT model calibration and validation results for the period 1998-2008 at Bétérou and Bonou stations within the Ouémé River Basin are summarised in Table 4.6. The calibration process at both stations demonstrated satisfactory performance, meeting the recommendation by Moriasi *et al.* (2007) and Gui *et al.* (2021). This satisfactory performance was also observed in the validation phase, indicating a good fit between the simulated and observed discharge at the two stations.

Table 4.6: SWAT Model Calibration and Validation Results

Station	**Model Performance**	**NSE**	**RSR**	**PBIAS**	**R^2**	**KGE**
Bétérou (upstream)	Calibration (1998-2002)	0.82	0.42	-6.6	0.85	0.74
	Validation (2003-2008)	0.81	0.43	-14.4	0.83	0.74
Bonou (downstream)	Calibration (1998-2002)	0.91	0.31	-12.8	0.92	0.82
	Validation (2003-2008)	0.89	0.33	-10.7	0.90	0.84

The four most sensitive parameters identified from the sensitivity analysis influencing the hydrology in the basin are: baseflow alpha factor, soil saturated hydraulic conductivity, curve number, and maximum canopy coverage (Table 4.7).

Table 4.7: Parameter Sensitivity Results from SWAT model calibration at Bonou

Parameter Name	t-statistic	P-Value
GW_DELAY	0.031	0.975
REVAPMN	-0.065	0.948
CH_N2	0.083	0.934
GE_REVAP	0.095	0.924
SOL_Z	0.096	0.923
EPCO	0.207	0.836
ESCO	0.271	0.787
SOL_ZMX	0.277	0.782
GWQMN	-0.341	0.733
SOL_BD	-0.771	0.441
CH_K2	-1.086	0.278
SOL_AWC	-1.804	0.072

CANMX	1.926	0.055
CN2	-3.484	0.001
SOL_K	-9.339	0.000
ALPHA_BF	10.160	0.000

4.2.2 Estimated Water Balance Components

The four classified maps from Objective 1 were used to simulate water balance to assess the effect of LULC change on water balance in the basin. The trend of LULC change revealed decreasing Forest and Savanna areas, with increasing Agricultural and Settlements/bare lands from 1986 to 2023. The analysis showed that Water bodies constituted less than 0.01 % of the basin area and exhibited irregular trends in change compared to other land cover types. Consequently, the impact of changes in water bodies on the water balance components was deemed negligible, and these areas were excluded from the statistical analyses to avoid potential inaccuracies in error estimation.

The average annual precipitation over the basin from 1998-2016 was 1155.3 mm and the values for the sub-basins differ (Fig. 4.6). Analysis of the proportions of average annual basin values for water balance components (Table 4.8), including surface runoff, baseflow, lateral flow, actual evapotranspiration, and total aquifer recharge, across different LULC maps and periods revealed significant insights. Among these components, evapotranspiration accounted for the largest fraction of precipitation (57%), followed by total aquifer recharge (approximately 27 %). Lateral flow and surface runoff contributed about 10 %, while baseflow accounted for the smallest fraction.

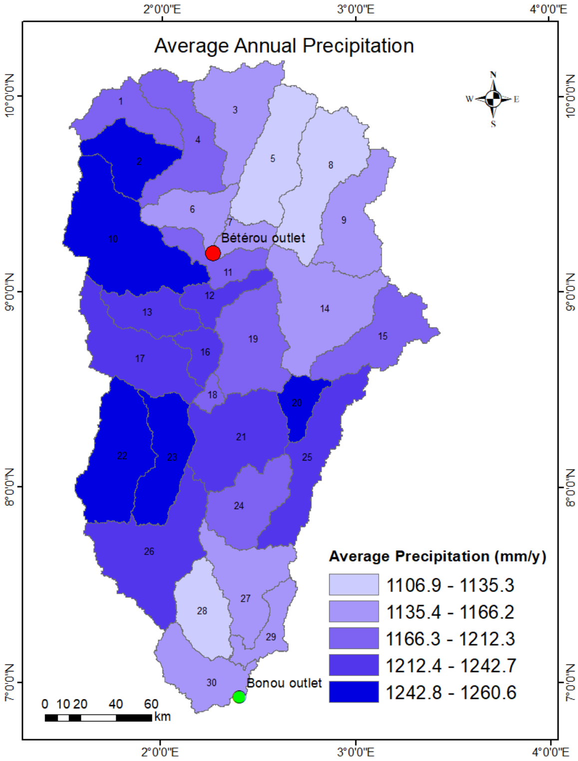

Figure 4.6: Average Annual Precipitation per Sub-basin from 1998-2016

Between 1986 and 2023 LULC maps, surface runoff increased by approximately 67 %, while baseflow, lateral flow, actual evapotranspiration, and aquifer recharge decreased across all periods. For instance, under the 1998-2016 simulation, a reduction of approximately 2,432 km² of Forest and 11,867 km² of Savanna areas, coupled with an increase of 534 km² in Settlements/bare lands and 13,776 km² in Agricultural lands, resulted in a 32 mm/y increase in surface runoff. Concurrently, baseflow, lateral flow, total aquifer recharge, and actual evapotranspiration, reduced by 12 mm/y, 6 mm/y, 26 mm/y, and 5.9 mm/y, respectively.

Table 4.8: Average Annual Water Balance Values for the LULC Maps across Simulation Periods

Period	LULC Map	Surface runoff (mm)	Baseflow (mmx)	Lateral flow (mm)	Total aquifer recharge (mm)	Actual evapotranspiration (mm)
1998-2008	1986	47.15	17.74	114.34	318.41	645.00
	2000	54.03	17.47	112.17	313.75	645.40
	2015	62.40	17.40	110.40	309.98	642.50
	2023	77.81	16.31	108.21	299.33	639.90
2008-2016	1986	50.79	20.03	119.02	338.03	692.70
	2000	58.86	20.77	116.58	332.33	692.80
	2015	68.65	19.50	114.50	327.63	689.80
	2023	85.13	18.04	112.10	316.40	686.90
1998-2016	1986	47.59	56.92	114.35	329.38	671.20
	2000	54.87	54.51	112.11	324.08	671.00
	2015	63.72	52.05	110.25	320.01	668.10
	2023	79.36	44.53	108.02	303.35	665.30

The increase in surface runoff between 2015 and 2023 LULC maps was higher compared to that between 1986 and 2000 maps, and 2000 and 2015 maps, contrary to the smaller number of years between 2015 and 2023 (Table 4.9). For the 1998-2016 simulation, for instance, surface runoff increased by 15.6 mm/y between 2015 and 2023, as compared to 7.28 mm/y and 8.6 mm/y increase from 1986 to 2000, and 2000 to 2015 maps, respectively. At the same time, a higher reduction was observed in baseflow, and total aquifer recharge between the 2000 and 2015 maps, than between 1986 and 2000 maps or 2000 and 2015 maps. This trend was similar across the other two simulation periods, except for baseflow which had much higher reduction over the 16-year simulation period (2.4 mm/y, 2.5 mm/y, and 7.5 mm/y between 1986-2000 maps, 2000-2015 maps and 2015-2023 maps, respectively) than across the two 8-year simulation periods (0.27 mm/y, 0.07 mm/y, 1.09 mm/y and 0.74 mm/y, 1.3 mm/y, and 1.5 mm/y). The trend of simulated discharge across the LULC maps showed increasing peak flows from 1986 > 2000 > 2015 > 2023, which agrees with some historical flood events in Benin such as in 2010 (Fig. 4.7). The Q-Q plots (refer to Appendix 2) indicated that these distributions were approximately normal.

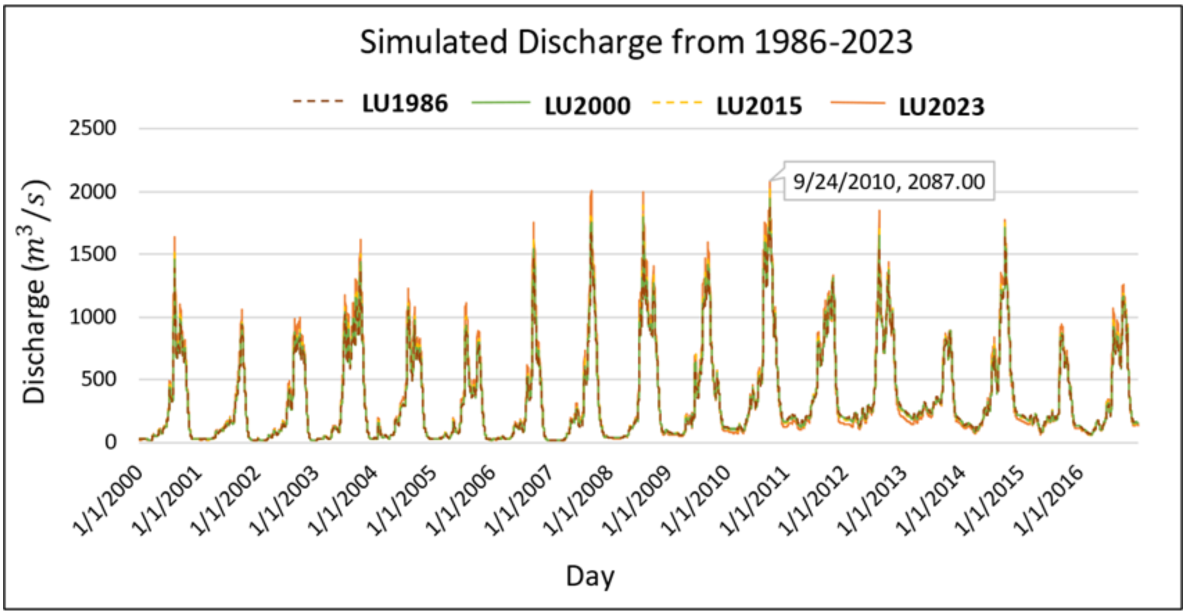

Figure 4.7: Increasing Simulated Peak Flows across the Historical LULC Maps at the Bonou Station

Table 4.9: Change in LULC Versus Change in Water Balance across the Simulation Periods

LULC map	Change in LULC				Change in water balance				
	Forest areas (%)	Settlements/ bare lands (%)	Savanna areas (%)	Agricultural lands (%)	Surface runoff (%)	Baseflow (%)	Lateral flow (%)	Total aquifer recharge (%)	Actual ET (%)
	1998 – 2008 Simulation								
1986-2000	-32.57	+36.30	-5.53	+24.58	+14.59	-1.52	-1.90	-1.46	+0.06
2000-2015	-44.42	+61.94	-11.52	+30.69	+15.49	-0.40	-1.58	-1.20	-0.45
2015-2023	-41.88	+33.77	-21.68	+35.08	+24.70	-6.26	-1.98	-3.44	-0.40
1986-2023	-78.22	+195.25	-34.53	+119.93	+65.03	-8.06	-5.36	-5.99	-0.79
	2008 – 2016 Simulation								
1986-2000	-32.57	+36.30	-5.53	+24.58	+15.89	+3.69	-2.05	-1.69	+0.01
2000-2015	-44.42	+61.94	-11.52	+30.69	+16.63	-6.11	-1.78	-1.41	-0.43
2015-2023	-41.88	+33.77	-21.68	+35.08	+24.01	-7.49	-2.10	-3.43	-0.42
1986-2023	-78.22	+195.25	-34.53	+119.93	+67.61	-9.94	-5.81	-6.40	-0.84
	1998 – 2016 Simulation								
1986-2000	-32.57	+36.30	-5.53	+24.58	+15.30	-4.23	-1.96	-1.61	-0.03
2000-2015	-44.42	+61.94	-11.52	+30.69	+16.13	-4.51	-1.66	-1.26	-0.43
2015-2023	-41.88	+33.77	-21.68	+35.08	+24.54	-14.45	-2.02	-5.21	-0.42
1986-2023	-78.22	+195.25	-34.53	+119.93	+66.76	-21.77	-5.54	-7.90	-0.88

4.2.3 Correlation between Historical LULC and Water Balance

The analysis revealed a strong positive correlation between the area of Forests and the amount of baseflow, lateral flow, total aquifer recharge, and actual evapotranspiration, but a strong negative correlation with the amount of surface runoff (Fig. 4.8). This was similar for Savanna areas. In contrast, the area of Agricultural and Settlements/bare lands had a strong positive correlation with the amount of surface runoff generated and a negative correlation with baseflow, lateral flow, total aquifer recharge and evapotranspiration. These findings indicate a substantial relation between changes in LULC and changes observed in the water balance components. Notably, the strong correlations remained consistent across the three simulated periods (Fig. 4.8), underscoring the persistent and significant influence of LULC changes on regional hydrology.

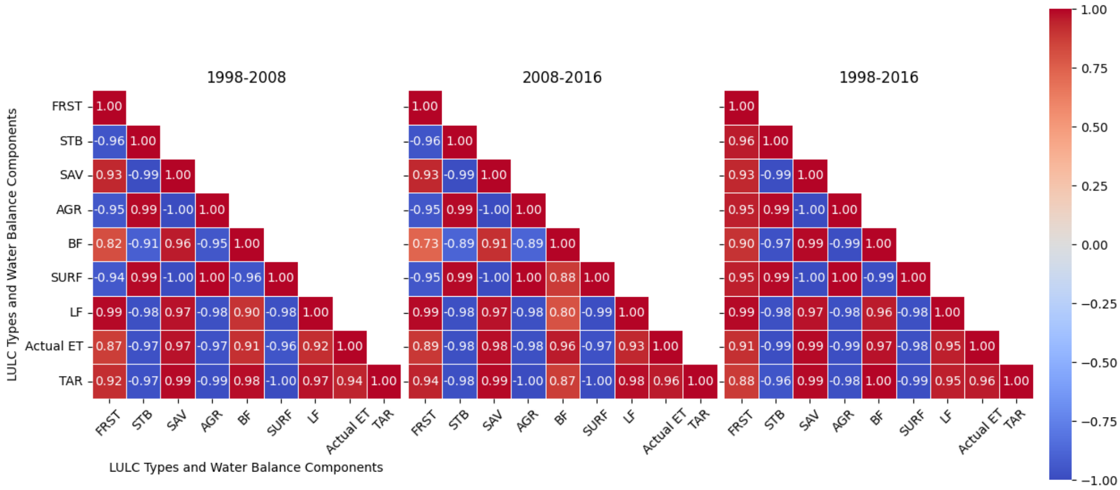

Figure 4.8: Correlation between LULC types and Water Balance Components for 1998-2008, 2008-2016, and 1998-2016[4]

4.2.4 Independent t-test Analysis

Independent t-test analyses were conducted to determine if there were significant differences in mean values of water balance components between the 1986 and 2023 LULC maps across the different periods. The results revealed significant differences

[4] Forest areas (*FRST*), settlements/bare lands (*STB*), savanna areas (*SAV*), agricultural lands (*AGR*), and water balance components, surface runoff (*SURF*), baseflow (*BF*), lateral flow (*LF*), actual evapotranspiration (*ET actual*)

($p<0.05$) for surface runoff, lateral flow, and total aquifer recharge, while baseflow and actual evapotranspiration showed no significant differences.

Specifically, the mean surface runoff of the 2023 LULC map (80.77 mm/y) was significantly higher compared to the 1986 (48.51 mm/y) with a difference of -32.26 ± 7.99 mm (Table 4.10). The t-statistic for surface runoff (-12.88) was notably higher than those for lateral flow (3.15) and total aquifer recharge (2.9), indicating a strong sensitivity of surface runoff to changes in LULC across the three simulated periods. The mean lateral flow obtained for the 2023 map (109.44 mm/y) was significantly lower than that obtained for the 1986 map (115.90 mm/y). The mean total aquifer recharge was significantly higher in the 1986 map (328.61 mm/y) compared to the 2023 map (306.36 mm/y). These findings suggest that the decrease in Forest and Savanna areas between 1986 and 2023 LULC maps together with the expansion of Settlements/bare lands and Agricultural lands led to a considerable increase in surface runoff and reduction in subsurface flow and evapotranspiration in the basin.

Table 4.10: Independent t-test between LULC Map for 1986 and 2023

Water Balance Component	**t-statistic**	**P-value**	**Difference (mm/y) ± 95 % CI**
Surface Runoff (mm/y)	-12.88	0.001	-32.26 ± 7.99
Lateral Flow (mm/y)	3.15	0.034	6.46 ± 5.74
Total Aquifer Recharge (mm/y)	2.90	0.044	22.25 ± 21.37
Baseflow (mm/y)	0.34	0.753	5.27 ± 45.21
Actual Evapotranspiration (mm/y)	0.29	0.788	5.60 ± 53.75

4.2.5 Partial Least Squares (PLS) Regression Analysis

Partial Least Squares (PLS) regression analyses were conducted to deepen the understanding of the relationship between LULC types and water balance components across the periods 1998-2008 (a), 2008-2016 (b), and 1998-2016 (c). The loading patterns for predictor variables (X) and response variables (Y) showed consistent trends over time (Figure 4.9). Components 1 and 2 are the latent variables unto which predictor and response variables were projected to reduce dimensionality. A higher loading value of a variable in a component means that this variable is strongly associated with that component, indicating that this variable plays an important role in explaining the relationship between the predictor and response variables.

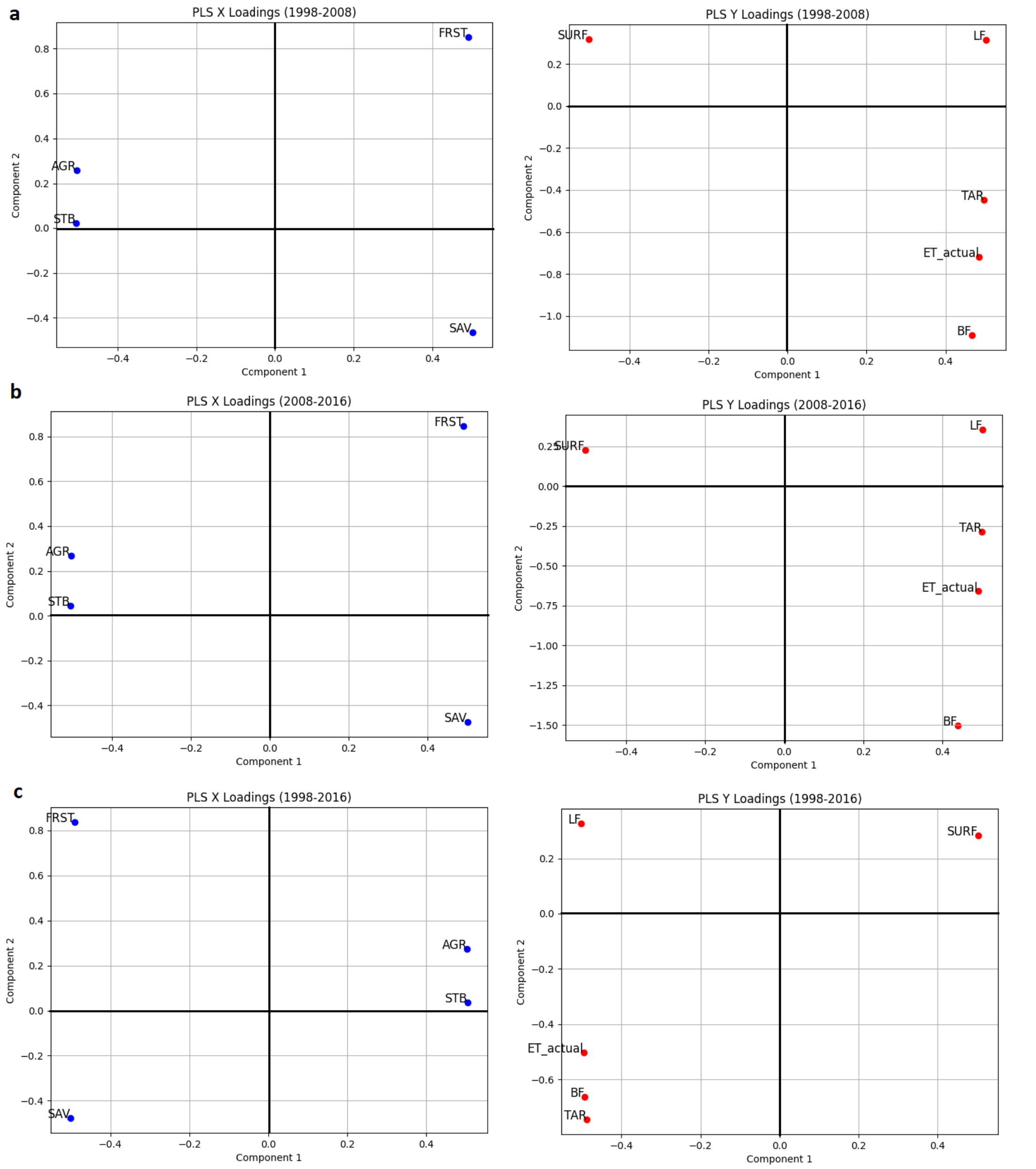

Figure 4.9: LULC (X) and Water Balance Components (Y) Loadings of the PLS Models across the Periods 1998-2008, 2008-2016 and 1998-2016

Component 1 was associated strongly with a reduction in Forest and Savanna areas and an expansion of Settlements/bare lands and Agricultural lands. This corresponds with a decrease in baseflow, lateral flow, total aquifer recharge, and actual evapotranspiration, but an increase in surface runoff. The second component displayed a strong association with Forest expansion and reduction in Savanna areas and a weaker correlation with increases in Agricultural and Settlements/bare lands. This corresponded with decreasing baseflow, total aquifer recharge, and actual evapotranspiration, with a lower increase in lateral flow and surface runoff.

The values of R^2 obtained for PLS1 in Component 1 confirmed the correlation results, demonstrating a strong relationship between the LULC types and the water balance components in ($R^2 \geq 0.85$) across the three periods (Table 4.11). This signifies that LULC changes explain more than 85 % of the variances in surface runoff, baseflow, lateral flow, aquifer recharge and evapotranspiration patterns. The root mean square error (RMSE) of the PLS1 model of all the water balance components ranged between 0.27 mm/y – 2.55 mm/y, signifying good predictive capability of the PLS1 model. Among the water balance components, actual evapotranspiration prediction had the highest RMSE value from the 1998-2016 simulation, while lateral flow had the least from the 1998-2008 simulation.

The results from PLS1 model coefficients show that a unit (1 km^2) increase in Settlements/bare lands led to the highest influence (14.7×10^{-3} mm/y) on surface runoff, increasing it consistently across the three periods in component 1. Agricultural lands also increased runoff (0.6×10^{-3} mm/y), while forest (-13.1×10^{-3} mm/y) and savanna areas (-0.7×10^{-3} mm/y) reduced it (where other LULC types are equal to zero) (Table 4.11). In contrast, lateral flow, baseflow, aquifer recharge, and actual evapotranspiration increased with a unit increase in Forest and Savanna areas, while the increase in Settlements/ bare lands and Agricultural lands decreased them. These trends were consistent across the three simulation periods.

Table 4.11: PLS1 Regression Coefficients of Historical LULC across the Simulation Periods

		PLS1 coefficients of LULC types per water balance component				
Period	LULC type	Surface runoff (10^{-3}mm/y) per km^2 ΔLULC	Lateral flow (10^{-3}mm/y) per km^2 ΔLULC	Baseflow (10^{-3}mm/y) per km^2 ΔLULC	Total aquifer recharge (10^{-3}mm/y) per km^2 ΔLULC	Actual evapotranspiration (10^{-3}mm/y) per km^2 ΔLULC
1998-2008	FRST	-2.96	0.61	0.12	1.79	0.53
	STB	13.95	-2.74	-0.61	-8.46	-2.64
	SAV	-0.65	0.12	0.03	0.40	0.12
	AGR	0.56	-0.11	-0.03	-0.34	-0.11
	Intercept	67.61	109.86	16.90	305.91	641.87
	R^2	0.987	0.986	0.851	0.966	0.918
	RMSE	1.301	0.269	0.210	1.290	0.631
2008-2016	FRST	-3.34	0.69	0.20	2.05	0.60
	STB	15.65	-3.12	-1.10	-9.62	-2.94
	SAV	-0.72	0.14	0.05	0.45	0.14
	AGR	0.63	-0.12	-0.04	-0.39	-0.12
	Intercept	73.98	113.95	19.03	323.55	689.07
	R^2	0.992	0.986	0.760	0.978	0.942
	RMSE	1.162	0.303	0.489	1.176	0.583
1998-2016	FRST	-3.08	0.63	1.15	2.37	0.61
	STB	14.47	-2.83	-5.55	-11.49	-2.95
	SAV	-0.367	0.13	0.26	0.54	0.14
	AGR	0.58	-0.11	-0.23	-0.47	-0.12
	Intercept	68.91	109.72	49.08	313.10	667.41
	R^2	0.989	0.986	0.950	0.961	0.932
	RMSE	1.223	0.278	1.038	0.474	2.548

Overall, changes in the area of Settlements/bare lands followed by changes in Forest areas, had the highest regression coefficients from model predictions of surface runoff, lateral flow, baseflow, total aquifer recharge, and actual evapotranspiration, indicating that they are key predictors of these water balance components in the basin. Component 2 showed inconsistent relationships between Forest areas and water balance, but Settlements/bare lands and Agricultural lands consistently increased runoff and reduced subsurface flow, aquifer recharge and actual evapotranspiration. Savanna areas reduced surface runoff and increased subsurface flows and aquifer recharge.

PLS2 was trained on data from the 1998-2008 simulation, and it gave R^2 values of 0.800 and 0.988 for predicted surface runoff for 2008-2016 and 1998-2016, respectively. Lower R^2 values were obtained for lateral flow, baseflow, total aquifer recharge, and actual evapotranspiration ($R^2 = 0$). This trend was similar for the PLS3 and PLS4 models. PLS3 trained on 2008-2016 simulation data gave R^2 of 0.749 and 0.847 for the period 1998-2008 and 1998-2016, respectively, for surface runoff predictions. Finally, PLS4, trained on 1998-2016 simulation data, also produced strong predictive power with R^2 values of 0.987 and 0.869 when used to predict surface runoff of the 1998-2008 and 2008-2016 periods. Prediction of lateral flow of the 1998-2008 period also gave high R^2 value of 0.991. The predictions of the remaining water balance components showed low predictability ($R^2 = 0$).

The Variable Importance in Projection (VIP) values revealed varying degrees of influence of the LULC types on the different water balance components with similar trends across all three periods (refer to Appendix 4). For surface runoff, aquifer recharge and actual evapotranspiration, changes in Settlements/bare lands, Savanna areas, and Agricultural lands had higher importance than changes in Forest areas (VIP scores ≥ 1). Changes in Settlement/bare lands and Forest areas had a higher influence on lateral flow, while baseflow was more influenced by changes in Savanna areas, Agricultural lands and Forest areas.

4.3 Impact of Projected Future LULC Change on Water Balance

4.3.1 Validation of 2023 Projected LULC

The simulated LULC map for 2023 showed good agreement with the classified map. The proportion of total, quantity, and location agreement are presented in Table 4.12. The CA-Markov projection used was able to predict the increase in agricultural lands from the north, south and northeast of the basin, similar to the pattern in the classified map (Fig. 4.10). However, it predicted fewer changes in the central part of the basin than is observed in the classified map. This is observable in how the validation showed a higher location disagreement than quantity disagreement. Overall agreement of greater than 70 % depicts acceptable projection performance (Leta *et al.*, 2021). The dominant cover projected in the 2023 simulated map based on the transition trend between 1986 and 2015 is Savanna, even though the dominant cover in the classified map is Agricultural lands. Hence, the model underestimated Agricultural lands by 12 %. It is imperative that most of the prediction errors were allocation errors, specifically misclassification between Savanna and Agricultural land. The model also projected more Forests than observed in the classified map, while underestimating settlements/bare lands. Overall, the model performed satisfactorily in predicting LULC for 2023, and the results highlight the strengths and shortcomings of the CA-Markov projections in this study.

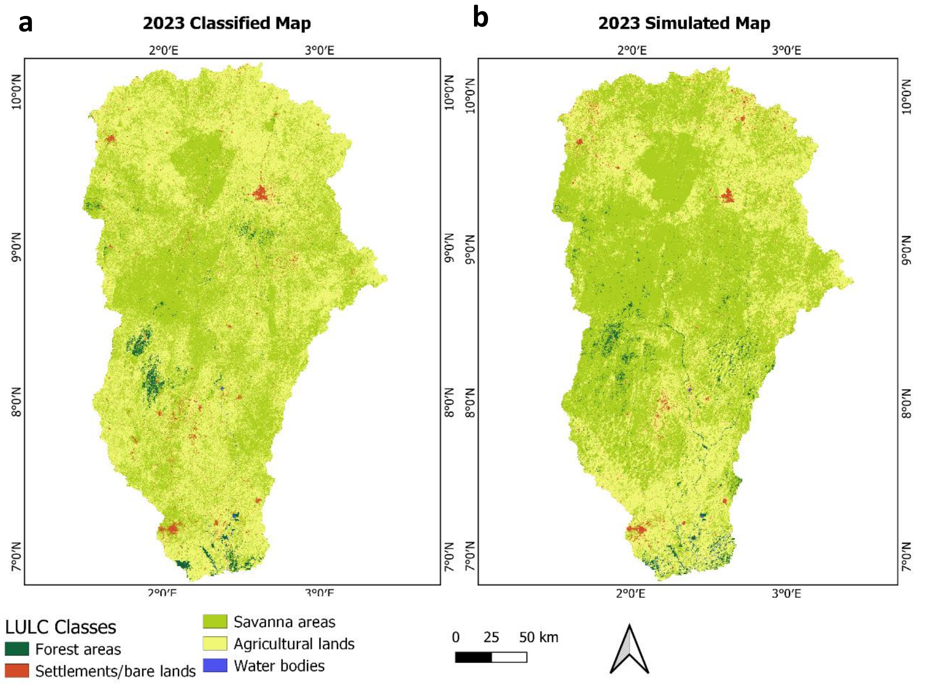

Figure 4.10: The classified 2023 LULC (a) and CA-Markov simulated 2023 LULC (b) Maps

Table 4.12: Area of LULC Types in the Classified and Simulated 2023 Maps

	Classified 2023 Map		**Simulated 2023 Map**		**Difference**	
LULC Type	km^2	(%)	km^2	(%)	km^2	(%)
Forest areas	677.08	(1.37)	1039.70	(2.11)	+362.62	(+0.74)
Settlements/bare lands	807.47	(1.64)	700.26	(1.42)	-107.21	(-0.22)
Savanna areas	22501.23	(45.66)	28266.09	(57.36)	+5764.86	(+11.70)
Agricultural lands	25263.42	(51.26)	19215.45	(38.99)	-6047.97	(-12.27)
Water bodies	31.03	(0.06)	58.73	(0.12)	+27.70	(+0.06)
Total	49280.23	(100)	49280.23	(100)		

Performance metrics	**Value**
Total agreement	0.74
Quantity agreement (disagreement)	0.69 (0.08)
Location agreement (disagreement)	0.70 (0.18)

4.3.2 Projected Future Change in LULC

The projected LULC for the years 2030, 2063 and 2100 under the 'business as usual' scenario are presented in Table 4.13. A general trend of reducing Forest areas, Savanna areas and water bodies, alongside increasing Settlements/bare lands and Agricultural lands was observed from 2030 to 2063 and 2063 to 2100 (Fig. 4.11). The absolute magnitude of change in LULC differs with the future period and LULC type. The highest reduction in Forests (311.4 km^2) and Savanna (2218.5 km^2), and increase in Agricultural land (2042.0 km^2) were observed between 2030 and 2063, while the highest increase in Settlements/bare land was observed from 2063-2100. Forest areas reduced by 125.9 km^2 from 2023 to 2030, while Savanna areas reduced by 1211.6 km^2, and Agricultural and Settlements/bare lands increased by 1234.6 km^2 and 114.6 km^2, respectively. From 2063 to 2100, Forests further reduced by 159.9 km^2 and Savanna by 2158.3 km^2, while Agricultural and Settlements/bare land increased by 1748.5 km^2 and 572.1 km^2, respectively. Overall, the highest average rates of change were reduction in Forest area (2.8 %/y) and Water bodies (7 %/y), followed by the rate of increase in Settlements/bare lands (1.4 %/y). The reduction in Savanna areas (0.5 %/y) and increase in Agricultural lands (0.4 %/y) had the lowest rates. The trend of projected LULC changes suggests continued deforestation and an increase in Agricultural and Settlements/bare land up to the end of the 21st century if activities on the land within the basin continue as have been in the past.

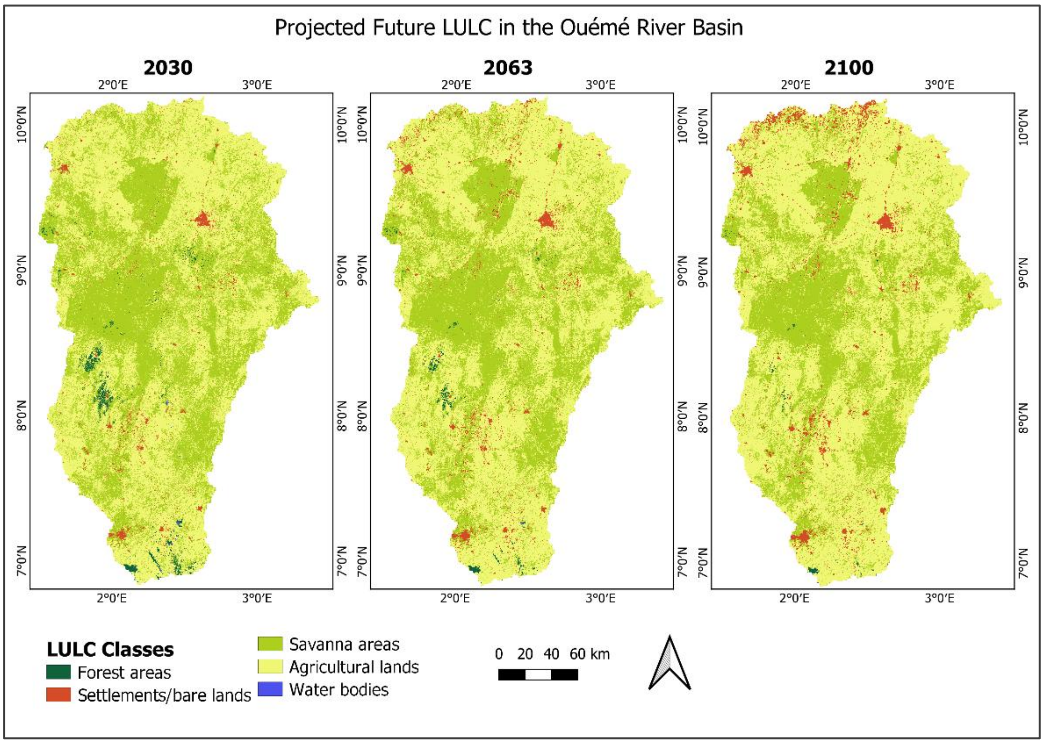

Figure 4.11: Projected LULC Maps for 2030, 2063, and 2100 using CA-Markov Projection

Table 4.13: Area of LULC Types in Projected 2030, 2063 and 2100 Maps

LULC type	Projected LULC Map						Change in LULC	
	2030		2063		2100		2063 – 2030	2100 – 2063
	km^2	(%)	km^2	(%)	km^2	(%)	%/y	%/y
Forest areas	551.15	(1.12)	239.76	(0.49)	79.89	(0.16)	-2.49	-3.28
Settlements/bare lands	922.11	(1.87)	1426.69	(2.90)	1998.81	(4.06)	+1.33	+1.03
Savanna areas	21289.64	(43.20)	19071.18	(38.70)	16912.85	(34.32)	-0.33	-0.36
Agricultural lands	26498.06	(53.77)	28540.09	(57.91)	30288.57	(61.46)	+0.23	+0.18
Water bodies	19.28	(0.04)	2.52	(0.01)	0.12	(0.00)	-5.98	-9.13
Total	49280.23	(100)	49280.23	(100)	49280.23	(100)		

Table 4.14: Change in Water Balance Based on Future LULC Maps

Projected LULC	Average Annual Amounts of Water Balance Components				
	Surface runoff (mm)	Lateral flow (mm)	Baseflow (mm)	Total aquifer recharge (mm)	Actual evapotranspiration (mm)
2023	79.36	108.02	44.53	303.35	665.3
2030	110.94	66.44	39.00	314.53	670.4
2063	119.42	65.36	35.88	307.71	669.8
2100	128.15	64.27	31.22	301.93	667.9
Change (%/y)					
2023-2030	+4.902	-6.708	-1.876	0.518	0.109
2030-2063	+0.223	-0.050	-0.252	-0.066	-0.003
2063-2100	+0.191	-0.045	-0.375	-0.051	-0.008

4.3.3 Relationship between Projected LULC Change and Water Balance

Results from simulating water balance using the projected LULC maps for 2030, 2063 and 2100 showed considerable differences (Table 4.14). Analysis of the changes in average annual surface runoff showed a steep increase between 2023 and 2030 (39.7 %), and a fairly steady increase from 2030-2063 (7.6 %) and 2063-2100 (7.3 %). Lateral flow decreased by 38.5 % between 2023-2030, 1.6 % from 2030-2063, and 1.7 % between 2063-2100. Baseflow showed similar rates of reduction for 2023-2030 (12.4 %) and 2063-2100 (12.9 %), and lower reduction from 2020-2063 (8 %). Total aquifer recharge and actual evapotranspiration increased from 2023-2030 but reduced from 2030 to 2100. Total aquifer recharge increased by 3.7 % from 2023-2030 but reduced between 2030-2063 (2.2 %) and 2063-2100 (1.9 %). Actual evapotranspiration showed the lowest change over time with an increase of 0.8 % from 2023-2030 and a reduction of 0.1 % and 0.3 % from 2030-2063 and 2063-2100, respectively.

The PLS model coefficients of the relationship between the absolute average annual values of the projected water balance and the projected area of LULC types from Component 1 are presented in Table 4.15. The regression coefficients show that an increase in Settlements/bare land and Agricultural land results in an increase in surface runoff, and a reduction in lateral flow, baseflow, total aquifer recharge, and actual evapotranspiration. The effect (magnitude of regression coefficient) of Settlements/bare land was higher than that of Agricultural land. An increase in Forest and Savanna areas reduced surface runoff while increasing lateral flow, baseflow, total aquifer recharge, and actual evapotranspiration, with a higher influence of Forests than Savanna.

Overall, the results show that in the future, further expansion in Settlements/bare land (e.g., urbanisation) and Agricultural land is projected to enhance surface runoff and reduce subsurface flow and aquifer recharge, while expansion in Forest and Savanna areas (e.g., reforestation) will reduce surface runoff and improve subsurface flow and aquifer recharge. Forest areas and settlements/bare lands had the highest coefficients, suggesting they are key predictors (indicators) of changes in the hydrological processes assessed. The PLS model shows LULC changes over time, which explained more than 90 % of the variances in the water balance components over time ($R^2>0.90$). The RMSE values <1 also depict the strong predictive capability of the model in predicting the changes in water balance in the basin from changes in LULC

.

Table 4.15: PLS Regression Coefficients, R^2 and RSME of Projected Future LULC Effect on Water Balance Components

Projected LULC (km^2)	Surface runoff 10^{-3}mm/y per km^2 ΔLULC	Lateral flow 10^{-3}mm/y per km^2 ΔLULC	Baseflow 10^{-3}mm/y per km^2 ΔLULC	Total aquifer recharge 10^{-3}mm/y per km^2 ΔLULC	Actual evapotranspiration 10^{-3}mm/y per km^2 ΔLULC
Forest Areas	-4.60	1.06	1.75	3.17	0.37
Settlements/bare land	2.36	-0.54	-0.91	-1.64	-0.18
Savanna areas	-0.52	0.12	0.20	0.36	0.04
Agricultural lands	0.57	-0.13	-0.22	-0.40	-0.04
Intercept	63.54	110.62	52.14	319.79	668.13
R^2	0.989	0.991	0.983	0.982	0.935
RMSE	0.465	0.092	0.221	0.416	0.090

4.4 Impact of Future Climate Change on Water Balance

4.4.1 Future Climate Projections for Scenarios SSP1-2.6 and SSP3-7.0

The bias correction of the precipitation and temperature data from the climate models using the Quantile Mapping approach performed well. The total mean bias error (*mbe*) of the corrected precipitation and temperature data was lower than the raw (uncorrected) data plotted against the reference. For instance, the raw (uncorrected) precipitation of the ACCESS-CM2 model data plotted against the reference (CHIRPS) data gave *mbe* of -34.31 mm and a correlation coefficient of 0.78, while the corrected data gave *mbe* of -0.07 mm with a correlation coefficient of 0.76. The correlation between the corrected and uncorrected model data was strongly positive ($r \geq 0.96$) across the six global climate models. The ACCESS-CM2 model precipitation performed better in capturing the trend in reference data, hence, it was chosen for water balance assessments. The bias-corrected ensemble mean performed better for the minimum and maximum temperature data with lower *mbe* and higher correlation than the uncorrected data. Plots of the bias-correction results of the other models are presented in Appendix 3.

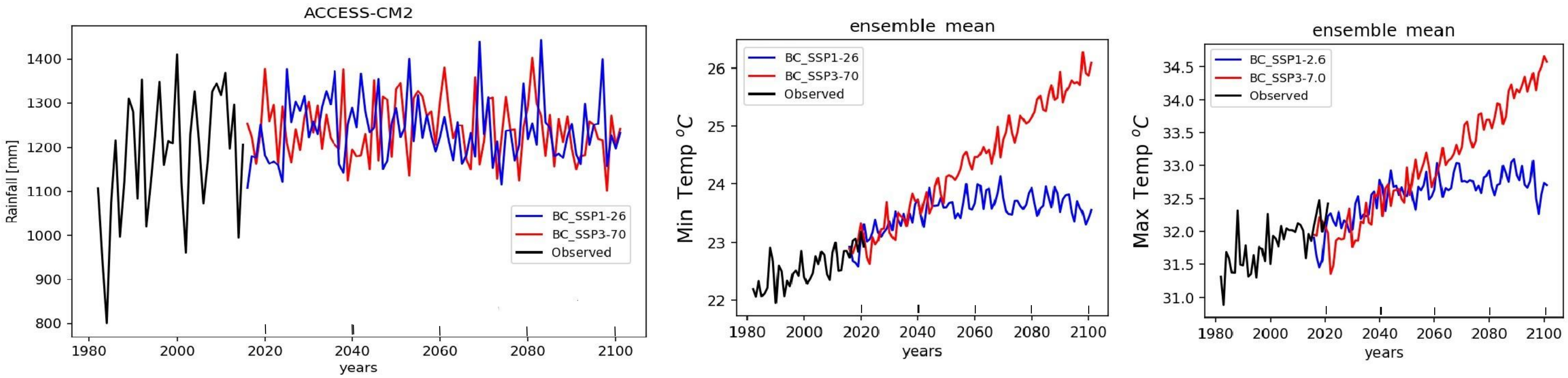

Figure 4.12 Bias-corrected Historical and Future precipitation (a), Minimum (b) and Maximum temperature (c) trends for the Ouémé River Basin, under SSP1-2.6 and SSP3-7.0 Scenarios for the Near, Mid-, and Long term future.

Average precipitation and minimum and maximum temperature across scenarios and periods (near term (2021-2040), mid-term (2041-2060) and long term (2081-2100)) over the catchment area are presented in Fig.4.12, together with the projected changes over the catchment area (Table 4.16).

The average precipitation of the baseline (historical) data (1995-2014) was 1223 mm, while the minimum temperature data ranged between 16 ^{o}C – 27 ^{o}C, and the maximum temperature between 22 ^{o}C – 38 ^{o}C (Fig. 4.13). Relative to the baseline, precipitation is projected to increase under SSP1-2.6 and SSP3-7.0 scenarios and across the future periods. In the near term, there is a higher increase in precipitation under SSP1-2.6 than under SSP3-7.0, similar to the long term. However, during the mid-term, precipitation is higher under SSP3-7.0 than SSP1-2.6. The precipitation under SSP1-2.6 generally increased from near term to mid-term (+0.4 %) and reduced from the mid-term to long-term (−1.4 %) more gradually compared to SSP3-7.0, where precipitation increases sharply from the near-term to mid-term (+2.8 %) and drops steeply from the mid-term to the long-term (−4.0 %). This suggests more extreme rainfall event scenarios under SSP3-7.0 compared to a gentler variability in rainfall under the SSP1-2.6 scenario.

The projected changes in minimum and maximum temperature were fairly similar under SSP1-2.6 and SSP3-7.0 scenarios in the near term (Table 4.16). From the near-term to mid-term, minimum temperature increases (+0.3 %) under SSP1-2.6 while maximum temperature reduces (−0.3 %). During the same period, the minimum temperature increases by 0.8 % under SSP3-7.0, while the maximum temperature increases by 0.7 %. Between the mid-term and long term, the minimum temperature reduces (−0.01 %) while the maximum temperature increases by 0.8 % under SSP1-2.6. Under SSP3-7.0, minimum and maximum temperatures increase by 1.6 % and 0.8 %, respectively.

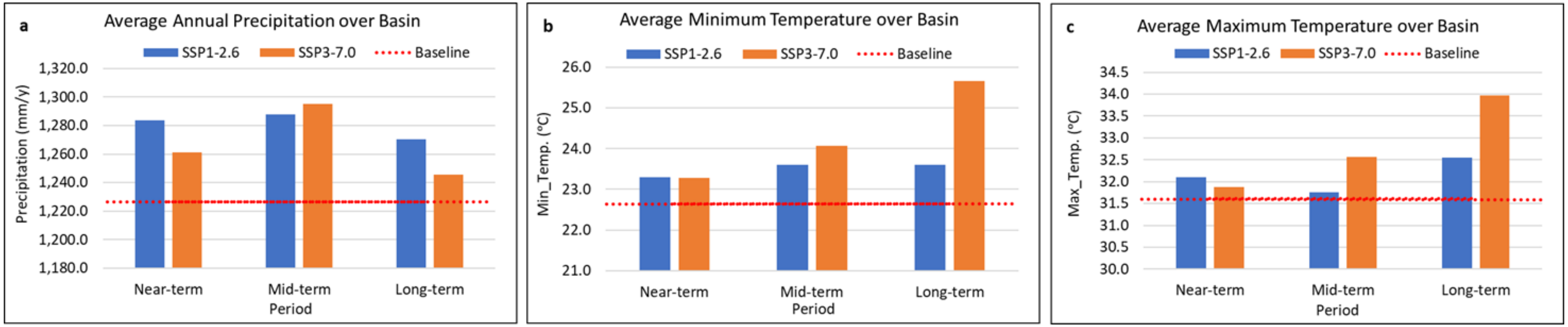

Figure 4.13: Projected Average Precipitation (a), Minimum (b) and Maximum (c) Temperature for Baseline Period, Near-term, Mid-term, and Long-term over the Basin under SSP1-2.6 and SSP3-7.0

Table 4.16: Projected Changes in Climate Change across Climate Scenarios and Future Periods

Change	Climate Scenario	Precipitation (%)	Minimum Temperature (°C)	Maximum Temperature (°C)
Near-term – historical	SSP 1-2.6	+4.66	+0.65	+0.49
	SSP 3-7.0	+2.83	+0.63	+0.25
Mid-term – historical	SSP 1-2.6	+5.01	+0.96	+0.14
	SSP 3-7.0	+5.61	+1.42	+0.96
Long-term - historical	SSP 1-2.6	+3.57	+0.95	+0.94
	SSP 3-7.0	+1.57	+3.01	+2.36

4.4.2 Future Water Balance Based on Future Climate

The projected precipitation for the three future periods (near term, mid-term and long term) was used to simulate water balance under constant LULC and soil conditions. This was done to ensure that changes in water balance were solely, a result of climate change. Only the 2023 LULC was used for this analysis because it represents the most current conditions, which serve as a baseline for future projections. The difference in water balance components between the future periods was also computed to ascertain the amount of change possible between those periods.

It can be observed from the change in water balance results in Fig. 4.14 and Table 4.17 that, under SSP1-2.6 scenarios, surface runoff reduced both from the near- to the mid-term and from the mid- to the long term. However, under scenario SSP3-7.0, surface runoff increased strongly from the near- to mid-term and reduced from the mid- to long term. Lateral flow and total aquifer recharge exhibited similar trends as surface runoff, with reductions from the near- to mid-term despite precipitation increase under SSP1-2.6 during the same period. Notwithstanding, lateral flow and aquifer recharge increased under SSP3-7.0 from the near to mid-term in response to a high increase in precipitation though temperature also increased within that period. From the mid- to long term, lateral flow, baseflow, and aquifer recharge reduced in response to the reduction in precipitation accompanied by increased temperature under SSP1-2.6 and SSP3-7.0. However, actual evapotranspiration reduced steadily under SSP1-2.6 mid-term to long term and increased from the near term to long term as temperature increased.

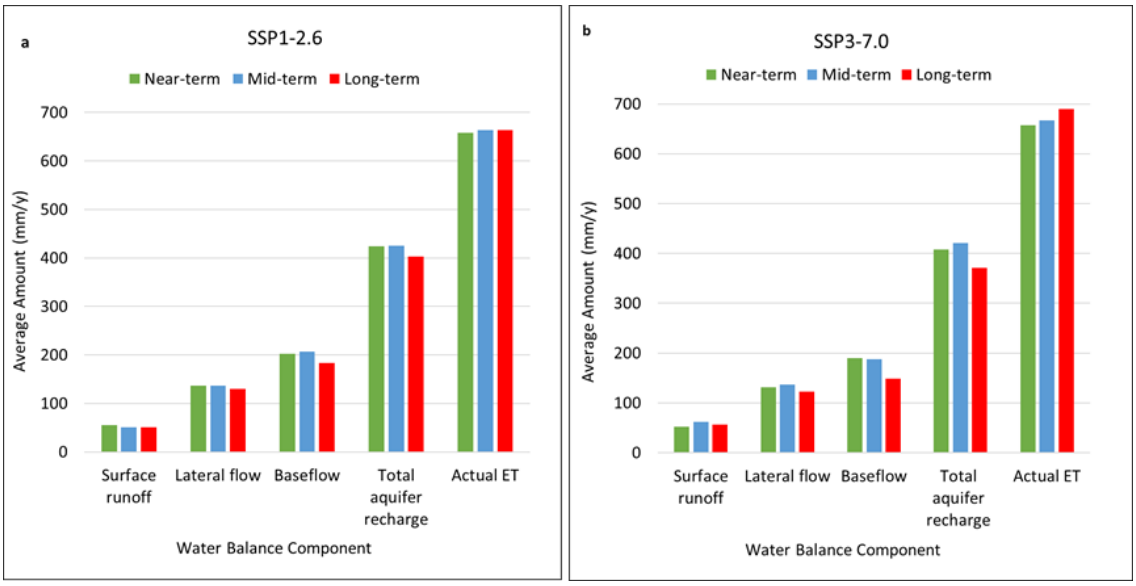

Figure 4.14: Estimated Water Balance Components based on Projected Climate in the near term, Mid-term and Long term Future

Table 4.17: Change in water balance components between the SSP1-2.6 and SSP3-7.0 future climate scenarios

Change	Climate Scenario	Surface runoff (%)	Lateral flow (%)	Baseflow (%)	Total aquifer recharge (%)	Actual evapotranspiration (%)
Near- to Mid-term	SSP1-2.6	-7.39	-0.60	+2.31	-0.13	+0.85
	SSP3-7.0	+20.01	+4.37	-0.83	+3.16	+1.60
Mid- to long-term	SSP1-2.6	-1.17	-4.64	-11.70	-5.15	-0.15
	SSP3-7.0	-9.20	-10.79	-20.97	-11.85	+3.37

4.4.3 Relationship between Future Climate and Water Balance

A PLS regression was employed to estimate the relationship between the projected climate variables and the amount of surface runoff, lateral flow, baseflow, total aquifer recharge and actual evapotranspiration. The regression coefficients gave higher values for both precipitation (P) and temperature (T) in predicting surface runoff, total aquifer recharge and actual evapotranspiration than lateral flow and baseflow (Table 4.18). This indicates that both precipitation and temperature changes affect the changes in Ouémé River Basin's hydrology. Particularly, a unit (mm/y) increase in average precipitation is projected to increase surface runoff, lateral flow, baseflow, and total aquifer recharge but reduce actual evapotranspiration. The increase in surface runoff and decrease in actual evapotranspiration were minute under SSP1-2.6 compared to SSP3-7.0. With a unit (°C) increase in mean temperature, surface runoff reduced under SSP1-2.6 but increased under SSP3-7.0. The higher coefficients of change in lateral flow, baseflow, and total aquifer recharge with a unit increase in temperature demonstrate the high sensitivity of these components, even when precipitation increases. Actual evapotranspiration increased with a unit increase in temperature due to the higher evaporative demand under warmer climate conditions. Baseflow and actual evapotranspiration predictions gave the highest errors, meaning the PLS model could not capture the variability in those components well enough.

Table 4.18: PLS Regression Coefficients of Future Climate Effect on Water Balance Components

		PLS model coefficients				
Climate scenario	Climate variable	Surface runoff (mm/y)	Lateral flow (mm/y)	Baseflow (mm/y)	Total aquifer recharge (mm/y)	Actual evapotranspiration (mm/y)
SSP 1-2.6	P (mm/y)	0.06	0.20	0.71	0.67	-0.02
	T (°C)	-3.49	-8.82	-28.89	-28.38	2.70
	RMSE	1.80	0.73	0.56	1.08	2.35
SSP 3-7.0	P (mm/y)	0.21	0.19	0.45	0.61	-0.24
	T (°C)	1.79	-3.31	-13.26	-12.72	10.65
	RMSE	0.86	0.76	2.6	0.68	4.34

4.5 Combined Impact of Future LULC and Climate Change on Water Balance

The projected future LULC for 2030 and climate for the near term (2021-2040) were used to simulate water balance. The 2063 and 2100 LULC maps were combined with climate for the mid-term (2041-2060) and long term (2081-2100), respectively. They were conducted under SSP1-2.6 and SSP3-7.0 to examine the combined impact of LULC and climate change on water balance.

Surface runoff increased steadily from 2030 to 2100 under SSP1-2.6, while under SSP3-7.0, it increased from 2030-2063 and decreased from 2063-2100 (Fig. 4.15). The rate of increase in surface runoff from 2030 to 2063 was higher under SSP3-7.0 than under SSP1-2.6 (Table 4.19). Lateral flow decreased from 2030-2100 under SSP1-2.6

while under SSP3-7.0, increased from 2030-2063 and decreased from 2063-2100. Baseflow increased from 2030-2063 and decreased largely under both SSPs from 2063-2100, with a higher magnitude of change under SSP3-7.0 than SSP1-2.6. Under SSP3-7.0, total aquifer recharge increased from 2030-2063 and decreased from 2063-2100. The decrease in total aquifer recharge from 2063-2100 was higher under SSP3-7.0 than under SSP1-2.6. Actual evapotranspiration under SSP1-2.6 increased from 2030-2063 and decreased from 2063-2100, while under SSP3-7.0, it increased over the period up to 2100. The results show that both LULC and climate changes influence water balance in the basin. The pattern of changes in water balance components was similar to the pattern of precipitation changes across the future periods for both SSP1-2.6 and SSP3-7.0. The average annual values of surface runoff and lateral flow obtained for the combined projected LULC and climate change scenario were higher than those obtained for the projected climate alone and lower than those for the projected LULC alone. Baseflow values for the combined LULC-climate scenario were similar to those obtained for the sole projected climate scenario but higher than those obtained for the sole projected LULC.

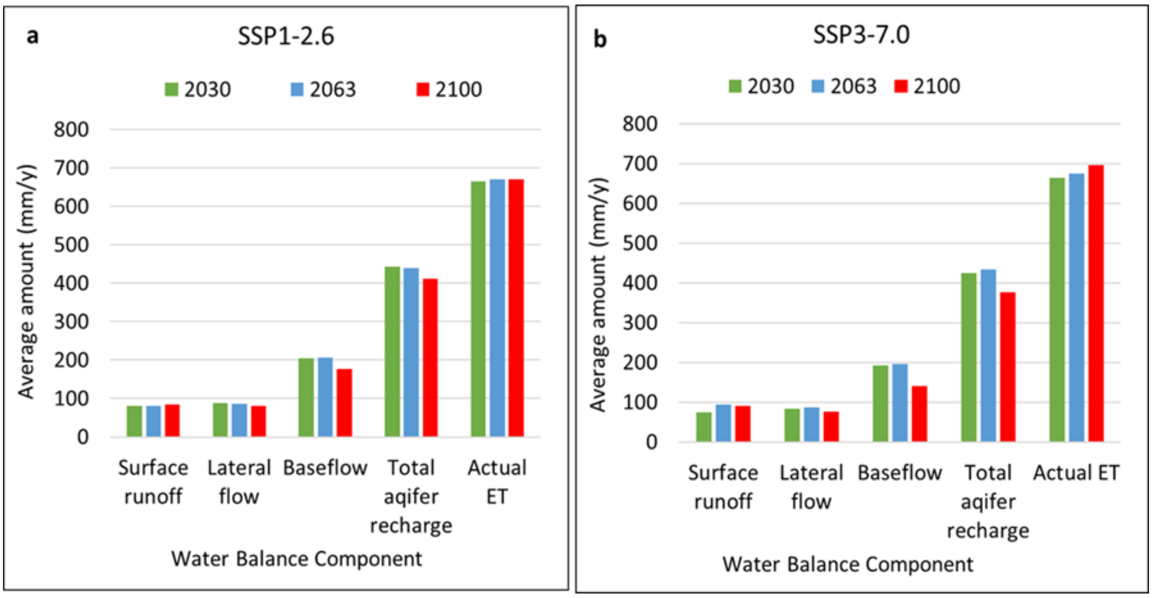

Figure 4.15: Estimated Water Balance Based on Combined Projected Future LULC and Climate under SSP1-2.6 (a) and SSP3-7.0 (b) Scenarios

Table 4.19: Change in Water Balance Components under Combined Projected LULC-Climate Change

Period	Scenario	Surface runoff (mm/y)	Lateral flow (mm/y)	Baseflow (mm/y)	Total aquifer recharge (mm/y)	Actual evapotranspiration (mm/y)
2030-2063	SSP1-2.6	+0.44	-1.14	+0.22	-3.99	+5.8
	SSP3-7.0	+18.95	+2.48	+3.59	+7.57	+10.6
2063-2100	SSP1-2.6	+3.46	-4.73	-28.5	-27.25	-1.6
	SSP3-.70	-2.82	-10.26	-54.24	-56.64	+|\\\\21.7

The PLS regression coefficients from Component 1 show that under both SSP1-2.6 and SSP3-7.0, an increase in precipitation, Forest and Savanna areas reduces surface runoff and actual evapotranspiration, while increasing lateral flow, baseflow and total aquifer recharge (Table 4.20). An increase in precipitation under SSP-3.70 increased surface runoff. However, an increase in temperature, Agricultural and Settlement/bare land increases surface runoff and actual evapotranspiration while reducing lateral flow, baseflow and aquifer recharge. Temperature had the highest coefficient, followed by precipitation, Forest areas, and Settlements/bare lands. Savanna and Agricultural land had the lowest coefficients. This signifies that, changes in temperature, precipitation, Forest areas and Settlements/bare land are key predictors (indicators) of changes in the basin's hydrological processes, as observed in Objectives 3 and 4. The variances in water balance components were reasonably explained by the variances in LULC and climate (R^2>0.7).

Table 4.20: PLS Regression Coefficients, R^2 and RSME of the Relationship between Combined LULC-Climate and Water Balance Components

Scenario	Variable	Surface runoff (mm/y)	Lateral flow (mm/y)	Baseflow (mm/y)	Total aquifer recharge (mm/y)	Actual evapotranspiration (mm/y)
SSP1-2.6	P (mm/y)	-0.04	0.06	0.33	0.33	-1.26 × 10^{-3}
	T (°C)	1.78	-2.57	-14.02	-14.27	0.70
	FRST	-1.38 × 10^{-3}	2.11 × 10^{-3}	9.83 × 10^{-3}	11.11 × 10^{-3}	-2.32 × 10^{-3}
	STB	0.69 × 10^{-3}	-1.04 × 10^{-3}	-5.10 × 10^{-3}	-5.55 × 10^{-3}	0.85 × 10^{-3}
	SAV	-0.17 × 10^{-3}	0.25 × 10^{-3}	1.22 × 10^{-3}	1.34 × 10^{-3}	-0.22 × 10^{-3}
	AGR	0.19 × 10^{-3}	-0.29 × 10^{-3}	-1.38 × 10^{-3}	-1.52 × 10^{-3}	0.26 × 10^{-3}
	R^2	0.950	0.976	0.901	0.955	0.502
	RMSE	0.390	0.392	4.215	2.934	1.726
SSP3-7.0	P (mm/y)	0.03	0.04	0.19	0.21	-0.63
	T (°C)	1.31	-0.86	-5.09	-5.09	2.86
	FRST	-8.42 × 10^{-3}	2.88 × 10^{-3}	18.97 × 10^{-3}	18.28 × 10^{-3}	-12.70 × 10^{-3}
	STB	3.23 × 10^{-3}	-1.63 × 10^{-3}	-10.01 × 10^{-3}	-9.88 × 10^{-3}	6.00 × 10^{-3}
	SAV	-0.82 × 10^{-3}	0.39 × 10^{-3}	2.39 × 10^{-3}	2.35 × 10^{-3}	-1.47 × 10^{-3}
	AGR	0.98 × 10^{-3}	-0.43 × 10^{-3}	-2.69 × 10^{-3}	-2.64 × 10^{-3}	1.68 × 10^{-3}
	R^2	0.716	0.742	0.843	0.807	0.990
	RMSE	4.448	2.221	9.798	11.021	1.376

CHAPTER 5 GENERAL DISCUSSION

5.1 Assessment of LULC Change in the Ouémé River Basin

The spatio-temporal trends in LULC showed significant changes in LULC within the Ouémé River Basin. The 1986 LULC map revealed that the basin was predominantly Savanna, however over time, these areas and Forests have been cleared, converted mainly into Agricultural land and Settlements. This corroborates with findings by (Bodjrènou *et al.,* 2023a) who observed a reduction in Savanna areas, and expansion in Agricultural land and urban areas. Studies within areas around the basin, such as in the Couffo catchment (Togbévi *et al.,* 2021) and Ouémé Delta (Osseni *et al.,* 2022) have also indicated the conversion of naturally vegetated areas into croplands. These trend of LULC change affect the basin by increasing soil erosion and vulnerability to floods through enhanced surface runoff. Erosion hotspots were identified in the Ouémé River Basin by Hiepe (2008) especially, in areas where Agricultural lands were rapidly expanding. Bossa (2012) also established that, LULC changes in the basin enhanced soil degradation and increased sediment yield. Furthermore, Dossou *et al.* (2021b) discovered that, intensive agriculture in the basin, particularly cotton and cowpea crops made the basin more vulnerable and fragile through land degradation. Communes (such as Djougou and Perere, and Bohicon, Covè, Glazoue, Zangnanado, Toffo and Djidja) within the basin, especially where Agricultural lands have expanded at the expense of natural vegetation, are more vulnerable to flooding (Hounkpè *et al.*, 2022).

The accuracy assessment of the classified maps demonstrated high agreement with the reference areas, indicating the reliability of the Simple Composite Landsat and the Random Forest Classifier algorithms with remotely sensed data in the GEE cloud computing platform for evaluating LULC information. However, challenges remain in accurately classifying Settlement areas and bare lands, which exhibit similarities in appearance and reflectance with Agricultural lands during the dry season for which images were used. The presence of clouds and the resolution of the Landsat image also influenced classification accuracy, highlighting the need for further refinement in classification methods and the potential benefits of higher-resolution satellite data ((Fisher *et al.,* 2018; Momeni *et al.,* 2016).

The findings also show that deforestation and expansion in Agricultural lands and Settlement areas over time have accelerated in recent years, particularly between 2015 and 2023. This agrees with assessments of LULC change in Benin by the US Geological Survey, which identified the country as experiencing high annual Agricultural land expansion (Tappan *et al.,* 2016). The rapid loss of tree cover in the basin affects ecosystem functioning, as Forests and Savanna serve as crucial carbon sinks (Wheeler *et al.,* 2016). Consequently, the degradation of natural vegetation contributes to increased carbon emissions and exacerbates global warming and changes in climate (McNicol *et al.,* 2018). Moreover, the susceptibility of the basin to extreme events like flooding is exacerbated by the degradation of natural vegetation, as highlighted by studies assessing flood risks in the region (Dossou *et al.,* 2021b; Hounkpè *et al.,* 2019).

Population growth within and around the basin emerges as a primary driver of anthropogenically influenced land use/cover change. Population growth leads to greater demand for food, water, and settlements, driving the expansion of Agricultural lands and Settlements/bare lands. Dense road networks (as seen around Bohicon, Djougou and Parakou) and access to water sources for irrigation further facilitate agricultural expansion. Soils in parts of the basin have also propelled the progressive expansion of agricultural and other economic activities within the basin, with different soil types supporting various agricultural activities (Osseni *et al.,* 2022). Ferralitic soils in the southern part of the basin are suitable for plantations and commercial vegetable production, while ferruginous soils in the central and northern parts support crops like cotton, peanut, sorghum, millet, and tobacco. Additionally, the lower zones prone to ponding during rainfall, known as the 'Bas-Fonds' are utilised for rice production (Sinsin and Kampmann, 2010).

Considering the projected continued population growth in Benin and Africa as a whole, as indicated by IPCC sixth report, it is important to manage LULC in the basin effectively, including reduced deforestation and more sustainable agricultural practices to ensure the sustainability of the environment and inherent resources including water and soil for improving food and water security.

5.2 Impact of Past LULC Change on Water Balance

The SWAT model calibration and validation at the upstream Bétérou and downstream Bonou stations yielded satisfactory results with higher values of NSE (0.81-0.91), PBIAS (-6.6 - (-14.4)), R^2 (0.83-0.92) similar to those obtained by (Moriasi *et al.* (2007) and Gui *et al.* (2021). Although negative PBIAS values indicated some overestimation, they remained within acceptable limits. This suggests that though the model captures the basin's overall hydrological processes well, there are some discrepancies, which could be attributed to the uncertainties in the input (e.g., climate data) and calibration procedure (Odusanya *et al.,* 2021). At Bétérou, the p-factor values of the model calibration and validation were above the recommended threshold (0.50), indicating that, more than half of the observed discharge data fell within the predicted uncertainty range, suggesting a reasonable predictive capacity of the model (Abbaspour, 2015).

On the contrary, at Bonou, the p-factor values were slightly below the threshold, signaling that more than half of the uncertainty in the observed discharge was not well captured by the calibration, due possibly to low-quality of input data or model parameterization (Fisher *et al.,* 2018; Hounkpè and Diekkrüger, 2018). The r-factor values obtained at Bonou exceeded 1.2, reflecting a wider uncertainty band, a common challenge when simulating hydrological processes in complex tropical basins (Bossa *et al.,* 2014; Saddique *et al.,* 2020). Such findings suggest further calibration efforts, including incorporating higher-resolution satellite data or refining key parameters that could reduce this uncertainty. In addition, other hydrological processes can be considered to address the uncertainty and improve the model parametrization, such as the actual evapotranspiration or the vegetation growth coupled with an evapotranspiration estimation (Odusanya *et al.,* 2021; Merk *et al.,* 2024).

The results from the independent t-test indicated significant differences between the mean surface runoff, lateral flow, and total aquifer recharge from the 1986 LULC map and the mean values from the 2023 map. This demonstrates that, these water balance components are very sensitive to LULC changes. Though the difference in baseflow and actual evapotranspiration showed no statistical significance, the results still reflect important ecological effects (White *et al.,* 2014), suggesting that, these components are affected by LULC changes, which could be more gradual or less immediate. These findings corroborate with studies in the Upper and Lower Ouémé Basin, which found that, degraded agricultural areas experienced lower soil infiltration capacity, resulting in higher runoff (Hounkpè and Diekkrüger, 2018; Abdulkadir *et al.,* 2022). The reduction in aquifer recharge and lateral flow emphasises the need for conservation agriculture practices such as cover cropping and minimum tillage (Togbèvi *et al.,* 2022), to limit the already low-fertility ferruginous soils from further degradation thereby affecting food productivity (Hounkpatin *et al.,* 2022; Dossou *et al.,* 2021b).

The PLS1 model in Component 1 demonstrated that, LULC changes explained most of the variations (>85 %) in surface runoff, baseflow, lateral flow, actual evapotranspiration and total aquifer recharge of the basin. The regression coefficients showed that area of Settlements/bare lands is consistently, a key predictor of surface runoff, with a unit increase in Settlements/bare lands enhancing runoff. This is likely due to restricted infiltration on impervious surfaces, and exposure of the bare soil surface to direct raindrops impact, that results in reducing infiltration and enhancing erosion (Togbévi *et al.,* 2022). The consequences of this phenomenon are floods and a reduction in groundwater replenishment which could affect water availability for farming, domestic and industrial purposes. An increase in Forest area was associated with a reduction in surface runoff, an increase in subsurface flow, aquifer recharge and actual evapotranspiration. This is attributable to the dense canopy of forests which enables interception of rainfall, and the forest litter which inhibits runoff, thereby enhancing infiltration rates (Honda and Durigan, 2016; Lokonon *et al.,* 2018). When Agricultural land increases, surface runoff increases, though lower compared to Settlements/bare lands, and reduces subsurface flow and aquifer recharge, thus, revealing the adverse impacts of extensive land degradation for agricultural expansion. An increase in Savanna areas reduces surface runoff and increases subsurface flow, aquifer recharge and evapotranspiration, but at a lower potential than Forests. This demonstrates the reduced ability of open tree canopy areas to effectively reduce runoff and enhance infiltration. These trends could aggravate water scarcity and reduction in ecosystem services in the basin (Togbévi *et al.,* 2020). Furthermore, in Component 2, the PLS models indicated an increase in Forest areas, Agricultural lands and settlement/bare areas which corresponded with an increase in surface runoff and a reduction in baseflow, aquifer recharge, and actual evapotranspiration. This suggests that, the hydrological response of Forests is more complex and potentially influenced by other factors such as land management practices (agro-forestry, selective logging, reforestation, impervious surfaces around trees) or fragmentation (continuous Forests or small patches). This implies that reforestation efforts should ensure continuous canopy coverage, while urban developments should also consider more green areas around trees to enhance infiltration and reduce runoff.

The high R^2 values obtained for surface runoff predictions across multiple periods suggest that the relationship between LULC change and runoff is robust and temporally consistent. This strong correlation reflects the immediate impact of reduced Forest and Savanna areas on surface runoff. However, the relatively lower R^2 values for baseflow, lateral flow, and total aquifer recharge across the three simulation periods (1998-2008, 2008-2016, and 1998-2016) indicate a low ability to generalise, suggesting that these components are less sensitive to short-term LULC changes. They are, therefore, more dependent on temporal variability (more sensitive to other factors such as climate) or may have a non-linear relationship with LULC changes. Higher baseflow was estimated during the 16-year simulation period compared to the two 8-year periods. The Dahomeyan Basement, which underlies the study area, consists of metamorphic and crystalline rocks with inherently lower porosity and permeability, except where fractures are present (Faure and Volkoff, 1998; Bossa, 2012). However, there is no established link between geomorphic parameters and baseflow, although watershed geomorphology influences baseflow (Price, 2011). Furthermore, the uncertainties in the SWAT model groundwater estimations could account for the inconsistencies in baseflow estimated for the different periods. This has necessitated the coupling of the SWAT model with groundwater models to adequately simulate baseflow (Bailey et al., 2020). Additionally, the minimal change in actual evapotranspiration, despite changes in LULC, can be attributed to the fact that, the expansion of tree crops such as cashew, orange, palm and other plantations which are quite abundant in the basin can maintain similar levels of evapotranspiration, compensating for the loss of natural Forest and Savanna (Ellison *et al.,* 2012). Assessing the impacts of Agricultural land expansion at the scale of specific crops may offer better insights into evapotranspiration trends.

The accurate prediction of surface runoff across the different periods indicates the consistency of its relationship with increasing Agricultural lands and Settlements/bare lands, and diminishing natural vegetation. The increasing runoff volumes across the LULC maps hint at increasing flood potential in rapidly urbanizing areas requiring urgent mitigation measures (Hounkpè *et al.,* 2019; Nyatuame *et al.,* 2020). At the same time, the reducing baseflow and aquifer recharge has implications for long-term water availability for farming and domestic needs during the dry season (Togbévi and Sintondji, 2021).

5.3 Impact of Future LULC Change Scenarios on Water Balance

Examining the projected LULC and associated changes in water balance components from 2023 to the end of the 21st century using the CA-Markov projection showed various trends. The results indicate that projected changes in LULC differ with both the LULC type and the future period, suggesting that, differences in demand for land resources (e.g., more food, industry expansion and processing companies), and surrounding conditions such as law enforcement (e.g., reforestation, ban deforestation) and climate limitations (less rainfall or droughts) could inform the type of LULC change that would occur. Over the period from 2023 to 2100, Forest cover was projected to decrease sharply, likely due to continued urban expansion and food demands from population growth, as evidenced by the sharp increase in Settlements/bare lands over the same period. On the other hand, Savanna shows a gradual decrease throughout the period, while Agricultural land exhibits consistent growth, increasing most sharply between 2030 – 2063. These changes indicate that the expansion of Agricultural land might be more targeted at Forests possibly due to the inherent high moisture-holding capacity and fertility of soils in forested areas (Osseni *et al.,* 2022) compared to Savanna areas. That study also projected a small increase in Forest and Savanna areas in the Ouémé Delta (below Bonou) for 2035. The expansion of Settlements/bare lands is attributable to the demand for settlements from the projected increase in population growth, and growth in industry operations such as the Special Economic Zones (SEZ) currently established in Benin under Law NO. 2022-38 as of 2023 to increase investments (Secrétariat Général du Gouvernement, 2023) in sectors including agricultural processing (e.g., soya bean, cashew, cotton, fruits) into end products such as oil, fruit juice and clothing for export.

The reflected impact of projected LULC changes on water balance shows that surface runoff increases throughout the period up to 2100. This trend corresponds with the decline in Forest cover and Savanna areas, and the increase in Agricultural land and Settlements/bare lands. However, a higher reduction in surface runoff with an increase in Forest cover than Savanna as observed from the PLS coefficients can be attributed to the denser tree canopy and litter in Forest areas compared to Savanna areas, to intercept rainfall and slow runoff. Additionally, a lower increase in surface runoff with an increase in Agricultural land than Settlements/bare land could be due to the availability of vegetation (crops) on Agricultural land which slows runoff to some extent compared to bare or impervious surfaces. The increase in surface runoff would increase the vulnerability of communes (Dossou *et al.,* 2021b) within and south of the basin to flooding, including Cotonou and Porto-Novo, Benin's capital, as projected by Hounkpè *et al.* (2019). Floods cause displacement of people and destruction of property as observed with the 2022 floods which affected over 70,000 people (International Federation of Red Cross and Red Crescent Societies (IFRC), 2023).

Base and lateral flows showed a decline over the period, while total aquifer recharge and actual evapotranspiration increased from 2023-2030, and then reduced from 2030-2100. This highlights the varying response of subsurface and groundwater to deforestation and land degradation (Sanström, 1995). A large reduction in lateral flow from 2023-2030 is possible because deforestation could reduce the preferential flow channels created by Forest and Savanna tree roots within the soil (Wiekenkamp *et al.,* 2019; Guan *et al.*, 2023). It could also reduce the horizontal flow of subsurface water, and promote higher percolation, resulting in more aquifer recharge (Wang *et al.,* 2024). The loss of Forest and Savanna vegetation could also reduce transpiration amounts and evaporation from rain interception, leading to more water stored in aquifers (Ranjan *et al.,* 2006). The post-deforestation surface condition (or land use) also affects water balance response (Peña-Arancibia *et al.,* 2019), where it is observed that actual evapotranspiration increased from 2023-2030, possibly due to the replacement of Forest trees with crops, which still contribute to evapotranspiration. The reduction in subsurface flow, aquifer recharge and evapotranspiration from 2030-2100 has implications for subsurface water availability, due to decreased infiltration caused by natural vegetation loss, coupled with an increase in abstractions (from projected population growth) and urbanisation. Particularly, they suggest potential risks for groundwater sources' sustainability and less water availability in the long term, especially given the national water supply services expansion initiative, where groundwater is the main source. Actual evapotranspiration remains relatively stable with a minimal decrease across the periods, likely because of the balance between Forest loss and increased tree crop areas (Lokonon, 2018). However, the steadily negative trend could reflect decreased vegetative transpiration as forested areas decline and the tree crops are harvested from time to time for building construction, logging for firewood, processing etc.

5.4 Impact of Future Climate Change Scenarios on Water Balance

The results indicate that the Quantile Mapping was able to reduce the biases in the precipitation and temperature data from the Global Climate Models, as similarly observed by M'Po *et al.* (2017a) when they compared Quantile Mapping with the Delta Approach and Linear Scaling bias correction method in the Ouémé basin. Generally, the results showed an increase in precipitation from the near- (2021-2040) to mid-term (2041-2060), and a decline from the mid- to long-term (2081-2100) under both Sustainability (SSP1-2.6) and Regional Rivalry (SSP3-7.0) scenarios, as similarly observed by Alamou *et al.* (2017) using the RCP scenarios. Surface temperature, however, increased from the near- to mid-term, and while it increases until the end of the 21st century under SSP3-7.0, there is a nearly constant trend from the mid- to long-term under SSP1-2.6. This suggests that, if activities within the basin focus on sustainable measures as in SSP1-2.6, less warm climate would be reached in the long-term, however if not, warmer climate conditions are expected up to the end of the 21st century (Lee *et al.,* 2021).

The projected climate change showed minimal difference in the temperature values in the near-term future between the Sustainability (SSP1-2.6) and Regional Rivalry (SSP3-7.0) scenarios. This agrees with the IPCC Fifth and Sixth Assessment Reports on future scenarios which have revealed that the near-term annual global surface air temperature (GSAT) levels depend less on the scenario chosen but are more influenced by the natural internal variabilities in the climate system such as ocean currents, atmospheric patterns, and uncertainties in models. This means that the absolute levels of annual GSAT are less sensitive to specific emission scenarios compared to long-term where scenarios become more influential due possibly to accumulated effects of greenhouse gas emissions on global warming. Change in precipitation in the long-term future relative to the baseline (1995-2014) values of 3.49 % and 1. 49 % for the SSP1-2.6 and SSP3-7.0 scenarios, respectively, corroborates with the IPCC ranges of 0.0 %-6.6 % and 0.5 % - 9.6 % for SSP1-2.6 and SSP3-7.0, respectively (Lee *et al.,* 2021). The changes in minimum and maximum temperatures of 0.95 ^{o}C (3.01 ^{o}C) and 0.94^{o}C (2.68^{o}C) for the SSP1-2.6 (SSP3-7.0) scenarios in the long-term also agrees with the projections by the IPCC sixth report, which outlined an increase within the ranges 0.5^{o}C – 1.5^{o}C, and 2.0^{o}C – 3.7^{o}C for the SSP1-2.6 and SSP3-7.0 scenarios, respectively.

The reduction in surface runoff under SSP1-2.6 from the near-term to the long-term can be explained by the sustainable measures such as reforestation, that are implemented under that scenario, which cover/protect and improve soil infiltration, thereby reducing runoff rates, even under increasing rainfall pattern observed from the near- to mid-term. The increase in runoff from the near- to mid-term under SSP3-7.0 can be attributed to the higher quantity of exposed land surface and impervious surfaces with no conservation measures in place, which enhance runoff, and the high magnitude can be explained by the sharp increase in rainfall from the near- to mid-term. From the mid-term to long-term under SSP3-7.0, however, the sharp reduction in surface runoff can be due to the sharp decline in rainfall during the same period, which makes less water available even for runoff.

Lateral flow and total aquifer recharge reduced from the near- to mid-term under SSP1-2.6 despite an increase in precipitation, and this can allude to a possible counter effect of surface temperature increase during the same period. Under SSP3-7.0, lateral flow and aquifer recharge increased from the near- to mid-term, possibly due to the higher increase in precipitation though temperature also increased within the same period. However, the mid- to long-term, lateral flow, baseflow, and reduced aquifer recharge was attributable to the high reduction in precipitation and the increase in temperature. It was also observed that, under the warmer SSP3-7.0 scenario where temperature increased, actual evapotranspiration increased possibly due to increased evaporation and transpiration demand from the warmer air (Houngué *et al.,* 2019). However, there was also a small reduction in actual evapotranspiration from the mid-term to long-term under SSP1-2.6 possibly due to the reduction in precipitation which would reduce the amount of water available for evapotranspiration.

The abrupt increase in precipitation from the near- to mid-term and sharp reduction from the mid- to long-term suggest more intense rainfall leading to floods (Hounkpè *et al.,* 2022) and extended dry periods under SSP3-7.0. The increase in high-intensity rainfall corroborates the study by Hounkpè (2016), who assessed the trend of heavy rainfall events over the basin from 1921 to 2012. The reduction in precipitation from the mid- to long-term under SSP1-2.6 and SSP3-7.0 suggests less frequent rainfall compared to the historical period (1995-2014), as similarly observed by M'Po *et al.* (2017b) who assessed the past and mid-century rainfall indices over the basin under RCP4.5 and RCP8.5 scenarios.

The increase in surface runoff under SSP1-2.6 and SSP3-7.0 scenarios from the near- to mid-term also aligns with the observation by Alamou *et al.,* (2017), who observed increased discharge under RCP2-4.5 and RCP5-8.5 climate scenarios from 2011-2100. These trends could lead to more flash floods, which cause displacement of communes and destruction of cultivated crops and properties as observed in the past. The extended dry periods could increase crop water stress leading to crop failure (Sonneveld *et al.,* 2012), especially under conditions of increased degradation and less/no sustainable environmental measures such as cover crops, reforestation, rain-harvesting systems, and green urban spaces. Moreover, the high reduction in subsurface flow and aquifer recharge with an increase in temperature indicates that, the availability of water to meet the household needs of the populace (Togbévi *et al.,* 2020), who mainly rely on groundwater sources might be limited in the future unless sustainable climate adaptation measures are used (Ariom *et al.,* 2022). Cotton production, for instance, could be intercropped or rotated with other crops to improve soil fertility and reduce the vulnerability of such areas to erosion and flooding under extreme rainfall (Dossou *et al.,* 2021a).

5.5 Combined Impact of Future LULC and Climate Change on Water Balance

Results from combining projected LULC for 2030, 2063, and 2100, with projected future climate in the near term (2021-2040), mid-term (2041-2063), and long term (2081-2100) revealed influences of both LULC and climate change on water balance components.

An increase in surface runoff from 2030-2063 depicts the reduction in natural vegetation (Forest and Savanna) and an increase in Agricultural and Settlements/bare land during that period as observed in Objective 3. The higher magnitude of surface runoff in 2030 under SSP1-2.6 than SSP3-7.0 is attributable to the higher precipitation under SSP1-2.6 in 2030. The larger increase in surface runoff from 2030-2063 under SSP3-7.0 than SSP1-2.6 depicts the adverse effects of continued unsustainable practices (e.g., deforestation, urbanisation without green infrastructure, agricultural expansion without conservation measures) in enhancing runoff (Hounkpè and Diekkrüger, 2018; Abdulkadir *et al.,* 2022). At the same time, the increase in lateral flow, baseflow, total aquifer recharge and actual evapotranspiration under SSP3-7.0 from 2030-2063 can be explained by the higher precipitation increase under SSP3-7.0 (34 mm/y) than SSP1-2.6 (4 mm/y) from the near term to mid-term. Actual evapotranspiration increased from 2030-2063 under SSP1-2.6 and SSP3-7.0 in response to increased precipitation, making more water available for evapotranspiration. An increase in deforestation, Settlements/bare and Agricultural land from 2030-2063 also increased the evaporative demand through higher land surface temperature. The high magnitude under SSP3-7.0 is attributable to the increase in temperature (0.75) while temperature reduced steadily under SSP1-2.6 (0.02).

Furthermore, the gentle decrease in surface runoff from 2063-2100 agrees with the huge precipitation decrease of 49 mm/y for that period, which makes less water available for runoff. The decrease in lateral flow depicts the effect of deforestation through a reduction in subsurface pathways created by Forest roots for preferential flow (Wiekenkamp *et al.,* 2019). The reduction in baseflow and total aquifer reflects the decrease in infiltration from increasing Agricultural and Settlements/bare lands. The higher reduction in magnitude reflects the large precipitation decline in the long term (M'Po *et al.,* 2017b) and the high sensitivity of baseflow and aquifer recharge to temperature rise as observed in Objective 4. Actual evapotranspiration reduced from 2063-2100 under SSP1-2.6 possibly due to the decrease in available water for evapotranspiration, despite the small increase in temperature (0.39 °C). However, the increase in actual evapotranspiration under SSP3-7.0 can be explained by the higher air temperature (1.5 °C) (Hounguè *et al.,* 2019), and unsustainable practices such as deforestation for agricultural and settlement expansion. More abrupt changes in water balance components under SSP3-7.0 indicate probable extreme climate events of floods (Hounkpè *et al.,* 2022) and droughts in the future.

The changes in the components of water balance showed responses to both LULC and climate change. This depicts the interrelatedness of LULC, climate and hydrology (Sandström, 1995). However, the trends in water balance components more closely followed the trend of climate changes (Sharma *et al.,* 2023), especially precipitation which is possible because precipitation is the main source of water in the hydrological processes.

The PLS model confirmed that, both LULC and climate change influence changes in water balance in the basin. An increase in precipitation and a corresponding increase in Forest and Savanna areas reduces surface runoff under SSP1-2.6 but increases runoff under SSP3-7.0. This emphasises the benefits of sustainable environmental practices such as reforestation prevalent under SSP1-2.6, which intercept rainfall and slow runoff as observed in Objective 4. As precipitation increases, more water is available for infiltration, explaining the increase in lateral flow, baseflow and total aquifer recharge under SSP1-2.6 and SSP3-7.0. An increase in temperature reduced surface runoff in SSP1-2.6 but increased runoff under SSP3-7.0, likely due to the absence of sustainable land practices under SSP3-7.0, which is compounded by deforestation and an increase in Settlements/bare and Agricultural lands. The coefficients also showed that Forests reduce runoff and improve subsurface flow at a higher potential than Savanna, while Settlements/bare land enhanced runoff and reduced subsurface flow at a higher potential than Agricultural land. This suggests the efficiency of dense vegetation cover and litter to reduce runoff and floods under peak flow events. This improves infiltration as well as aquifer recharge, which is crucial for groundwater availability for domestic, farming and industrial purposes.

These findings highlight the interactions among LULC, climate and the hydrological processes in the basin, underscoring the need for sustainable land and water management and climate adaptation measures to improve food and water security and reduce extreme events such as floods and droughts.

5.6 Contribution to Knowledge

1. This study used multiple historical LULC maps over the Ouémé River Basin to assess changes in LULC, and examined the relationship between each LULC type and water balance components using linear regression analysis.
2. Additionally, this study assessed the consistency of the relationships over different periods by simulating water balance over multiple periods.
3. Furthermore, projections of future scenarios of LULC for 2030, 2063, and 2100 and its impact on water balance were assessed.
4. Finally, projections of future climate change from the IPCC CMIP6 data and scenarios were used to project future changes in water balance that can be expected up to 2100.
5. The impact of combined projected changes in LULC and climate on water balance was assessed.

CHAPTER 6 CONCLUSIONS AND RECOMMENDATIONS

6.1 Conclusions

This study assessed the impact of land use/cover and climate change on water balance in the Ouémé River Basin by examining past trends and projecting future trends. The study has shown that, deforestation as a result of the expansion of Agricultural lands and increasing Settlements/bare areas, and increase in precipitation and temperature have a strong influence on hydrological processes such as water balance components of surface runoff, lateral flow, baseflow, aquifer recharge, and evapotranspiration. The key conclusions are as follows:

1. Spatio-temporal changes in LULC showed a reduction in Forests (-4.9 %) and Savanna (-24.1 %), with increasing Settlements/bare lands (1.1 %) and Agricultural land (28.0 %) from 1986-2023 (i.e., 38 years).
2. The LULC change from 1986-2023 increased surface runoff (32 mm/y) and peak flows, suggesting high flooding vulnerability. Lateral flow (6 mm/y), baseflow (5 mm/y), aquifer recharge (22 mm/y), and reduced actual evapotranspiration (6 mm/y), potentially led to limited water availability for domestic and farming purposes. Changes in Settlements/bare land and Forests were key predictors.
3. Future LULC projections for 2030, 2063 and 2100 suggest that, continued trends of increasing Agricultural land and Settlements/bare land will increase surface runoff (31.6 mm/y relative to 2023) and reduce lateral flow, baseflow, aquifer recharge and actual evapotranspiration. The increase in runoff could lead to floods and increase water insecurity through reduced water availability due to reduced groundwater recharge in the future.
4. The projected future climate for 2021-2100 under the SSP1-2.6 and SSP3-7.0 scenarios showed highly variable rainfall and temperature patterns, that strongly influenced water balance. This might aggravate the hydrological trends, leading to more extreme drought conditions, and intense rains, causing more floods, which could affect people, properties and crop production.

5. The combined projected future LULC and climate revealed the interactive impact of LULC and climate changes on surface runoff and higher sensitivity sub-surface flow values closer to sole climate. compared to the sole projected LULC and climate scenarios. Air temperature had the highest influence on water balance changes, though the water balance changes trend was similar to that of precipitation changes.

6.2 Recommendations

Policy

1. It was recommended that the Ministry of the Living Environment and Sustainable Development (MCVDD) in Benin should embark on more reforestation activities and discourage deforestation through regulation enforcement.
2. The Ministry of Agriculture, Livestock and Fisheries should also promote agricultural intensification with conservation agriculture practices, such as minimum soil disturbance, planting cover crops, diversified plant species (water efficient crops), and intercropping to protect the soil and reduce runoff.
3. NGOs, Research Institutes, and the Ministry of Agriculture, Livestock and Fisheries should train farmers on the effect of continuous agricultural land expansion and the benefits of conservation agriculture practices to limit future runoff impacts. Green urban infrastructure and vertical expansion of cities are also recommended for the Ministry of Planning and Development to reduce runoff.
4. Finally, the Ministry of Planning and Development should encourage and incorporate adequate green spaces in development plans to reduce the impacts of extreme rainfall and temperature, which lead to floods and heat-related illnesses.

Research

1. Alternative satellite data (higher resolution if possible) and LULC classification algorithms should be considered to validate the results from this study.

2. Further investigation into the impact of specific crop types on surface runoff, subsurface flows, and aquifer recharge, testing other hydrological models or coupling SWAT with a groundwater model (e.g., MODFLOW) to validate water balance estimations.

3. The projection of LULC considering multiple land change models is suggested for further studies to improve the results from this study.

CHAPTER 7 REFERENCES

Abbaspour, K. C. (2015) *SWAT-CUP SWAT calibration and uncertainty programs*. Eawag: Swiss Federal Institute of Aquatic Science and Technology, pp. 6-66.

Abdi, H. (2010) 'Partial least squares regression and projection on latent structure regression (PLS Regression)', *Wiley Interdisciplinary Reviews: Computational Statistics*, 2(1), pp. 97–106.

Abdulkadir, T. S., Idrissou, A. Y., Salami, A. W., Aremu, S. A., Ayanshola, M. A., Surajudeen, M., Yusuf, I. T. and Aboshio, A. (2022) 'Prediction of water yield and balance in Upper Ouémé River Catchment in Benin Republic', *Bayero Journal of Engineering and Technology (BJET),* 17(1), pp. 41–52.

Adjei, F. O., Obuobie, E., Adjei, K. A. and Odai, S. N. (2023) 'Evaluation of potential evapotranspiration assessment methods for hydrological modelling with SWAT in the Densu river basin in Ghana', *International Journal of Environmental Science and Technology*, 20(1), pp. 921-930.

Aladejana, O.O., Salami, A. T. and Adetoro, O. I. O. (2018) 'Hydrological responses to land degradation in the Northwest Benin Owena River Basin, Nigeria', *Journal of Environmental Management*, 225, pp. 300–312.

Alamou, E. A., Obada, E. and Afouda, A. (2017) 'Assessment of future water resources availability under climate change scenarios in the Mékrou Basin, Benin', *Hydrology*, 4(4), pp. 1-21.

Aldwaik, S. Z. and Pontius Jr, R. G. (2012) 'Intensity analysis to unify measurements of size and stationarity of land changes by interval, category, and transition', *Landscape and Urban Planning*, 106(1), pp. 103–114.

Allen, R. G., Pereira, L. S., Raes, D. and Smith, M. (1998) *Crop evapotranspiration: Guidelines for computing crop water requirements (FAO Irrigation and Drainage Paper 56*). FAO.

Almazroui, M., Saeed, F., Saeed, S., Islam, M. N., Ismail, M., Klutse, N. A. B and Siddiqui, M. H. (2020) 'Projected Change in Temperature and Precipitation Over Africa from CMIP6', *Earth Systems and Environment*, 4, pp. 455-475.

Al-Naji, A., Fakhri, A. B., Gharghan, S. K. and Chahl, J. (2021) 'Soil color analysis based on a RGB camera and an artificial neural network towards smart irrigation: A pilot study', *Heliyon*, 7(1), pp. 1-5.

Ariom, T.O., Dimon, E., Nambeye, E., Diouf, N. S., Adelusi, O. O. and Boudalia, S. (2022) 'Climate-Smart Agriculture in African Countries: A Review of Strategies and Impacts on Smallholder Farmers', *Sustainability (Switzerland)*, 14(18), pp. 1-32.

Arnold, J. G., Srinivasan, R., Muttiah, R. S. and Williams, J. R. (1998) 'Large area hydrologic modeling and assessment part I: Model development', *Journal of the American Water Resources Association,* 34(1), pp. 73–89.

Ayanshola, A., Olofintoye, O. and Obadofin, E. (2018) 'The Impact of Global Warming on Precipitation Pattern in Iloron and the Hydrological Balance of the Awun Basin', *Slovak Journal of Civil Engineering,* 26(1), pp. 40–46.

Bailey, R. T., Park, S., Biegar, K., Arnold, J. G. and Allen, P. M. (2020) 'Enhancing SWAT+ Simulation of Groundwater Flow and Groundwater-surface Water Interactions using MODFLOW Routines'. *Environmental Modelling and Software*, 126, 104660, pp. 1-14.

Barbier, E.B. and Hochard, J.P. (2018) 'Land degradation and poverty' *Nature Sustainability*, 1(11), pp. 623–631.

Belgiu, M. and Drăgut, L. (2016) 'Random Forest in Remote Sensing: A Review of Applications and Future Directions', *ISPRS Journal of Photogrammetry and Remote Sensing*, 114, pp. 24-31.

Beven, K. (2012) *Rainfall-Runoff Modelling: The Primer.* Second Edition. John Wiley & Sons, Ltd, Chichester, England.

Biao, E. I. (2017) 'Assessing the impacts of climate change on river discharge dynamics in Ouémé River basin (Benin, West Africa)', *Hydrology*, 4(4), pp. 1-16.

Bliefernicht, J., Rauch, M., Laux, P. and Kunstmann, H. (2022) 'Atmospheric Circulation Patterns that Trigger Heavy Rainfall in West Africa', *International Journal of Climatology*, 42, 6515-6536.

Bodjrènou, R., Comandan, F. and Danso, D. K. (2023a) 'Assessment of Current and Future Land Use and Land Cover in the Ouémé basin for Hydrological Studies', *Sustainability (Switzerland)* 15(3), pp. 1-16.

Bodjrènou, R., Sintondji, L. O. and Comandan, F. (2023b) 'Hydrological modeling with physics-based models in the Ouémé basin: Issues and perspectives for simulation optimization', *Journal of Hydrology: Regional Studies*, 48, 101448, pp. 1-14.

Bossa, A. Y., Diekkrüger, B. and Agbossou, E. K. (2014) 'Scenario-based impacts of land use and climate change on land and water degradation from the meso to regional scale', *Water (Switzerland),* 6(10), pp. 3152–3181.

Bossa, Y. A. (2012) *Multi-scale modeling of sediment and nutrient flow dynamics in the Ouémé catchment (Benin) – towards an assessment of global change effects on soil degradation and water quality*. Universität Bonn, Bonn, Germany.

Card, D.H. (1982) 'Using known map category marginal frequencies to improve estimates of thematic map accuracy', *Photogrammetric Engineering and Remote Sensing*, 48(3), 431–439.

Chakravarty, P. and Kumar, M. (2019) 'Chapter 6 - Floral species in pollution remediation and augmentation of micrometeorological conditions and microclimate: An integrated approach', *Phytomanagement of Polluted Sites: Market Opportunities in Sustainable Phytoremediation*, pp. 203–219.

Chalid, A. and Mulyadi, A. (2021) ‘Study of climate change effect on water balance in upper Citarum Watershed, the Krueng Cunda Watershed, and the Woske Watershed, Indonesia’, *IOP Conference Series: Earth and Environmental Science*, 930, 012074, pp. 1-10.

Chander, G., Markham, B. I. and Helder, D. I. (2009) ‘Summary of current radiometric calibration for Landsat MSS, TM, ETM+ and EO-1 ALI sensors’, *Remote Sensing of the Environment*, 113, pp. 893-903.

Chen, D, Rojas, M., Samset, B. H., Cobb, K., Diongue Niang, A., Edwards, P., Emori, S., Faria, S. H., Hawkins, E., Hope, P., Huybrechts, P., Meinshausen, M., Mustafa, S. K., Plattner, G. K. and Tréguier, A.-M. (2021) Framing, Context, and Methods. In Climate Change 2021: *The physical science basis. contribution of working group I to the Sixth Assessment Report of the Intergovernmental Panel on Climate Change* [[Masson-De;motte, V., Zhai, P., Pirani, A., Connors, S. L., Péan, C., Berger, S., Caud, N., Chen, Y., Goldfarb, L., Gomis, M. I., Huang, M., Leitzell, K., Lonnoy, E., Matthews, J. B. R., Maycook, T. K., Waterfield, T., Yelekçi, O., Yu, R. and Zhou, B. (eds)]. Cambridge University Press, Cambridge, United Kingdom and New York, NY, USA. 147-286.’

Chun, J. A., Baik, J., Kim, D. and Choi, M. (2018) ‘A Comparative assessment of SWAT-Model-Based evapotranspiration against regional-scale estimates’, *Ecological Engineering*, 122, pp. 1-9.

Copernicus Climate Change Service – Climate Data Store, (2021a) *CMIP6 climate projections,* Copernicus Climate Change Service (C3S) Climate Data (CDS). Available at: https://cds.climate.copernicus.eu/datasets/projections-cmip6?tab=overview Accessed: 06/07/2024.

Copernicus Climate Change Service – Climate Data Store, (2021b) *Temperature and Precipitation Gridded Data for Global and Regional Domains Derived from In-situ and Satellite Observations*, Copernicus Climate Change Services (C3S) Climate Data Store (CDS). Available at: https://cds.climate.copernicus.eu/datasets/insitu-gridded-observations-global-and-regional?tab=overview Accessed: 04/07/2024.

Copernicus Climate Change Service – Climate Data Store, (2023) *ERA5 Hourly Data on Single Levels from 1940 to Present*, Copernicus Climate Change Services (C3S) Climate Data Store (CDS). Available at: https://cds.climate.copernicus.eu/datasets/reanalysis-era5-single-levels?tab=overview Accessed: 29/06/2024.

Cornelissen, T., Diekkrüger, B. and Giertz, S. (2013) ‘A comparison of hydrological models for assessing the impact of land use and climate change on discharge in a tropical catchment’, *Journal of Hydrology*, 498, pp. 221–236.

Darko, J. A. A., Ahenkorah, I. and Aakyiir, M. N. (2019) ‘Petrogenesis, geochemistry and structural evidence of the Neoproterozoic Pan-African Orogenic Event in Ghana, West Africa’, *Springer Nature Applied Science,* 1 (293).

Di Gregorio, A., Mushtaq, F., Tchana, E., Aw, M., D'Annunzio, R., Muchoney, D., Mamane, B., Mahamane, M., Assoumana, B. T., Mimouni, M., Aubee, E., Enaruvbe, G. O., Mensah, F., Bartel, P. and Henry, M. (2022) *West African land cover reference system*. Rome, FAO, AGRHYMET, ECOWAS and OSS.

Dossou, J. F., Li, X. X., Kang, H. and Boré, A. (2021a) 'Impact of climate change on the Ouémé basin in Benin', *Global Ecology and Conservation*, 28, e01692, pp. 1-17.

Dossou, J. F., Li, X. X., Kouhoundji, N. K. and Vissin, E. W. (2021b) 'Impact of agriculture on the Ouémé basin in Benin', *Water, Air, and Soil Pollution*, 232(479), pp. 1-21.

Ellison, D., Futter, M. N. and Bishop, K. (2012) 'On the forest cover-water yield debate: From demand- to supply-side thinking', *Global Change Biology,* 18(3), pp. 806–820.

Eltahir, E. and Krol, A. (2021) *Climate models*, MIT Climate Portal. Available at: https://climate.mit.edu/explainers/climate-models. Accessed: 10/10/2024.

Faure, P. and Volkoff, B. (1998) 'Some factors affecting regional differentiation of the soils in the Republic of Benin (West Africa)', *Catena*, 32, pp. 281-306.

Fisher, J. R. B., Acosta, E. A., Dennedy-Frank, P.J., Kroeger, T. and Boucher, T.M. (2018) 'Impact of satellite imagery spatial resolution on land use classification accuracy and modeled water quality', *Remote Sensing in Ecology and Conservation*, 4(2), pp. 137–149.

Foody, G. M. (2010) 'Assessing the Accuracy of Land Cover Change with Imperfect Ground Reference Data', *Remote Sensing of the Environment,* 114(10), pp. 2271-2285.

Fujita, M. and Thisse, J. (2013) *The von Thünen Model and Land Rent Formation. In: Economics of Agglomeration: Cities, Industrial Location, and Globalization*. Cambridge University Press, pp. 59-98.

García-Álvarez, D., Olmedo, M. T. C., Paegelow, M., and Mas, F. J. (eds.) (2022) *Validation Practices with QGIS Land Use Cover Datasets and Validation Tools*. Springer Nature, Switzerland.

Geladi, P. and Kowalski, B. R. (1986) *Partial Least-Squares Regression: A Tutorial*. Elsevier Science Publishers B.V, Amsterdam, Netherlands.

Gharun, M., Possell, M., Bell, T. L. and Adams, M. A. (2017) 'Optimisation of fuel reduction burning regimes for carbon, water and vegetation outcomes', *Journal of Environmental Management*, 203, pp. 157-170.

Giertz, S., Diekkrüger, B. and Steup, G. (2006) 'Hydrology and Earth System Sciences Physically-based modelling of hydrological processes in a tropical headwater catchment (West Africa)-process representation and multi-criteria validation', *Hydrology and Earth System Sciences*, 10, pp. 829-847.

Green, W. H. and Ampt, G. A. (1911) ‘Studies on Soil Physics, 1. The Flow of Air and Water through Soils’, *Journal of Agricultural Sciences*, 4, pp. 11-24.

Guan, N., Cheng, J. and Shi, X. (2023) ‘Preferential flow and preferential path characteristics of the typical forests in the Karst Region of Southwest China’, *Forests,* 14(6), p. 1248.

Gui, H., Wu, Z. and Zhang, C. (2021) ‘Comparative Study of Different Types of Hydrological Models Applied to Hydrological Simulation’, *Clean-Soil, Air, Water,* 49, p. 2000381.

Guo, Y., Zhang, Y., Zhang, T., Wang, K., Ding, J. and Gao, H. (2019) ‘Surface Runoff’. In: Li, X. and Vereecken, H. (eds). *Observation and Measurement of Ecohydrological Processes*, Ecohydrology, 2, Springer, Berlin, Heidelberg.

Hargreaves, G. H. and Samani, Z. A. (1985) ‘Reference crop evapotranspiration from temperature’, *Applied Engineering in Agriculture*. 1(2), pp. 96-99.

Hayhoe, K., Edmonds, J., Kopp, R. E., LeGrande, A. N., Sanderson, B. M., Wehner, M. F. and Wuebbles, D. J. (2017) *Climate models, scenarios, and projections. In: Climate science special report: fourth national climate assessment*, 1 [Wuebbles, D. J., Fahey, D. W., Hibbard, K. A., Dokken, D. J., Stewart, B. C., Maycok, T. K. (eds)]. U.S. Global Change Research Program, Washington, DC, USA, p. 133-160.

Hengle, T., Heuvelink, G. B. M., Kempen, B., Leenaars, J. G. B., Walsh, M. G. and Shepherd, K. D. (2015) ‘Mapping soil properties of Africa at 250 m resolution: Random forests significantly improve current predictions’. *PLoS ONE*, 10 (6), pp. 1-26.

Her, Y., Frankenberger, J., Chaubey, I. and Srinivasan, R. (2015) ‘Threshold effects in HRU definition of the Soil and Water Assessment Tool’, *Transaction of American Society of Agricultural and Biological Engineers*, 58(2), pp. 367-378.

Hiepe, C. (2008) *Soil degradation by water erosion in a sub-humid West-African catchment: a modelling approach considering land use and climate change in Benin*, Universität Bonn, Bonn, pp. 79-177.

Höllermann, B., Giertz, S. and Diekkrüger, B. (2010) ‘Benin 2025-Balancing future water availability and demand using the WEAP ‘Water Evaluation and Planning’ System’, *Water Resources Management*, 24(13), pp. 3591–3613.

Honda, E. A. and Durigan, G. (2016) ‘Woody encroachment and its consequences on hydrological processes in the savannah’, *Philosophical Transactions of the Royal Society B*’, 371(1703), pp. 1-9.

Hounguè, R., Lawin, A. E., Moumouni, S. and Afouda, A. A. (2019) ‘Change in climate extremes and pan evaporation influencing factors over Ouémé Delta in Bénin’, *Climate*, 7, 2, pp. 1-22.

Hounkpatin, K. O. L., Bossa, A. Y., Yira, Y., Igue, M. A. and Sinsin, B. A. (2022) 'Assessment of the soil fertility status in Benin (West Africa) – Digital soil mapping using machine learning', *Geoderma Regional*, 28, e00444, pp. 1-14.

Hounkpè, J. (2016) *Assessing the climate and land use changes impact on flood hazard in Ouémé River Basin, Benin (West Africa)*. University of Abomey Calavi, Benin, pp. 9-102.

Hounkpè, J. and Diekkrüger, B. (2018) 'Challenges in calibrating hydrological models to simultaneously evaluate water resources and flood hazard: A case study of Zou basin, Benin', *Episodes*, 41(2), pp. 105–114.

Hounkpè, J., Badou, D. F., Ahouansou, D. M. M., Totin, E. and Sintondji, L. O. C. (2022) 'Assessing observed and projected flood vulnerability under climate change using multi-modeling statistical approaches in the Ouémé River Basin, Benin (West Africa)', *Regional Environmental Change*, 22(4), p. 112.

Hounkpè, J., Diekkrüger, B., Afouda, A. A. and Sintondji, L. O. C. (2019) 'Land use change increases flood hazard: a multi-modelling approach to assess change in flood characteristics driven by socio-economic land use change scenarios', *Natural Hazards*, 98(3), pp 1021–1050.

Incoom, A. B. M., Amaning, K. A. and Odai, N., S. (2020) 'Rainfall variabilities and droughts in the Savannah zone of Ghana from 1960-2015', *Scientific African*, 10, e00571, pp. 1-16.

International Federation of Red Cross and Red Crescent Societies (IFRC) (2023) *Benin Floods 2022 DREF Final Report (MDRBJ017)*. Available at: ReliefWeb.https://reliefweb.int/report/benin/benin-floods-2022-dref-final-report-mdrbj017. Accessed: 15/10/2024.

Jajarmizad, M., Harun, S. and Salarpour, M. (2012) 'A review on theoretical consideration and types of models in hydrology', *Journal of Environmental Science and Technology,* 5(5), pp. 249–261.

Kilinzo, F., Van Griensven, A., Obando, J., Lens, P. and Bauwens, W. (2011) *Selecting a Potential Evapotranspiration (PET) method in the absence of essential climatic input data*. SWAT International Conference – TOLEDO, Spain.

Kirkham, M. B. (2005) *26 Potential Evapotranspiration*: *Principles of Soil and Plant Water Relations*. Academic Press, pp. 455-468.

Lamboni, B., Emmanuel, L. A., Manirakiza, C. and Djibib, Z. M. (2019) 'Variability of Future Rainfall over the Mono River Basin of West-Africa', *American Journal of Climate Change,* 8, pp. 137–155.

Lawin, A. E., Yèkambèssoun, N. T. M., Biaou, C. A., Komi, K., Hounguè, R., Yao, K. B. and Afouda, A. A. (2019) 'Mid-century daily discharge scenarios based on climate and land use change in Ouémé River Basin at Bétérou outlet', *Hydrology*, 5(69), pp.1–14.

Lee, J.-Y., Marotzek, J., Bala, G., Cao, L., Corti, S., Dunne, J. P., Engelbrecht, F., Fischer, E., Fyfe, J. C., Jones, C., Maycock, A., Mutemi, J., Ndiaye, O., Panickal, S. and Zhou, T. (2021) *Future global climate: scenario-based projections and near-term information*. In climate change 2021: The physical science basis. contribution of Working Group I to Sixth Assessment Report of the Intergovernmental Panel on Climate Change [Masson-De;motte, V., Zhai, P., Pirani, A., Connors, S. L., Péan, C., Berger, S., Caud, N., Chen, Y., Goldfarb, L., Gomis, M. I., Huang, M., Leitzell, K., Lonnoy, E., Matthews, J. B. R., Maycook, T. K., Waterfield, T., Yelekçi, O., Yu, R. and Zhou, B. (eds)]. Cambridge University Press, Cambridge, United Kingdom and New York, NY, USA, pp. 533-672.

Leta, M. K., Demissie, T. A. and Tränckner, J. (2021) 'Modeling and prediction of land use land cover change dynamics based on land change modeler (LCM) in Nashe Watershed, Upper Blue Nile Basin, Ethiopia', *Sustainability*, 13, p. 3740.

Lillesand, T., Kiefer, R. W. and Chipman, J. (2015) *Remote sensing and image interpretation (7th ed.)*, John Wiley & Sons, pp. 485-561.

Liu, H. and Wu, Q. (2017) 'Supervised and unsupervised image classification with radial basis function neural networks', *IEEE Transactions on Neural Networks and Learning Systems*, 28(5), pp. 1103-1115.

Lokonon, B.E., Tchandao Mangamana, E., Gnonlonfoun, I., Akpona, T.J.D., Assogbadjo, A.E., Glèlè Kakaï, R. and Sinsin, B. (2018) 'Knowledge, valuation and prioritization of 46 woody species for conservation in agroforestry systems along Ouémé catchment in Benin (West Africa)', *Environment, Development and Sustainability*, 21(5), pp. 2377–2399.

Lokonon, B.E., Tchandao Mangamana, E., Kakaï, R.G. and Sinsin, B. (2017) 'Assessing use, diversity and local conservation priorities of woody species within agroforestry systems along Ouémé catchment in Benin (West Africa)', *Ethnobiology and Conservation*, 6(4), pp. 1-19.

M'Po, Y. N., Lawin, A. E., Oyerinde, G. T., Yao, B. K., Afouda, A. A. (2017a) 'Comparison of daily precipitation bias correction methods, based on four regional climate model outputs in the Ouémé Basin, Benin', *Hydrology*, 4(6), pp. 58-71.

M'Po, Y. N., Lawin, E. A., Yao, B. K., Oyerinde, G. T., Attogouinon, A. and Afouda, A. A. (2017b) 'Decreasing past and mid-century rainfall indices over the Ouémé River Basin, Benin (West Africa)', *Climate*, 5, p. 74.

Maforikan, E.S., Hammani, A., Ahouansou, M.D. and Anthony-Krueger, C. (2023) Estimating water Balance at Bétérou Watershed, Benin Using Soil and Water Assessment Tool (SWAT) Model, Preprints.

Maxwell, A. E., Warner, T. A. and Fang, F. (2018) 'Implementation of machine-learning classification in remote sensing: An applied review', *International Journal of Remote Sensing,* 39(9), pp. 2784-2817.

Mbaye, M. L., Hagemann, S., Haensler, A., Stacke, T., Gaye, A. T. and Afouda, A. (2015) ‘Assessment of Climate Change Impact on Water Resources in the Upper Senegal Basin (West Africa)’, *American Journal of Climate Change*, 04(01), pp. 77–93.

McDonald, J. F. (2018) ‘Mr. Ricardo’s Theory of Land Rent’, *Journal of Real Estate Practice and Education*, 21(1), pp. 1–15.

Mclntyre, O. (2023) SDG 6 *‘Ensure Availability and Sustainable Management of Water and Sanitation for All’*. The UN Development Goals: A Commentary, Oxford Commentaries on International Law, pp. 441-508.

McNicol, L. M., Ryan, C. M. and Mitchard, E. T. A. (2018) ‘Carbon losses from deforestation and widespread degradation offset by extensive growth in African woodlands’, *Nature Communications*, 9, pp. 1-11.

Merk, F., Schaffhauser, T., Anwar, F., Tuo, Y., Cohard, J.-M., Disse, M. (2024) ‘The significance of the Leaf-Area-Index on the eevapotranspiration estimation in SWAT-T for characteristic land cover types of Western Africa’, *Hydrology and Earth System Sciences*, 28, pp. 5511-5539.

Momeni, R., Aplin, P. and Boyd, D.S. (2016) ‘Mapping complex urban land cover from spaceborne imagery: The influence of spatial resolution, spectral band set and classification approach’, *Remote Sensing*, 8(2), pp. 1-23.

Monteith, J. L. (1965) *Evaporation and the Environment. In the State and Movement of Water in Living Organisms.* 19th Symposia of the Society for Experimental Biology. Cambridge University Press, London, UK.

Moriasi, D. N., Arnold, J. G., Liew, M. W. Van, Bingner, R.L., Harmel, R.D. and Veith, T.L. (2007) ‘Model evaluation guidelines for systematic quantification of accuracy in watershed simulations’, *Transactions of American Society of Agricultural and Biological Engineers*, 50(3), pp. 885-900.

Mosavi, A., Sajedi-Hosseni, F., Choubin, B., Taromideh, F., Rahi, G. and Dineva, A. (2020) Susceptibility Mapping of Soil Water Erosion using Machine Learning Models. Water (Switzerland), 12(7), pp.1-17.

NASA- Applied Remote Sensing Training Program, (2018) *Advanced webinar: accuracy assessment of a land cover classification*, NASA Earth Science Division, Washington DC, USA.

Neitsch, S. L., Arnold, J. G., Kiniry, J. R. and Williams, J. R. (2011) *Soil and Water Assessment Tool Theoretical Documentation Version 2009*, Texas Water Resources Institute technical report No. 406. Texas Water Resources Institute, Texas A&M University, Texas.

Neitsch, S. L., Arnold, J. G., Kiniry, J. R., Srinivasan, R. and Williams, J. R. (2002) *Soil and Water Assessment Tool user’s manual version 2000*, Grassland, Soil and Water Research Laboratory, Agricultural Research Service, 808 East Blackland Road, Temple, Texas 76502.

Noi Phan, T., Kuch, V. and Lehnert, L. W. (2020) 'Land cover classification using Google Earth Engine and Random Forest Classifier- The role of image composition', *Remote Sensing*, 12(15), pp. 1-22.

Nounangnonhou, T. C., Acakpovi, A., Lokonon, B. E. and Sanya, A. E. (2018) 'Modelling and prediction of Ouémé (Benin) River flows by 2040 based on GR2M approach', *Larhyss Journal,* 33(2018), pp. 71–91.

Nyatuame, M., Amekudzi, L. K. and Agodzo, S. K. (2020) 'Assessing the land use/land cover and climate change impact on water balance on Tordzie watershed', *Remote Sensing Applications: Society and Environment,* 20, pp. 1-10.

O'Neill, B. C., Kriegler, E., Ebi, K. L., Kemp-Benedict, E., Riahi, K., Rothman, D. S., van Ruijven, B. J., van Vuuren, D. P., Birkmann, J., Kok, K., Levy, M. and Solecki, W. (2017) 'The roads ahead: Narratives for shared socioeconomic pathways describing world futures in the 21st century', *Global Environmental Change*, 42, pp. 169–180.

Obodai, J., Adjei, K. A., Odai, S. N. and Lumor, M. (2019) 'Land use/land cover dynamics using Landsat data in a gold mining basin-the Ankobra, Ghana', *Remote Sensing Applications: Society and Environment*, 13, pp. 247–256.

Odusanya, A. E., Schulz, K., Biao, E. I., Degan, B. A. S. and Mehdi-Schulz, B. (2021) 'Evaluating the performance of streamflow simulated by an eco-hydrological model calibrated and validated with global land surface actual evapotranspiration from remote sensing at a catchment scale in West Africa', *Journal of Hydrology: Regional Studies*, 37(100893), pp. 1-22.

Olofintoye, O. O., Ayanshola, A. M., Salami, A. W., Idrissiou, A., Iji, J. O. and Adeleke, O. O. (2022) 'A study on the applicability of a SWAT model in predicting the water yield and water balance of the Upper Ouémé Catchment in the Republic of Benin', *Slovak Journal of Civil Engineering*, 30(1), pp. 57–66.

Olofsson, P., Foody, G. M., Herold, M., Stehman, S. V., Woodcock, C. E. and Wulder, M. A. (2014) 'Good practices for estimating area and assessing accuracy of land change', *Remote Sensing of Environment*, 148, pp. 42–57.

Osseni, A. A., Dossou-Yovo, H. O., Gbesso, G. H. F., Lougbegnon, T. O. and Sinsin, B. (2022) 'Spatial dynamics and predictive analysis of vegetation cover in the Ouémé River Delta in Benin (West Africa)', *Remote Sensing*, 14(6165), pp. 1-19.

Padial-Iglesias, M., Serra, P., Ninyerola, M. and Pons, X. (2021) 'A Framework of filtering rules over ground truth samples to achieve higher accuracy in land cover maps', *Remote Sensing*, 13, p. 2662.

Paudel, M., Nelson, E. J., Downer, C. W. and Hotchkiss, R. (2011) 'Comparing the capability of distributed and lumped hydrologic models for analyzing the effects of land use change', *Journal of Hydroinformatics*, 13(3), pp. 461-473.

Pazou, E. Y. A., Lalèyè, P., Boko, M., van Gestel, C.A.M., Ahissou, H., Akpona, S., van Hattum, B., Swart, K. and van Straalen, N. M. (2017) 'Contamination of fish by organochlorine pesticide residues in the Ouémé River Catchment in the Republic of Bénin', *Environment International,* 32, pp. 594-599.

Peel, M. C., Finlayson, B. L. and McMahon, T. A. (2007) 'Updated world map of the Köppen-Geiger climate classification', *Hydrology and Earth System Sciences*, 11, pp. 1633–1644.

Peña-Arancibia, J. L., Bruijnzeel, L. A., Mulligan, M. and Van Dijk, A. I. (2019) 'Forests as 'Sponges' and 'Pumps': Assessing the impact of deforestation on dry-season flows across the Tropics', *Journal of Hydrology*, 574, pp. 946-963.

Perron-Welch, F., Medaglia, J. C., Piselli, D., Goodman, A. and Spasevski, A. (2023) *SDG 15 'Protect, restore and promote sustainable use of terrestrial ecosystems, sustainability manage forests, combat desertification, and halt and reverse land degradation and halt biodiversity loss'*. The UN Sustainable Development Goals: A Commentary, Oxford Commentaries on International Law, pp. 1077-1156.

Polykretis, C., Grillakis, M. G. and Alexakis, D. D. (2020) 'Exploring the impact of various spectral indices on land cover change detection using change vector analysis: A case study of Crete Island, Greece', *Remote Sensing*, 12(2), pp. 1-25.

Pontius Jr, R. G. (2022) *Metrics that make a difference,* Balram, S. and Burnaby, C. (eds.). Cham: Springer International Publishing.

Pontius Jr, R. G. and Malanson, J. (2005) 'Comparison of the structure and accuracy of two land change models', *International Journal of Geographical Information Science,* 19(2), pp. 243–265.

Pontius Jr, R. G. and Millones, M. (2011) 'Death to kappa: Birth of quantity disagreement and allocation disagreement for accuracy assessment', *International Journal of Remote Sensing*, 32(15), pp. 4407–4429.

Price, K. (2011) 'Effects of watershed topography, soils, land use, and climate on baseflow hydrology in humid regions: A review', *Progress in Physical Geography*, 35(4), pp. 465–492.

Priestly, C. H. B. and Taylor, R. J. (1972) 'On the Assessment of surface heat flux and evaporation using large-scale parameters', *Monthly Weather Review* 100, pp. 81-92.

Puyravaud, J-P. (2003) 'Standardizing the calculation of the annual rate of deforestation', *Forest Ecology and Management*, 177(1-3), pp. 593-596.

Qiu, S., Zhu, Zhe, Olofsson, P., Woodcook, C. E. and Jin, S. (2023) 'Evaluation of Landsat image compositing algorithms', *Remote Sensing of Environment*, 285, pp. 1-23.

Randall, D. A., Wood, R. A., Bony, S., Colman, R., Fichefet, T., Fyfe, J., Kattsov, V., Pitman, A., Shukla, J., Srinivasan, J., Stouffer, R. J., Sumi, A. and Taylor, K.E. (2007) *Climate models and their evaluation.* In: Climate change 2007: The physical science basis. Contribution of Working Group I to the Fourth Assessment Report of the Intergovernmental Panel on Climate Change [Solomon, S., D. Qin, M. Manning, Z. Chen, M. Marquis, K.B. Averyt, M. Tignor and H.L. Miller (eds.)]. Cambridge University Press, Cambridge, United Kingdom and New York, NY, USA.

Ranjan, S. P., Kazama, S. and Sawamoto, M. (2006) 'Effects of climate and land use changes on groundwater resources in coastal aquifers', *Journal of Environmental Management,* 80(1), pp. 25-35.

Riahi, K., van Vuuren, D.P., Kriegler, E., Edmonds, J., O'Neill, B.C., Fujimori, S., Bauer, N., Calvin, K., Dellink, R., Fricko, O., Lutz, W., Popp, A., Cuaresma, J.C., KC, S., Leimbach, M., Jiang, L., Kram, T., Rao, S., Emmerling, J., Ebi, K., Hasegawa, T., Havlik, P., Humpenöder, F., Da Silva, L.A., Smith, S., Stehfest, E., Bosetti, V., Eom, J., Gernaat, D., Masui, T., Rogelj, J., Strefler, J., Drouet, L., Krey, V., Luderer, G., Harmsen, M., Takahashi, K., Baumstark, L., Doelman, J.C., Kainuma, M., Klimont, Z., Marangoni, G., Lotze-Campen, H., Obersteiner, M., Tabeau, A. and Tavoni, M. (2017) 'The shared socioeconomic pathways and their energy, land use, and greenhouse gas emissions implications: An overview', *Global Environmental Change*, 42, pp. 153–168.

Ritchie, J. T. (1972) 'A Model for predicting evaporation from a row crop with incomplete cover', *Water Resources Resources*, 8, pp. 1204-1213.

Saddique, N., Mahmood, T. and Bernhofer, C. (2020) 'Quantifying the impacts of land use/land cover change on the water balance in the afforested River Basin, Pakistan', *Environmental Earth Sciences,* 79(19), pp. 1–13.

Sandström, K. (1995) 'Differences in groundwater response to deforestation – A continuum of interactions between hydroclimate, landscape characteristics and time', *GeoJournal,* 35(4), pp. 539-546.

Santpoort, R. (2020) 'The drivers of maize area expansion in sub-Saharan Africa. How policies to boost maize production overlook the interests of smallholder farmers' *Land*, 9(3), pp. 1-13.

Sathya, R. and Abraham, A. (2013) 'Comparison of supervised and unsupervised Learning Algorithms for Pattern Classification', *International Journal of Advanced Research in Artificial Intelligence*, 2(2), pp. 34-38.

Schulla, J. (2014) *Model description WaSiM (Water balance Simulation Model)*. Zurich.

Secrétariat Général du Gouvernement (2023) *Law No. 2022-38 of 03 January 2023: Establishing the regime of special economic zones in the Republic of Benin*. Available at: https://sgg.gouv.bj/doc/loi-2022-38/.

Sharma, S. K., Sinha, R. K., Eldho, T. I. and Patel, H. M. (2023) Individual and combined impacts of land use/cover and climate change on water balance components of a tropical river basin, *Environmental Modeling and Assessment*, 29, 67-90.

Sinsin, B. and Kampmann, D. (eds.) (2010). *Biodiversity Atlas of West Africa, volume I: Benin*. Cotonou & Frankfurt/Main.

Sintondji, L. O., Zokpodo, B., Ahouansou, D. M., Vissin, W. E. and Agbossou, K. E. (2014) 'Modelling the water balance of Ouémé catchment', *International Journal of AgriScience*, 4(1), pp. 74–88.

Sloan, P. G. and Moore, I. D. (1984) 'Modeling subsurface stormflow on steeply sloping forested watersheds', *Water Resources Research*, 20, pp. 1815-1822.

Sonneveld, B.G.J.S., Keyzer, M.A., Adegbola, P. and Pande, S. (2012) The Impact of Climate Change on Crop Production in West Africa: An Assessment for the Ouémé River Basin in Benin, *Water Resources Management,* 26, pp. 553–579.

Soumaoro, T. (2021) 'Assessment of climate change impacts on agriculture in Mali', *International Journal of Scientific Research and Management*, 9(1), pp. 313–329.

Tanimu, B., Bello, A. D., Abdullahi, S. A., Ajibike, M. A., Muhammad, M. K. I. and Shahid, S. (2024) 'Enhancing reliability in climate projections: A novel approach for selecting Global Climate Models', *Physics and Chemistry of the Earth, Parts A/B/C*, 134, 103598.

Taonda, A., Zerbo, I., Da, S. S., Traoré, I. C. E., N'Guessan, A. E., Kassi, J. N. and Thiombiano, A. (2024) 'Potential distribution of detarium microcarpum under different climate change scenarios in Burkina Faso', *Journal for Nature Conservation,* 82, pp. 126737.

Tappan, G. G., Cushing, W.M., Cotillon, S.E., Mathis, M.L., Hutchinson, J.A., Herrmann, S.M. and Dalsted, K. J. (2016) *West Africa land use land cover time series: U.S. Geological Survey data release,* Earth Resources Observation and Science (EROS) Centre, United States.

Tassi, A. and Vizzari, M. (2020) 'Object-oriented LULC classification in Google Earth Engine combining SNIC, GLCM, and Machine Learning algorithms', *Remote Sensing*, 12(22), pp. 1–17.

Togbévi, Q.F. and Sintondji, L.O. (2021) 'Hydrological response to land use and land cover changes in a tropical West African catchment (Couffo, Benin)', *AIMS Geosciences*, 7(3), pp. 338–354.

Togbévi, Q.F., Bossa, A.Y., Yira, Y., Preko, K. (2020) 'A multi-model approach for analysing water balance and water-related ecosystem services in the Ouriyori catchment (Benin)', *Hydrological Sciences Journal*, 65(14), pp. 2453–2465.

Togbévi, Q.F., Van Der Ploeg, M., Tohoun, K.A., Agodzo, S.K. and Preko, K. (2022) 'Assessing the Effects of Anthropogenic Land Use on Soil Infiltration

Rate in a Tropical West African Watershed (Ouriyori, Benin)', *Applied and Environmental Soil Science*, 2022, pp. 1-11.

United Nations Environment Programme (2021) *Progress on Integrated Water Resources Management. Tracking SDG 6 series: global indicator 6.5.1 updates and acceleration needs*, UN-Water, Geneva, Switzerland.

US Geological Survey (2019) *Landsat 8 (L8) data users handbook, Version 5.0,* Landsat Missions, USGS Earth Resources Observation and Science Centre, Siuox Falls, South Dakota.

van Engelen, V. and Ting-tiang, W. (eds.) (1993) *Global and National Soils and Terrain Digital Databases (SOTER): Procedures Manual.* World Soil Resources Reports 74, ISRIC, Wageningen [etc.].

Varga, O. G., Pontius Jr, R. G., Singh, S. K. and Szabo, S. (2019) 'Intensity analysis and the figure of merit's components for assessment of a Cellular Automata – Markov simulation model'*, Ecological Indicators*, 101, pp. 933-942.

Viana, C. M., Pontius Jr, R. G., Rocha, J. (2023) 'Four fundamental questions to evaluate Land Change Models with an illustration of a Cellular Automata-Markov model', *Annals of American Association of Geographers*, 113(10), pp. 2497-2511.

Walling, E. and Vaneeckhaute, C. (2020) 'Greenhouse gas emissions from inorganic and organic fertilizer production and use: A review of emission factors and their variability', *Journal of Environmental Management*, 276, pp. 1-16.

Wang, D., Niu, J., Dai, Z., Yang, T., Miao, Y., Zhang, L., Chen, X. and Berndtsson, R. (2024) 'Forest restoration effects on soil preferential flow in the Paleo-periglacial Eastern Liaoning Mountainous Regions, China', *Journal of Cleaner Production*, 467, pp. 142974.

Werther, M., Spyrakos, E., Simis, S. G. H., Odermatt, D., Stelzer, K., Krawczyk, H., Berlage, O., Hunter, P. and Tyler, A. (2021) 'Meta-classification of remote sensing reflectance to estimate trophic status of inland and nearshore waters', *ISPRS Journal of Photogrammetry and Remote Sensing,* 176, pp. 109–126.

Wheeler, C. E., Omeja, P. A., Chapman, C. A., Glipin, M., Tumwesigye, C. and Lewis, S. L. (2016) 'Carbon sequestration and biodiversity following 18 years of active tropical forest restoration', *Forest Ecology and Management*, 373, pp. 44-53.

White, J. W., Rassweiler, A., Samhouri, J. F., Stier, A. C. and White, C. (2014) 'Ecologists should not use statistical significance tests to interpret simulation model results', *Oikos*, 123(4), pp. 385–388.

Wiekenkamp, I., Huisman, J. A., Bogena, H. R. and Vereecken, H. (2019) 'Effects of deforestation on water flow in the vadose zone', *Water*, 12, pp. 35.

World Bank (2018) Benin: *Broader Access to Water for Rural Communities*, World Bank Group, NW Washington DC, USA.

World Bank (2022) *Agriculture, forestry, and fishing, value added (5 of GDP) – Benin*. World Bank national accounts data, and OECD National Accounts data files, World Bank Group, NW Washington DC, USA.

Wright, J. B., Jones, Hastings, D. A., Jones, W. B. and Williams, H. R. (1985) *Geology and Mineral Resources of West Africa*, London (George Allen and Unwin).

Xie, S., Liu, L., Zhang, X., Yang, J., Chen, X. and Gao, Y. (2019) 'Automatic land-cover mapping using Landsat time-series data based on Google Earth Engine', *Remote Sensing*, 11(24), pp. 1-20.

Zhou, S., Yu, B., Lintner, B. R., Findell, K. L. and Zhang, Y. (2023) 'Projected increase in global runoff dominated by land surface changes' *Nature Climate Change*, 13(5), pp. 442–449.

Zoungrana, B. J., Ouedraogo, B. and Yanono, I. P. (2024) 'Potential Impact of Future Climate Change on Grassland Cover in Burkina Faso', *Environmental Science and Pollution Research*, 31, pp. 57229-57241.

Appendix

1. Area-based accuracy assessment computations

1. $\text{Stratus weight}, W_i = \dfrac{\text{Total Individual Class Area (km}^2\text{)}}{\text{Total Area of the classified pixels (km}^2\text{)}}$

2. $\text{Area proportion} = W_i \times \left(\dfrac{\text{Pixels in each LULC class}}{\text{Toral pixels for each LULC class}}\right)$

3. $S(A\hat{}) = \sqrt{\sum_{i=1}^{5} \dfrac{W_i \times \acute{P}_{ij} - \acute{P}_{ij}^2}{n_i - 1}}$

   Where:

   $S(A\hat{})$ is the standard error of area estimate for LULC class i

   $\acute{P}_{ij}$ is the value of LULC class i against class j in the area-based error matrix

   n_i is the total number of classified pixels for LULC class i

2. Water Balance Simulation

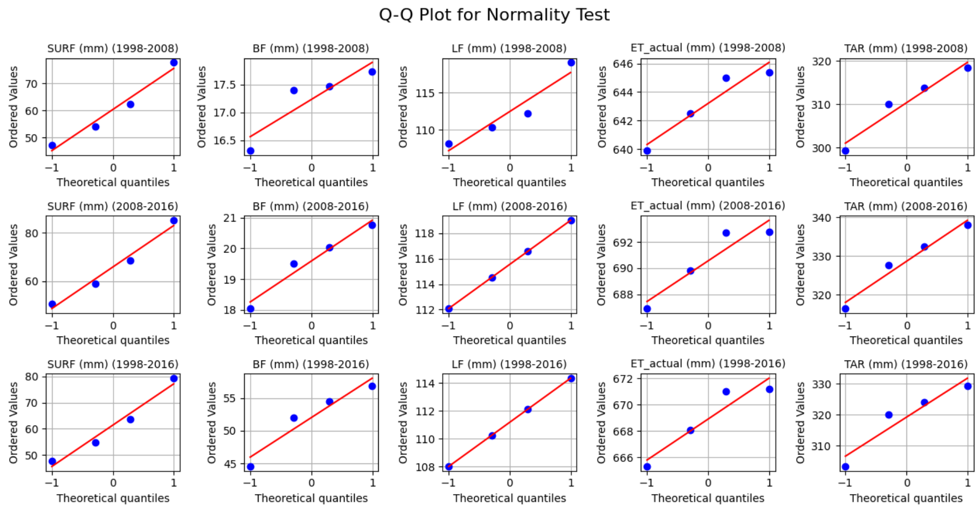

Figure 2A: Quantile-Quantile Plot of Average Annual Water Balance across Historical LULC Maps (1986, 2000, 2015, and 2023) and different Simulation Periods

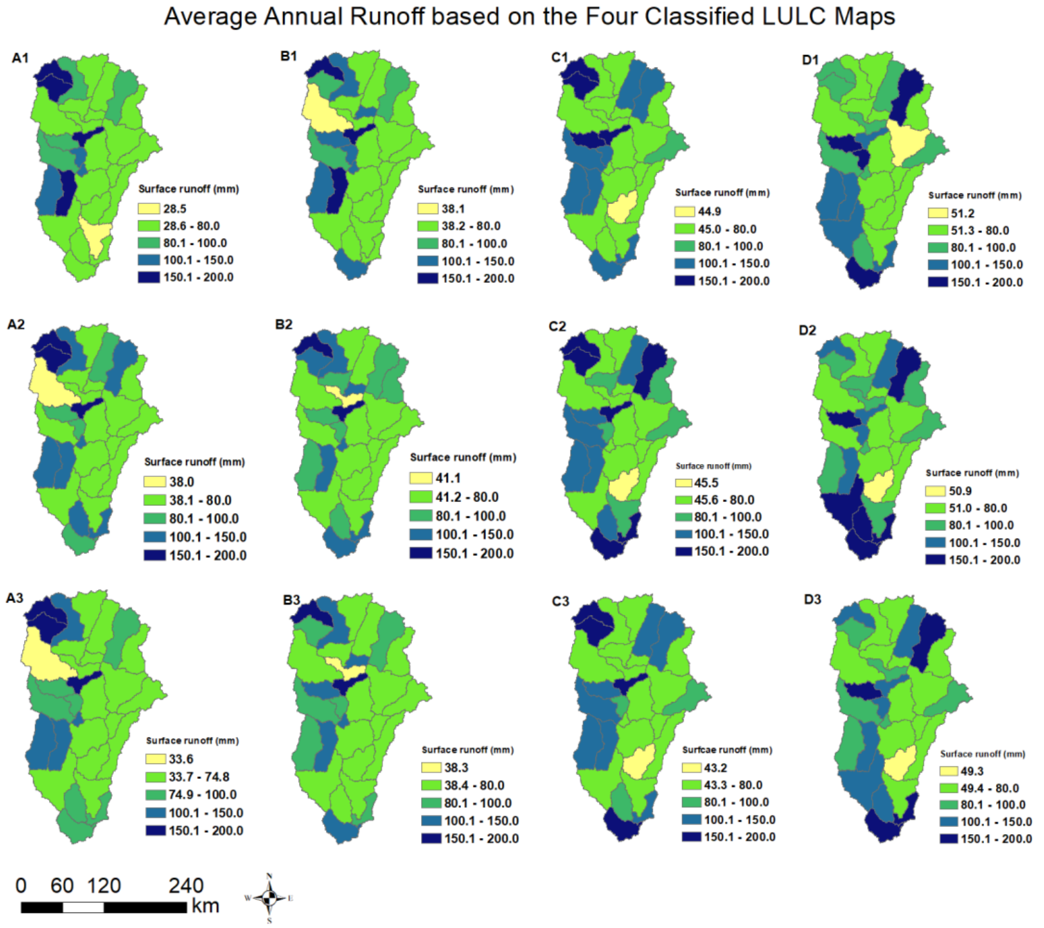

Figure 2B: Average annual surface runoff based on the four LULC across the three simulation periods. The label "letters" stand for the LULC map (A-1986, B-2000, C-2015 and D-2023), and the "numbers" for the simulation period (1 is period 1998-2008, 2 is period 2008-2016, and 3 is period 1998-2016)

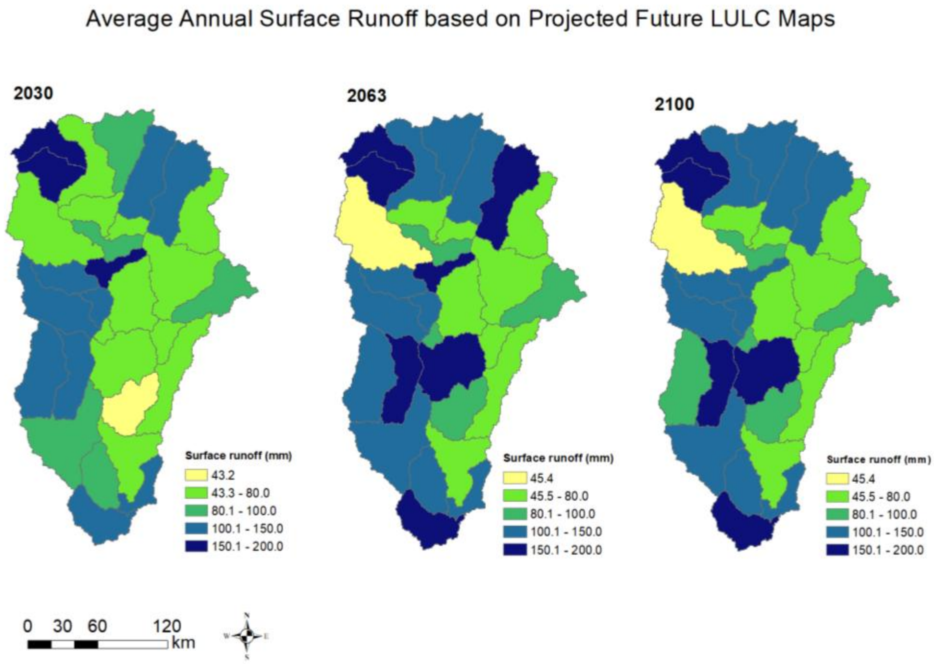

Figure 2C: Average annual surface runoff simulated based on future LULC maps for 2030, 2063 and 2100 over the basin

3. Future Climate Projections (Bais-Correction results)

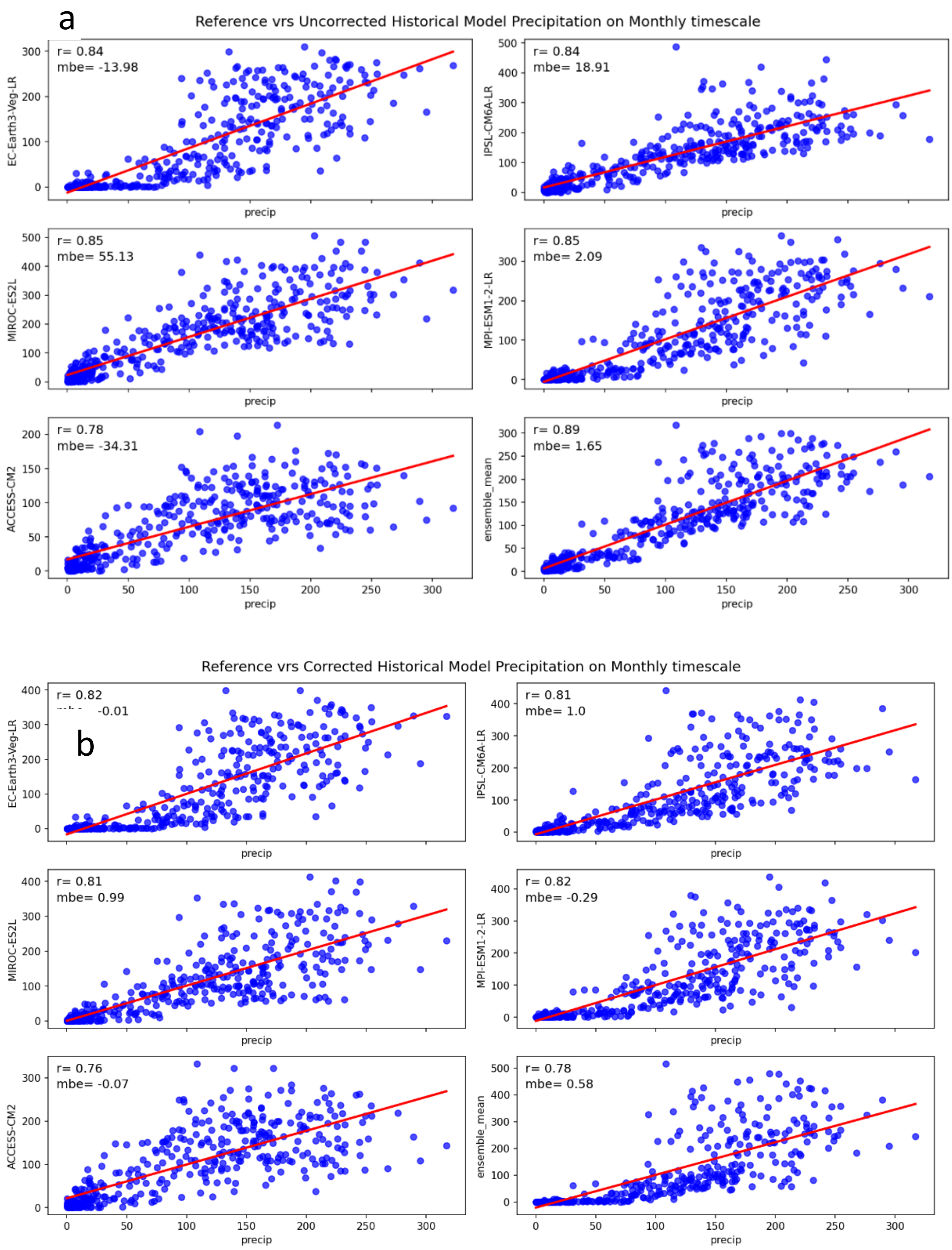

Figure 3A: Reference (CHIRPS) Precipitation versus Uncorrected (a) and Corrected (b) Climate Model Data, showing lower mbe for the bias-corrected model data

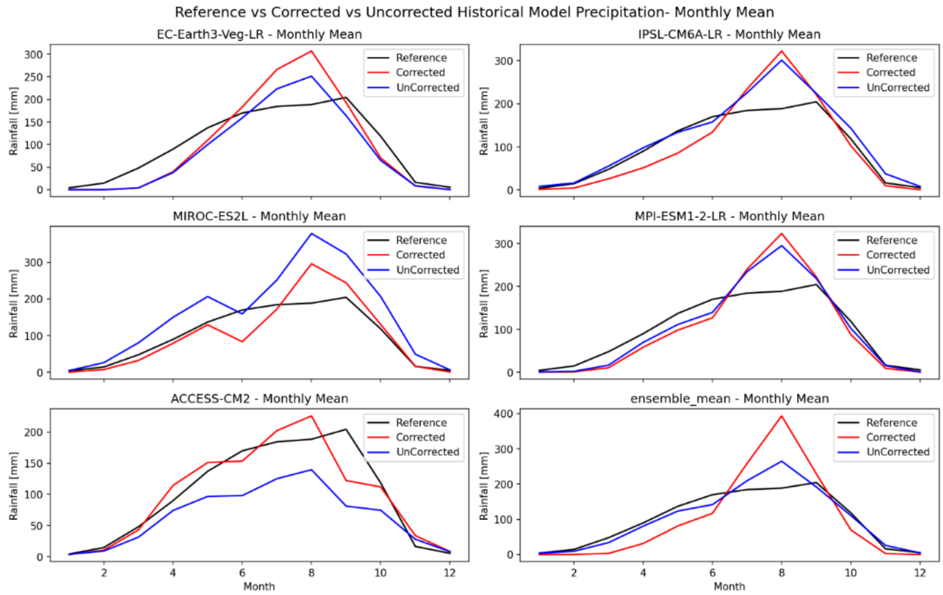

Figure 3B: Precipitation data from the ACCESS-CM2, MIROC-ES2L, MPI-ESM1-2-LR, IPSL-CM6A-LR, EC-EARTH3-Veg-LR and the ensemble mean, showing the bias-corrected, uncorrected (raw model data) and reference (CHIRPS)

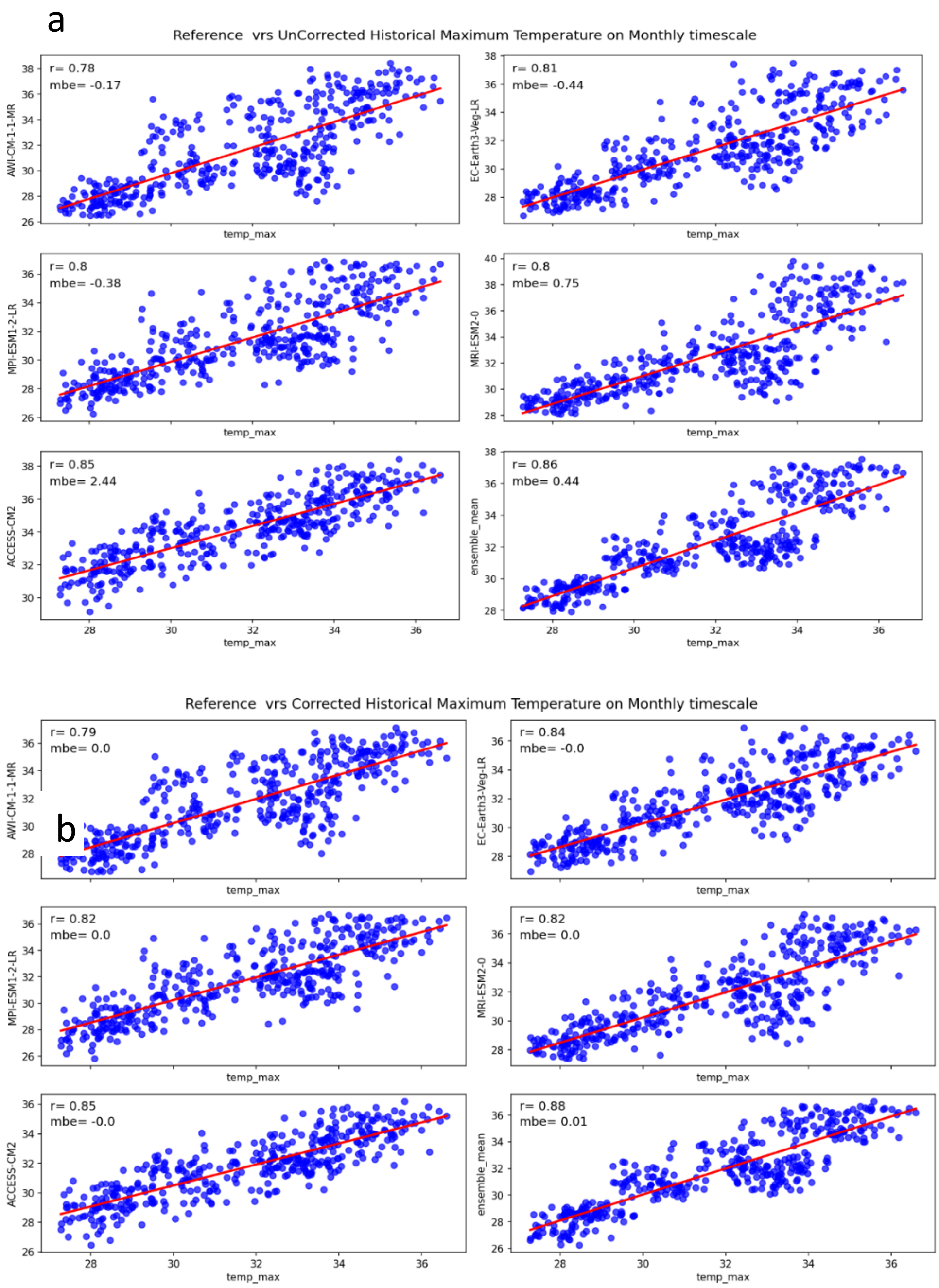

Figure 3C: Reference (ERA5) Maximum Temperature versus Uncorrected (a) and Corrected (b) Climate Model Data, showing lower mbe for the bias-corrected model data

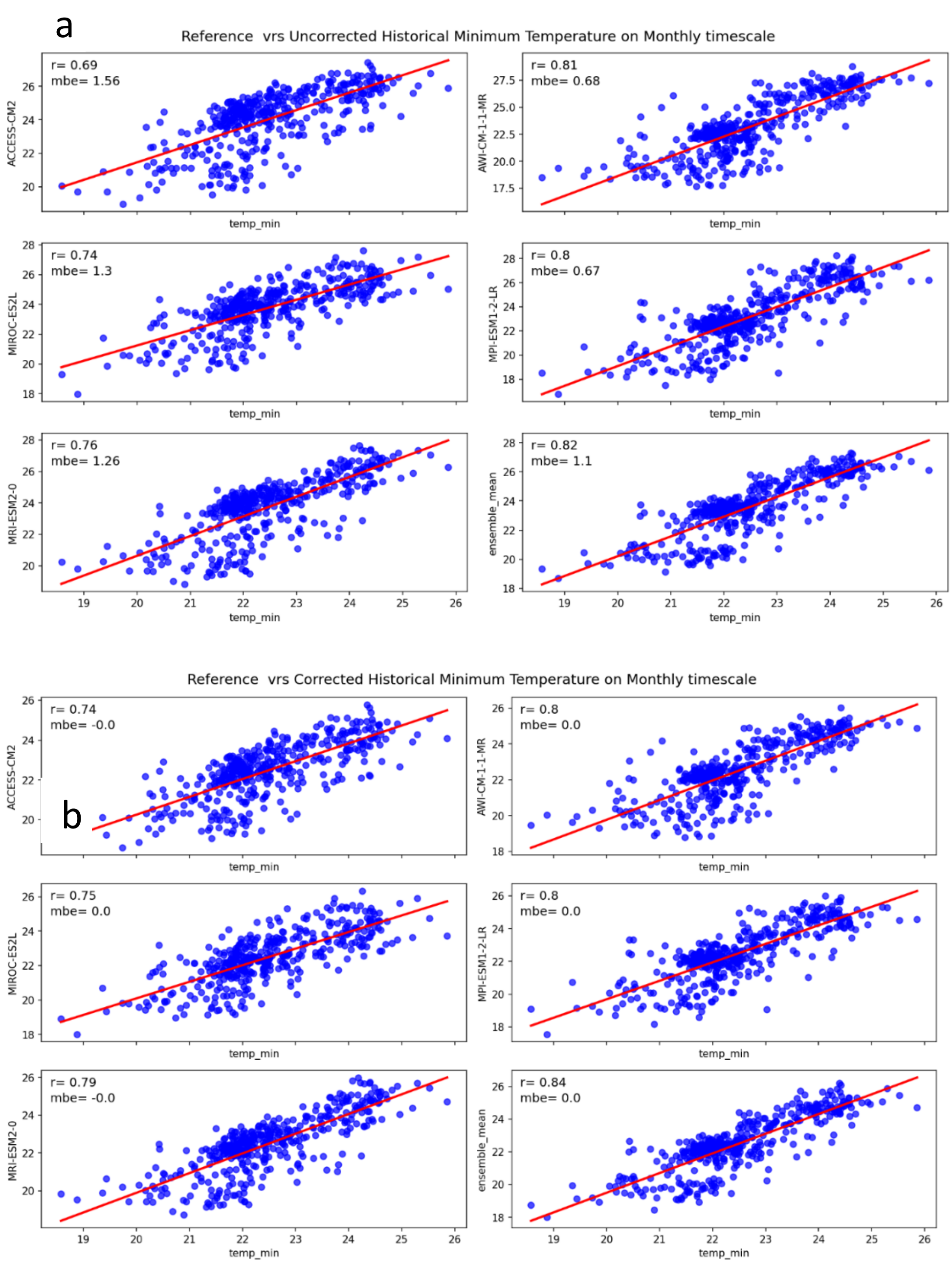

Figure 3D: Reference (ERA5) Minimum Temperature versus Uncorrected (a) and Corrected (b) Climate Model Data, showing lower mbe for the bias-corrected model data

4. Variable Importance in Projection (VIP)

Table 1A: VIP scores obtained for the LULC types depicting their importance in influencing surface runoff (SURF), lateral flow (LATF), baseflow (BF), total aquifer recharge (TAR) and actual evapotranspiration (ET_actual) across the three periods.

Variable Importance in Projection (VIP) scores					
1998-2008					
LULC type	SURF	LATF	BF	TAR	Actual ET
FRST	0.966	1.445	0.998	0.964	0.981
STB	1.002	0.639	0.946	0.994	1.003
SAV	1.016	0.962	1.048	1.024	1.018
AGR	1.015	0.759	1.005	1.017	0.997
R^2	0.996	0.934	0.954	0.985	0.968
2008-2016					
LULC type	SURF	LATF	BASF	TAR	ET
FRST	0.969	1.016	1.096	0.970	0.974
STB	1.004	0.999	0.933	0.979	1.005
SAV	1.013	0.987	1.017	1.035	1.018
AGR	1.014	0.997	0.946	1.015	1.002
R^2	0.997	0.995	0.946	0.980	0.980
1998-2016					
LULC type	SURF	LATF	BASF	TAR	ET
FRST	0.967	1.014	0.967	0.966	0.968
STB	1.003	0.999	0.985	0.999	1.009
SAV	1.015	0.988	1.031	1.017	1.016
AGR	1.014	0.998	1.015	1.016	1.006
R^2	0.997	0.995	0.988	0.98	0.986